

**Process planning methodology and evaluation of tool
life for micromilling with an application to the
fabrication of thin wall structure**



Amin Dadgari

School of Engineering

Newcastle University

A thesis submitted for the degree of

Doctor of philosophy

June 2019

(Intentionally left blank)

Abstract

The scaling down effect on feature geometries and tools used in micromilling results in low feature stiffness and excessive tool wear. To achieve the required costs and tolerances, optimisation of the machining processes and their associated parameters are necessary which requires a thorough understanding of machining characteristics. Furthermore, the compensation must be sought for downscaling issues that arise at the process planning stage. Hence, the effect of the characteristics of the cutting tool, workpiece material and machining parameters are investigated in this research through a critical review of the literature followed by a numerical and experimental study of the impact of process variables. The research findings are used in the development of a process planning methodology for micromilling of components with application to high aspect ratio structures, to assist machine operators and to fill the gap between industrial and academic machining knowledge.

From the investigation of machining sequences, the study of machining layer strategy considering the sequence of removal of excess material using numerical simulation, strategic planning of machining layers in relation to feature stiffness is required, in particular to the machining of high aspect ratio features. The results from numerical simulation recommend an improved layer strategy for micromilling of thin wall structures, which were then experimentally validated in relation to machining time and geometrical and surface accuracy. The importance of planning tool entry and exit position in relation to feature rigidity was highlighted. The increase in depth of cut shows to improve the tool engagement reducing the thin wall deflection by 168 μm and appearance of the burr along the wall edge indicated by up to 200% drop in burr width. The investigation of tool paths showed the suitability of strategies for machining of circular and linear geometries. Also, the experimental findings emphasise on considering the feature geometry type in the selection of tool paths to achieve a balance between high-performance machining and improved productivity.

This study also investigates tool life, associated with flank wear rate, surface roughness, volumetric tool loss and the degradation of the cutting edge radius for micro endmills where a direct correlation between cutting speed and tool wear rate has been found. The new procedure for tool life prediction in conjunction with clear tool rejection criteria for the micro end mill is recommended. Along with standard procedure for the evaluation of tool change intervals to avoid tool failure and consequential defects in parts produced. In addition to the findings in the literature on machine process planning and findings from the study of machining sequence on the thin wall structure and tool life investigation conducted, a new process planning methodology for micromilling has been proposed. The process planning methodology includes

four distinct modules *i.e.* feature recognition, tool selection, machining parameter selection and machining sequence planning. The feature recognition module proposes a new approach to identify key feature faces and their corresponding machining attributes required for tasks in process planning. In the tool selection module, a new methodology for the evaluation of the machinability index and the tool replacement strategy for micro endmills are proposed to guide the operator in the task of tool selection and estimating tool replacement intervals. The machining parameter module provides a systematic approach for the selection spindle speed, feedrate and depth of cut. The machine sequence planning module assists the operator in selecting a suitable tool path and tool layer strategy along with a compensate technique for tool path errors.

An artefact with thin wall features has been fabricated using the methodology proposed and the conventional process planning method. The results show the part processed using the proposed methodology achieved better geometrical tolerance, and improved repeatability. It also show a 17% improvement in mean surface roughness, which demonstrates the effectiveness of the proposed methodology.

Acknowledgement

First and foremost, I would like to acknowledge and extend my gratitude to my supervisors, Dr Dehong Huo and Dr David Swailes for continues support, patient and encouragement that have led me to get through the most difficult stages during the completion of my PhD studies.

Beside my advisory team, I would like to thank the member of my panel: Dr Oana Bretcanu, Dr Jinju Chen, Dr John Hedley, Dr Yaodong Wang and Prof Kenneth Dalgarno for providing me with feedback and guidance. As well as all member of staff especially technician team in school of mechanical engineering for their assistance with experimental work during this project.

My gratitude also goes to my employer DAIKIN APPLIED UK, especially to Bob Cowlard, Clive Parkman and Tracy Turnbull for supporting me with my personal career development goal.

Last, but by no means least, my heartfelt gratitude goes to my family Majid, Maryam, Golnaz and Andrea for their selflessness, unconditional, loving and tremendous moral support that has encouraged me to achieve better and live the life fully. I wouldn't be where I am today without them.

List of Publications

1. Dadgari, Amin, Dehong Huo, and David Swailes. "Investigation on tool wear and tool life prediction in micro-milling of Ti-6Al-4V." *Nanotechnology and Precision Engineering* 1.4 (2018): 218-225.
2. Dadgari, Amin, Dehong Huo, and David Swailes. "Investigation of Machining Tool Path on Surface Roughness and Dimensional Accuracy for High-Speed Micro Milling." *International Journal of Robotics and Mechatronics* (2017).
3. Dadgari, Amin, De Hong Huo, and David Swailes. "The Effect of Machining Toolpath on Surface Roughness and Dimensional Accuracy for High-Speed Micro Milling." *Solid State Phenomena*. Vol. 261. Trans Tech Publications, 2017.

Table of Content

Abstract.....	iii
Acknowledgement	v
List of Publications.....	vi
Table of Content.....	vii
List of Figures.....	x
List of Tables.....	xiii
List of Abbreviation.....	xiv
List of Nomenclature	xvi
Chapter 1. Introduction.....	1
1.1 Background and motivation.....	1
1.1.1 <i>Application of micromilling</i>	2
1.2 Aims and Objectives.....	5
1.3 Scope of this research.....	6
Chapter 2. Literature review	8
2.1 Introduction.....	8
2.2 Micro cutting mechanics	8
2.2.1 <i>Size effect and minimum chip thickness</i>	9
2.2.2 <i>Understanding the process of chip formation</i>	11
2.3 Evaluation of cutting conditions in process planning.....	13
2.3.1 <i>Machining parameters</i>	13
2.3.2 <i>Machining strategies</i>	14
2.3.3 <i>Tool wear</i>	17
2.4 Overview of process planning methodologies	28
2.5 Summary of gaps in knowledge.....	33
Chapter 3. Research approach and experimental procedure	35
3.1 Experimental setup	35
3.1.1 <i>Machining setup</i>	35
3.1.2 <i>FE model setup</i>	36
3.2 Experimental planning.....	39
3.2.1 <i>Tool life</i>	39
3.2.2 <i>Study of thin wall structure</i>	40
3.3 Methodology.....	42
3.3.1 <i>Tool wear</i>	42
3.3.2 <i>Geometrical accuracy and burr height</i>	43

3.3.3	<i>Surface roughness</i>	44
3.4	Equipment	45
3.4.1	<i>Hitachi scanning electron microscope (SEM)</i>	45
3.4.2	<i>Alicona InfiniteFocusSL</i>	46
3.4.3	<i>Kisler Dynamometer</i>	46
3.4.4	<i>High speed air spindle</i>	47
3.4.5	<i>Precision scale</i>	47
3.4.6	<i>Micro end mill</i>	48
Chapter 4.	Tool wear and tool life prediction in micromilling	49
4.1	Introduction	49
4.2	Experimental Results and Discussion	50
4.2.1	<i>Flank wear</i>	50
4.2.2	<i>Tool diameter reduction</i>	53
4.2.3	<i>Cutting edge radius</i>	57
4.2.4	<i>Surface roughness</i>	60
4.2.5	<i>Volumetric change</i>	62
4.2.6	<i>Discussion of tool wear</i>	68
4.3	Tool life prediction	71
4.4	Conclusion and remarks	72
Chapter 5.	Investigation of machining sequence for thin wall structures	74
5.1	Introduction	74
5.2	Simulation results and discussion	75
5.3	Experimental results and discussion	86
5.3.1	<i>Machining layers validation</i>	86
5.3.2	<i>Study of milling technology and radial depth</i>	91
5.3.3	<i>Study of machining tool path strategy</i>	95
5.3.4	<i>Summary</i>	98
5.4	Optimisation of machining sequence	98
5.5	Conclusion and remarks	101
Chapter 6.	Process planning methodology for micromilling	103
6.1	Introduction	103
6.2	Proposal of process planning for micromilling	104
6.2.1	<i>Proposed process planning methodology for micromilling</i>	105
6.2.2	<i>Feature recognition module</i>	106
6.2.3	<i>Tool selection module</i>	111
6.2.4	<i>Machining parameters selection module</i>	115
6.2.5	<i>Machining sequence module</i>	118

6.3 Experimental validation	122
6.3.1 Results and discussion	127
6.4 Conclusion and remarks	129
Chapter 7. Conclusions and future work	131
7.1 Conclusions	131
7.2 Contributions to knowledge	133
7.3 Future work	134
Appendix	143

List of Figures

Figure 1: Overview of existing technology courtesy of WETC [12].....	3
Figure 2: Common material used for micro components [6].....	4
Figure 3: (a) Comparison of a commercial tool with an object [14], (b) Carbide Ball Nose End Mill [Courtesy of Associated Production Tools], (c) CVD diamond tool [Courtesy of Contour Fine Tooling Ltd].	4
Figure 4: Example of micro features: (a) Micro grooves [16], (b) Thin wall [17], (c) Microneedle [18]5	
Figure 5: Schematic of research methodology.....	7
Figure 6: Schematic of the cutting zone (left) and cutting sweep path characteristic (right) [27].	9
Figure 7: Effect of tool edge radius on formed chip thickness [36].	10
Figure 8: Plot of measured cutting forces and its behaviour when size effect occurs in micromachining [39].....	11
Figure 9: Detailed comparison of cutting processes [41].	12
Figure 10: Different machining strategies [59].	15
Figure 11: Demonstration of the conventional (Left) improved tool path (Right) [61].	15
Figure 12: Set of vT resulting from the use of multiple criteria [80]	20
Figure 13: Effect of flank wear (a) 0 μ m, (b) 5 μ m, (c) 10 μ m, and (d) 20 μ m on the shear plane and contact surface area [91].	23
Figure 14: Link between process planning stages and the required inputs	29
Figure 15: Variant CAPP approach [116]	32
Figure 16: Hurco CNC-VM10 (left), Illustration of the experimental set-up (right)	35
Figure 17: Predefine boundary constrains on thin wall model	36
Figure 18: Schematic diagram of slot milling.....	39
Figure 19: Schematic of the machine layer strategy “Step”	40
Figure 20: Schematic diagram of strategies used in this experiment.....	41
Figure 21: Schematic diagram of the cutting edge radius (left), SEM image of tool edge (right).....	42
Figure 22: Schematic diagram of tool (left), SEM image of Tungsten carbide tool endmills from the top (right).....	42
Figure 23: Schematic diagram of typical flank wear modes [80]	43
Figure 24: Processed SEM image of tool wear land width	43
Figure 25: Example of an SEM image processed using Image J	44
Figure 26: Example of measurement of thin wall deflection and burr size.....	44
Figure 27: Map of evaluated finished surface area.....	45
Figure 28: Hitachi TM3030 SEM and Bruker Quantax 70 EDX.....	45
Figure 29: Alicona infinite focus SL optical 3D profilometer.....	46
Figure 30: Dynamometer experimental set-up.....	47
Figure 31: NE211 Series control unit (left), High-speed spindle NAKANISHI -HES810 (right).....	47
Figure 32: Sartorius Semi- Microbalance R 200 D.....	48
Figure 33: Schematic diagram of Tungsten carbide tool geometry.....	48
Figure 34: Average width of flank wear land (VB2) recorded for different cutting speeds. Error bars represent standard deviation.	50
Figure 35: Localized flank wear land (VB3) recorded for different cutting speeds. Error bars represent standard deviation.....	51
Figure 36: Average width of non-uniform flank wear (VB2) recorded for different feed rate. Error bars represent standard deviation.	52
Figure 37: Localized flank wear land (VB3) recorded for different feed rate. Error bars represent standard deviation.	53
Figure 38: Tool diameters reduction for different cutting speed. Error bars represent standard deviation.	54
Figure 39: Tool diameter reduction for different feed rates. Error bars represent standard deviation. .	55

Figure 40: Measured width of the channels machined using different cutting speed. Error bars represent standard deviation.	56
Figure 41: Measured width of channels machined using different feedrate. Error bars represent standard deviation.	57
Figure 42: Tool cutting edge radius using different cutting speed. Error bars represent standard deviation.	58
Figure 43: Tool cutting edge radius using the different feed rate. Error bars represent standard deviation.	59
Figure 44: Measured surface roughness for different cutting speeds. Error bars represent standard deviation.	61
Figure 45: Measured surface roughness for different feed rates. Error bars represent standard deviation.	62
Figure 46: Volumetric change of micro-tools at different cutting speeds. Error bars represent standard deviation.	63
Figure 47: SEM micrographs and EDX spectra of tools for different cutting speed	64
Figure 48: SEM micrographs and EDX spectra of tools for different cutting speed	65
Figure 49: Volumetric change of micro-tools at different feedrate. Error bars represent standard deviation.	66
Figure 50: SEM micrographs and EDX spectra of tools for different feedrate	67
Figure 51: Set of three vT graph, resulting from the use of attributes proposed as criteria for micromilling	71
Figure 52: Layer strategy one - front and side view (right and left image respectively) of thin wall and the sequence of material removal layer overlaid by deformation probe locations.	75
Figure 53: Maximum deflection recorded across of the thin wall structure using machining layer strategy “one”	76
Figure 54: Layer strategy two - front and side view (right and left image respectively) of thin wall and the sequence of material removal layer overlaid by deformation probe locations.	77
Figure 55: Maximum deflection recorded across of the thin wall structure using machining layer strategy “Two”	78
Figure 56: Layer strategy three - front and side view (right and left image respectively) of thin wall and the sequence of material removal layer overlaid by deformation probe locations.	79
Figure 57: Maximum deflection recorded across of the thin wall structure using machining layer strategy “Three”	80
Figure 58: Layer strategy four - front and side view (right and left image respectively) of thin wall and the sequence of material removal layer overlaid by deformation probe locations.	81
Figure 59: Maximum deflection recorded across of the thin wall structure using machining layer strategy “Four”	82
Figure 60: Layer strategy Five - front and side view (right and left image respectively) of thin wall and the sequence of material removal layer overlaid by deformation probe locations.	83
Figure 61: Maximum deflection recorded across of the thin wall structure using machining layer strategy “Five”	84
Figure 62: Layer strategy six - front and side view (right and left image respectively) of thin wall and the sequence of material removal layer overlaid by deformation probe locations.	85
Figure 63: SEM image of the front and top view of the machined thin wall (Image on the right and middle top) using the layer strategy one (Left and middle bottom image)	86
Figure 64: SEM image of the front and top view of the machined thin wall (Image on the right and middle top) using the layer strategy two (Left and middle bottom image)	86
Figure 65: SEM image of the front and top view of the machined thin wall (Image on the right and middle top) using the layer strategy three (Left and middle bottom image)	87
Figure 66: SEM image of the front and top view of the machined thin wall (Image on the right and middle top) using the layer strategy four (Left and middle bottom image)	87

Figure 67: SEM image of the front and top view of the machined thin wall (Image on the right and middle top) using the layer strategy five (Left and middle bottom image).....	88
Figure 68: SEM image of the front and top view of the machined thin wall (Image on the right and middle top) using the layer strategy six (Left and middle bottom image)	88
Figure 69: SEM image of the front and top view of the machined thin wall (Image on the right and middle top) using the layer strategy seven (Left and middle bottom image)	89
Figure 70: SEM image of the front and top view of the machined thin wall (Image on the right and middle top) using the layer strategy eight (Left and middle bottom image)	89
Figure 71: Top view of thin walls machined using up and down milling technology at the tool exit position.....	91
Figure 72: Top view of thin walls machined using up and down milling technology at the tool entry position.....	92
Figure 73: SEM images of side view for 40 μ m thin walls using up and down milling technology	92
Figure 74: Qualitative damage score evaluated in relation to wall edge visibility and smoothness	94
Figure 75: Simulated tool motion corresponding to tool path strategies tested.....	95
Figure 76: Preview of machined geometries using different tool path strategies	96
Figure 77: Surface roughness and machining time measured experimentally.....	97
Figure 78: Proposed process planning methodology for micromilling.....	105
Figure 79: Overview of feature recognition module for micromilling	107
Figure 80: Rectangular corner slots with rounded edge.....	108
Figure 81: Object Multi Attributed Adjacency Matrix (OMAAM) for rectangular corner slots with round edge.....	109
Figure 82: Feature Multi Attributed Adjacency Matrixes (FMAAM) for rectangular corner slots with round edge.....	109
Figure 83: Output-Manufacturing part feature list and corresponding manufacturing attributes	111
Figure 84: Overview of material module proposed for micromilling.....	112
Figure 85: Example of tool datasheet for individual tool within the tool store	114
Figure 86: The outline of the machining parameters selection process	116
Figure 87: Flow chart of machining toolpath and strategic sequence selection for micromilling	119
Figure 88: Artefact model - micro impeller.....	122
Figure 89: Process datasheet for the fabrication of micro impeller.....	123
Figure 90: Maximum deflection angle of micro blades	127
Figure 91: Web thickness of the micro blades.....	127
Figure 92: Mean surface roughness of micro blades side face	128
Figure 93: Comparison of tool diameter (SEM image-Left) with the resultant slot width measured using Alicona (Right).....	143
Figure 94: Alicona measurement interface.....	144
Figure 95: Cutting forces measured in full slot milling of Aluminum 6061-T6 using 1 mm uncoated tungsten carbide endmill	145
Figure 96: Average cutting forces measured for 1 mm uncoated tungsten carbide endmill	145

List of Tables

Table 1: Tool deterioration is defined by ISO-8688 for endmills [80].....	19
Table 2: Summary of significant findings in micromilling field	25
Table 3: Material properties of Aluminium 6061-T6.....	36
Table 4: Johnson-Cook material constants for Aluminium 6061-T6 [126].....	37
Table 5: Measured cutting forces in machining of Aluminium 6061-T6 using 1 mm Tungsten Carbide tool.....	39
Table 6: Cutting conditions	40
Table 7: Summary of cutting parameters.....	40
Table 8: Machining parameters used in the experimental comparison of machining tool paths	41
Table 9: Micro tool geometries used in this experiment.....	48
Table 10: Experimental data measured from SEM images of machined thin wall and corresponding layer strategy used.....	90
Table 11: Thin wall deflection measured through the processing of SEM images.....	93
Table 12: Burr size measured through the processing of SEM images	93
Table 13: Experimentally measured data for surface roughness, accuracy and machining time	96
Table 14: Corresponding weight factors to manufacturing aims.....	99
Table 15: Toolpath strategy scores for different weightings of each scenario	100
Table 16: Cutting layer strategy scores for different weightings of each scenario	100
Table 17: Schematics of the vector and corresponding attributes.....	108
Table 18: Feature properties for rectangular corner slots with round edge.....	110
Table 19: Material categories and colour codes define by ISO513.....	113
Table 20: The Step procedure in generating the NC code	124
Table 21: Machining parameters used in tool run out experiment.....	143

List of Abbreviation

AE	Acoustic emission
AFR	Automatic feature recognition
CAD	Computer-aided design
CAM	Computer-aided manufacturing
CAPP	Computer-aided process planning
CF	Catastrophic failure
CL	Cutter location
CNC	Computer numerical control
CSG	Constructive Solid Geometries
EDM	Electric discharge Machine
EDX	Energy Dispersive X-Ray
FEA	Finite Element Analysis
FL	Flaking
GA	General arrangement
GT	Group Technology
MEMS	Micro Electro Mechanical System
MMR	Material Removal Rate
MQL	Minimum quantity lubrication
NURBS	Non-uniform B spline
PMJIC	Pneumatic mist jet impinging cooling
RPM	Revolution Per Minute
RTS	Relative tool sharpness
SEM	Scanning electron microscope
SHPB	Split Hopkinson pressure bar

TFC Total flood cooling

VB Flank wear

List of Nomenclature

α, β, γ	Weight factors
γ	Rake angle
δ	Chord error
δ_0	Stagnation angle
ε	Interpolation error
ε^{pl}	Plastic strain
λ	Thermal conductivity
ρ	Density
σ^0	Strain rate
σ_p	Proportional stress limit
τ_s	Shear stress
φ	Shear plane angle
A	Constant- yield
a_p	Depth of cut
a_p	Depth of cut
B	Constant- strain hardening
C_p	Specific heat
$C_{p,u,p,d}$	Surface Heat capacity
E	Elastic modulus
F	Friction
f	Feed rate
F_c	Cutting force
F_s	Shear force
f_z	Feed rate

h_m	Minimum chip thickness
h_r	Elastic recovery height
$K_{rc}, K_{tc}, K_{rc}, K_{ac},$ K_{te}, K_{ae}	Cutting coefficients
n	Number of flute
$N, C, m, d_1, d_2, d_3, d_4, d_5$	Constant
P_c	Cutting power
\dot{q}	Heat input
r, r_e	Cutting edge Radius
R_a	Surface roughness
R_e	Radial depth of cut
S	Spindle speed
T	Tool life
t_0	Depth of cut
T_{room}	Room temperature
T_{melt}, θ_{melt}	Melting temperature
U_f	Friction energy
U_s	Shear energy
U_t	Specific cutting energy
V	Cutting velocity
v_c	Cutting speed
V_{fL}	Operation speed- lower bound
V_{fU}	Operation speed- Upper bound
V_s	Shear velocity
w	Width of cut

Chapter 1. Introduction

1.1 Background and motivation

In the past decade, the use of miniature components have increased in various industries, including biomedical, electronics and moldmaking, to reduce the cost and the energy used by the manufacturing sector [1]. The rapid development of technology-driven consumer demand for multipurpose parts and longer life cycle lead to a complex component design with high relative accuracy and selection of difficult-to-machine materials that challenged the advancement of manufacturing processes [2]. The strong desire to directly produce 3-dimensional geometries using a wide range of materials, including metallic components, cannot be performed by non-conventional manufacturing processes such as photolithography, chemical machining, and electrical-discharge machining (EDM) [3, 4]. Therefore, it is necessary to step up the application of conventional processes such as micromilling, microturning and microdrilling. Micromilling involves changing the shape of the workpiece using an implement made of a harder material which is known as a cutting tool, where the material is removed as a result of direct contact between the workpiece and the cutting tool. Hence, a preparatory step, known as process planning, is required to translate the design specifications to transform the block of raw material into the desired part. Therefore, process planning can be described as the act of preparing detailed work operations to produce the part

from initial form (block of raw material) and transforming it into the required shape (finished part), as pre-determined by part design given by model or drawings. In conventional milling, protocols are described which define the machining parameters and steps employed for particular features [5]. Since micromilling is kinematically similar to the conventional scale, it involves many characteristics of conventional milling, including the principle of process planning which remains the same [6].

However, as a result of downscaling, the mechanism of surface generation and the behaviour of the material microstructure dramatically change [7]. The ratio of the cutting edge radius to chip thickness is much lower and any run out of the tooltip will have a significant effect on the geometrical accuracy of the finished part. Chip formation in micromilling is affected by the phenomenon of size effect which can result in an interruption of chip formation as opposed to conventional milling where the chip is formed as the tool and the workpiece are engaged. Also, the insignificant impact of deformation of the cutting tool and workpiece during conventional milling have a major effect on part accuracy and surface generation in micromilling.

Besides differences in cutting mechanics, there are other fundamental dissimilarities between the two methods such as fixture type, process monitoring procedure and machining stability. In micromilling, dynamic forces that are transferred to the workpiece results in a reduction in stiffness of the clamp that can lead to higher vibrations, directly affecting the accuracy of the parts [8]. Furthermore, the formation of burrs and the difficulty of burr removal from the micro features can lead to the rejection of manufactured parts [9]. At conventional milling, the machine operator can assess the health of the cutter to estimate tool change intervals by visual inspection and monitoring the noise produced during the material removal process. However in micromilling, monitoring the process at the microscale is difficult without the use of special equipment, as well as the need to monitor other factors such as the influence of machine dynamics on micro features, to ensure a high quality finish part is produced [10].

Hence, the direct use of process planning protocols of conventional milling is not applicable. Therefore, it is necessary to modify the protocols adopted from conventional milling to include discarded flaw factors due to process downscaling and effect of miniaturisation. The process parameters should also be optimised to stabilise the material removal process before it can be used in the task of process planning for micromilling [11].

1.1.1 Application of micromilling

The scope of micromilling has gradually expanded over the past 25 years. The demand for micro components by various industries, with different functions, geometries and made of

different materials, led to the development of new categories known as micro/mesoscale manufacturing. This is fundamentally different from MEMS micro manufacturing shown in Figure 1.

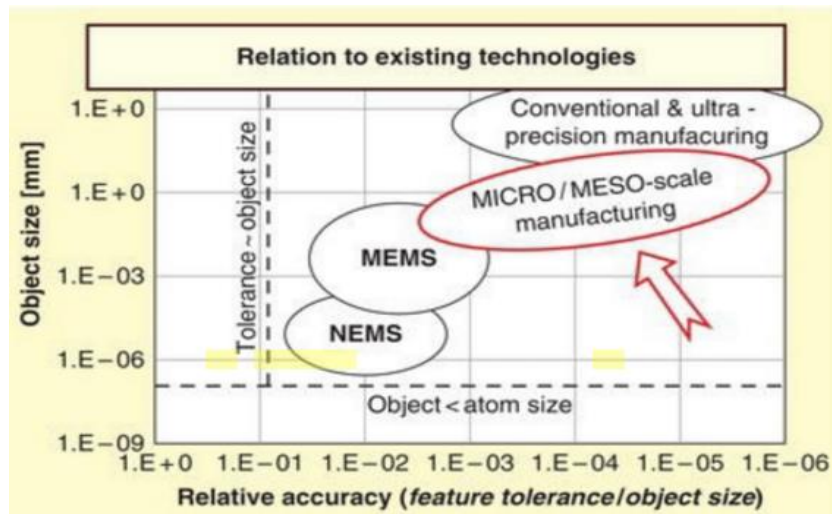


Figure 1: Overview of existing technology courtesy of WETC [12].

Huge numbers of micro products from key application areas (e.g. in biomedical engineering, MEMS, sensors, optical and microfluidic), such as biosensors, micro-actuators and implants, are being widely spread using materials with superior properties. The development of machinery and an increase in demand for more complex parts resulted in the development of innovative, more versatile and rapid methods of machining. Therefore machinists and engineers have been striving for higher accuracy and faster production [11]. Non-lithography based micro manufacturing has been described by the world technology evaluation centre (WETC) panel, as the creation of a 3-dimensional high precision product for various materials with a size range changing from tens of micron up to a few millimetres. Other lithography based or non-lithography based manufacturing technologies have rapidly developed over the years, including micro EDM, laser cutting, micro-extrusion, micro-embossing, microstamping and microinjection molding [11]. The ability to manufacture 3-dimensional geometries, from a broad range of materials with low manufacturing costs and high finished accuracy, benefits the micromechanical material removal over other processes. Overview of the common materials used in micro-component is shown in Figure 2.

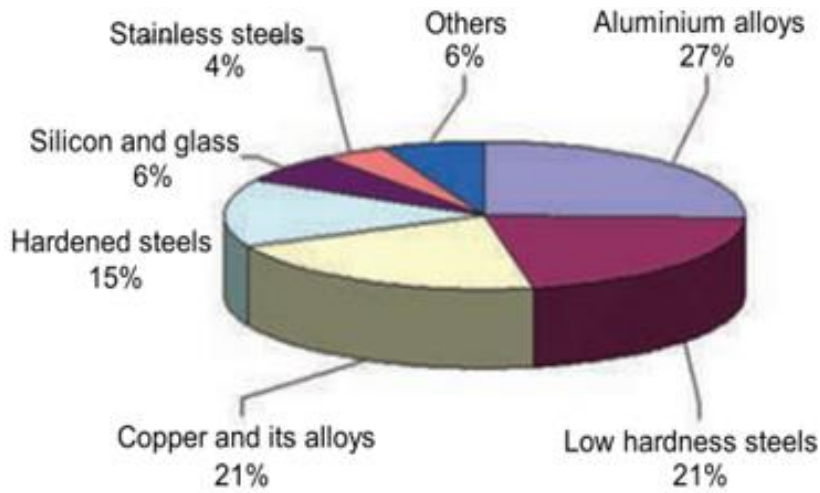


Figure 2: Common material used for micro components [6].

Currently, tools with diameters of 1mm or less have been considered as micro tools, and those with diameters of 0.05 mm or less have been introduced commercially are shown in Figure 3 [13].

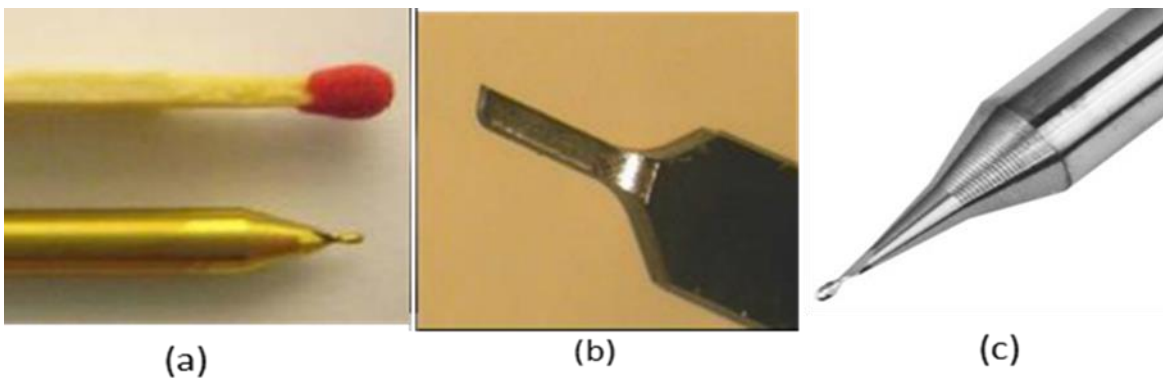


Figure 3: (a) Comparison of a commercial tool with an object [14], (b) Carbide Ball Nose End Mill [Courtesy of Associated Production Tools], (c) CVD diamond tool [Courtesy of Contour Fine Tooling Ltd].

Among the primary principle of manufacturing processes, micromilling has played a key role in the fabrication of components with dimensions that range between 10 μm -10 mm [13]. The tendency towards miniaturisation in the manufacturing industry has dramatically increased in many applications. Especially in electronics, the use of semiconductor devices in electrical boards has increased the need of micro parts to match the compactness of packages and micro switches. Similarly, in the medical field, demand for painless surgery brings the necessity of miniaturising medical equipment. Accuracy and surface finish achieved using micromilling was identified as a key element and is linked to the fundamental aspects of product performance, with features including high aspect ratio. Machining materials with low rigidity and high aspect

ratio feature are widely researched, and aerospace and power sectors are major investors of these advancements [15]. Examples of micro features and high aspect ratios are shown in Figure 4.

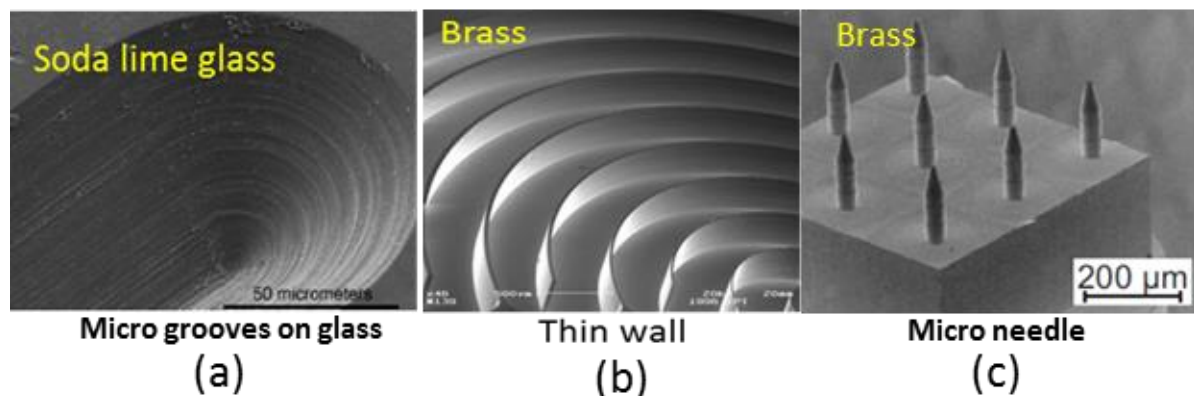


Figure 4: Example of micro features: (a) Micro grooves [16], (b) Thin wall [17], (c) Microneedle [18]

1.2 Aims and Objectives

This project aims to improve finished part quality and process efficiency in micromilling by addressing the scale difference between conventional milling and micromilling, and by standardising the procedure concerning protocols used in process planning for micromilling. Therefore following objectives are established for this project:

- Review the literature in order to compare the processes used in micromilling with the ones used in conventional milling to construct a better understanding of scale differences concerning process planning. Also, collect and combine the body of knowledge on the impact of miniaturisation in relation to tool and material used in micromilling.
- Critically review the approach and methodologies used in the evaluation of cutting conditions specified at the process planning stage for micromilling as well as establishing a standard procedure for operators to use in the evaluation of cutting conditions.
- Review the ISO standard procedure used in the life evaluation of micro tools and estimation tool change interval as well as establishing a machinability index associated with tool and material properties to assist the operator in the task of tool selection.
- Construct a methodological approach for the operator to use in process planning for micromilling of components including applications with high aspect ratio geometries.

1.3 Scope of this research

This section outlines the structure of this thesis while summarising the content and contribution to knowledge for each chapter. To demonstrate the linkage between the chapters, a flow chart is produced shown in Figure 5.

Chapter 1 gives an insight into the motivation for miniaturisation of components and the application of micromilling. It also outlines the dissimilarity between conventional milling and micromilling based on the task of process planning. The aim and objectives of this project are stated and the scope of this research is summarised. The link between other chapters to chapter 6 (Proposed Process Planning and Methodology) is demonstrated using a flow chart.

Chapter 2 initially reviews the dissimilarity between the different processes and discusses the effect of minimum chip thickness and size effect in micromilling. Subsequently, it reviews state-of-the-art research and engineering practices used to underly the theory in the areas where micromilling differs from conventional scale milling, as outlined by the aim and objectives of this project. Gaps identified in the literature are summarised at the end of this chapter.

Chapter 3 provides details of the experimental setup, experimental planning and methodology used in the evaluation of samples. Also, the specification for pieces of equipment and software used in this project are provided in this chapter.

Chapter 4 studies the wear of uncoated tungsten carbide endmills while evaluating the life of micro endmills following ISO procedure (ISO 8688-2 for evaluation of the life of endmills). Tool rejection criteria for the micromilling of hard-to-cut materials (Titanium alloy Ti-6Al-4V) and a methodology for evaluating the machinability index associated with tool and material properties are recommended.

Chapter 5 studies the effect of machining layer strategy using numerical simulation on the accuracy of the thin wall structure. It also investigates the effect of tool path strategy on the performance of micro endmills and geometry type. Strategies for machining thin wall structures and toolpath selection is proposed.

Chapter 6 outlines the proposed process planning methodology for micromilling that is made of four modules. The function of the individual modules and their internal processes are discussed and the input and output of each module are stated. The proposed process planning methodology is compared to conventional process planning methodology, through the fabrication of an artefact, to demonstrate the effectiveness of the proposed methodology.

Chapter 7 summarises the main findings of this research, states the main contributions to knowledge and recommends future directions in this field.

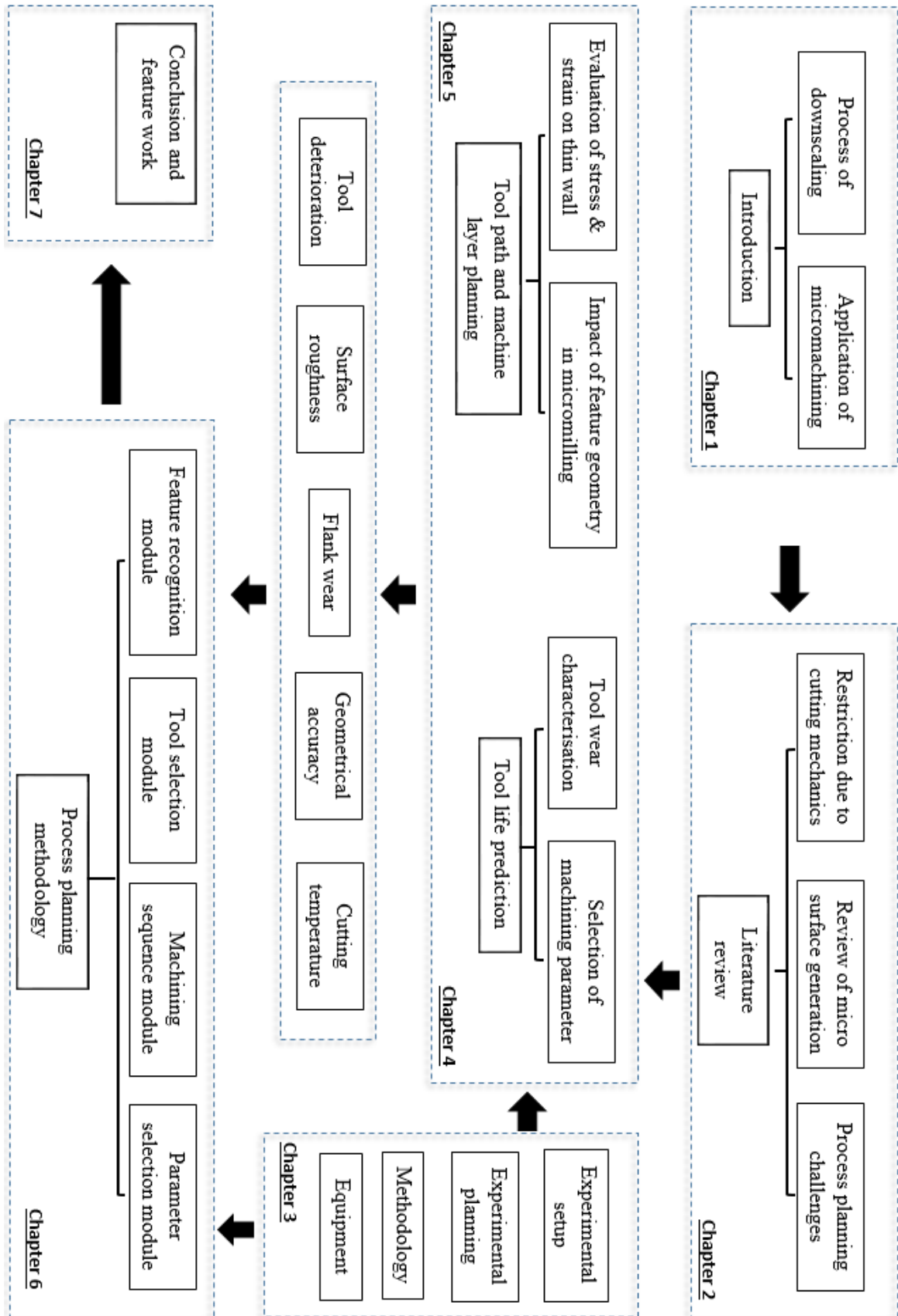


Figure 5: Schematic of research methodology

Chapter 2. Literature review

2.1 Introduction

This chapter initially reviews the dissimilarity of processes and chip formation in micromilling. Subsequently discusses state-of-the-art research and engineering practices used to underly the theory in the areas where micromilling differs from conventional milling. Also, review the relevant research methodologies and latest development of machining knowledge concerning process planning for micromilling. Which are outlined by aim and objectives of this project. In addition, a framework of process planning system is discussed and the gaps in knowledge related to the subjects concerning process planning are identified.

2.2 Micro cutting mechanics

The aim of this section is to review the differences between conventional milling and micromilling. Since machine kinematics are similar for both machining scales, process planning protocols used in processing of micro parts are the same [19]. However, miniaturisation of tool and component geometries lead to change in material removal characteristics and influence the system dynamic performance, that leads to feature excitation (also known as chatter) and deformation of tool and part geometries [20]. Other differences in micromilling, such as the change in material removal process that is characterised by the transition between chip formations to ploughing, and the chip flow direction and high friction between chip and tool, influence the chip removal from the cutting zone [21, 22]. The machine dynamic differences

arise from the limitations of equipment precision and capability to satisfy the cutting parameters required by micro tools [22]. Also invalid assumptions are made such as when tool penetration and the impact of vibration are not considered [23]. The miniaturisation of geometries results in low stiffness and high aspect ratio geometries that are affected by cutting forces and machining vibration. These are neglected and not compensated for by conventional processes used in process planning. Also, commonly used secondary finishing processes (e.g. polishing and deburring) are difficult to achieve on low stiffness geometries, which degrades the quality of the finished part [24]. Therefore, in process planning, applying conventional processes directly to micromilling is inappropriate due to different process responses and invalid assumptions made.

2.2.1 Size effect and minimum chip thickness

In conventional milling, the material is assumed to be homogenous due to the high ratio of uncut chip thickness to grain size, with chip formation expected at every sweep of the tool [19]. However, when the chip is formed from a countable material grain with an uncut chip thickness comparable to grain size, this has a non-homogeneous effect and results in interruption in chip formation [25]. Large ratio of chip thickness to tool edge radius in conventional milling always results in positive rake angle; nevertheless, in micromilling comparable chip thickness with tool edge radius and excessive edge wear results in negative rake angle as shown in Figure 6 [26].

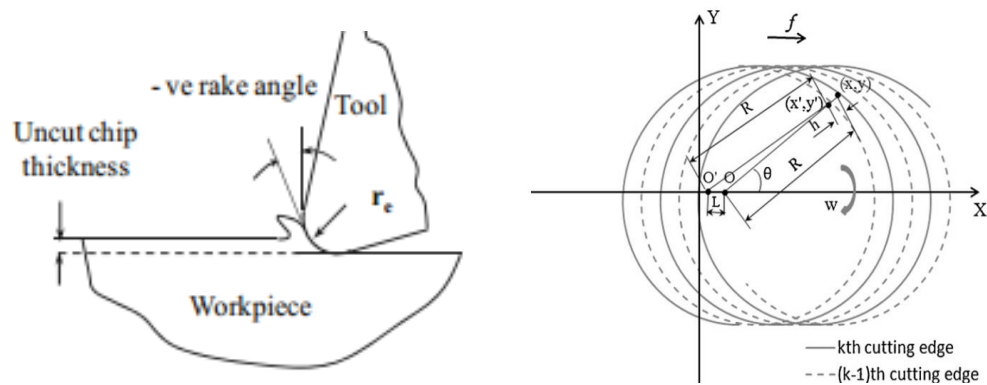


Figure 6: Schematic of the cutting zone (left) and cutting sweep path characteristic (right) [27].

Size effect is described by violating the minimum uncut chip thickness value that is associated with the characteristics of the workpiece material and process conditions, making its evaluation complicated [28]. This phenomenon is a result of reducing uncut chip thickness below a critical value where material removal process is transformed from shear to a slipping process. The contact surface area between tool and workpiece undergoes elastic-plastic deformation is shown

in Figure 7. Due to the complexity in the measurement of minimum chip thickness directly, many researchers have attempted to estimate this value numerically [29]. One of the earliest model established and used as a foundation to further development of this method, estimated the neutral angle corresponding to the critical depth of cut assuming isotropic material with non-strain hardening and constant chip flow rate [30]. Further development of numerical method using molecular dynamics, included the effect of grain size and grain boundary effect to consider strain hardening of the material [31]. The molecular dynamic model is used in estimating the minimum chip thickness value to be between 1/20 to 1/10 of tool edge radius, assuming perfect tool motion during material removal process. Due to altering cutting parameters and a change in rake angle, a numerical model is developed to correlate the rake angle to the natural angle [32]. The model is used to evaluate the minimum chip thickness for AISI 4340 to be approximately 2 μm but excluding the effect of chip separation criteria. To consider the effect of material properties and cutting parameters, surface roughness model is built and used to estimate minimum chip thickness ratio as 0.14-0.25 but this model is limited for the use of single-phase materials [33]. Similarly, a theoretical model is designed which includes the effect of cutting temperature, material strain and strain rate; using an iterative method to compute the minimum chip thickness ratio in relation to cutting speeds and tool edge radius [34]. The model accounting for the thermal softening and strain hardening estimated the ranges minimum chip thickness from 0.2-0.4 for of AL6082-T6. When the effect of cutting forces and material hardening are considered, an analytical force model is developed based on FE simulation, analysing stress flow in the material to estimate the minimum chip thickness ratio which is 0.25 times the cutter edge radius for OFHC copper [35].

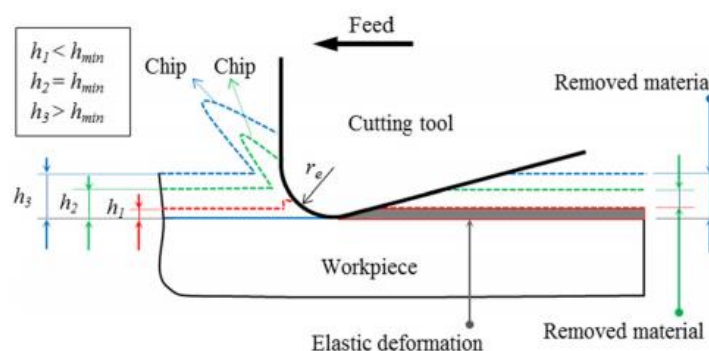


Figure 7: Effect of tool edge radius on formed chip thickness [36].

Many researchers also attempt to measure the minimum chip thickness experimentally [37-40]. The analysis of variance (ANOVA) on specific cutting forces in machining AISI 1045 steel in relation to tool edge radius, workpiece roughness, cutting force and chip formation shows a range of minimum chip thickness ratio from 0.22 to 0.33 [37]. When the material friction

coefficients in micromilling of copper, brass and aluminium in relation to burnishing are compared, the minimum uncut chip thicknesses are estimated to range from 0.09 μm to 0.12 μm [38]. Similarly minimum chip thickness value is measured in relation to the transition in plot of cutting forces as indicated by the drop shown in Figure 8. The experimental values shows the range of minimum chip thickness ratio to be between 0.14 to 0.35 of the cutting edge radius interrelated with material properties and cutting conditions [39]. Furthermore, the non-linear positive trend suggests that this behaviour is influenced by feed rate (f_z), depth of cut (a_p), cutting speed (v_c) and lubrication [39]. Similarly using acoustic emissions signalling method during machining of Inconel 718 estimated the minimum chip thickness to be 1.41 μm for tools with an edge radius of 6 μm [40].

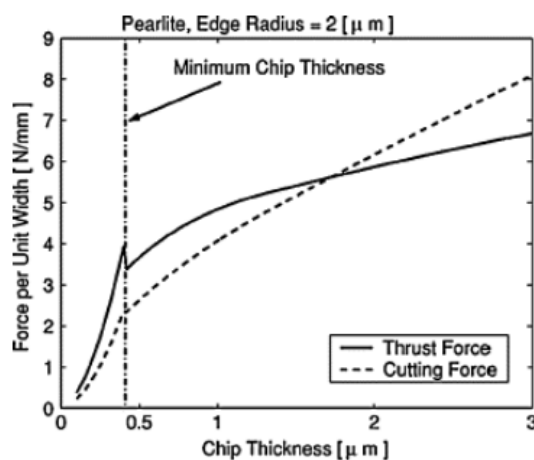


Figure 8: Plot of measured cutting forces and its behaviour when size effect occurs in micromachining [39].

The knowledge gained from the previous work shows the different approach and methodology used by most researchers in estimating the minimum chip thickness. The variation in the ratio of minimum chip thickness to tool edge radius ranges from 0.1 to 0.35 predominantly driven by material properties and cutting conditions used. The sharpness of the tool edge radius shows to drive the lower limit of machining parameters that can be used. Therefore advancement in tool manufacturing that leads to sharper tools can improve the restrictions on machining parameters used in micromilling.

2.2.2 Understanding the process of chip formation

In macro-scale machining, the uncut chip is made from hundreds of material grains with varieties of shapes and sizes that have a negligible effect on the material removal process. However, in micromilling the uncut chip is made of far fewer material grains where the tool's cutting edge passes through individual grain boundaries. Therefore differences in the physical

characteristics of the material grains can affect the aspect ratio of the material removal process and chip formation. Due to the variations in the elastic recovery of each grain, the properties of the workpiece material cannot be considered as homogenous, as the average value of microstructure suggests. The chip formation differs for single and multi-phase material, since in single-phase material the cutting edge radius of the tool goes through a single grain of the material. While, in multi-phase material the cutting edge goes through grain boundaries, as shown in Figure 9, with a higher resistance compared to regular grains and resulting in break-in continuity of chip formation [41].

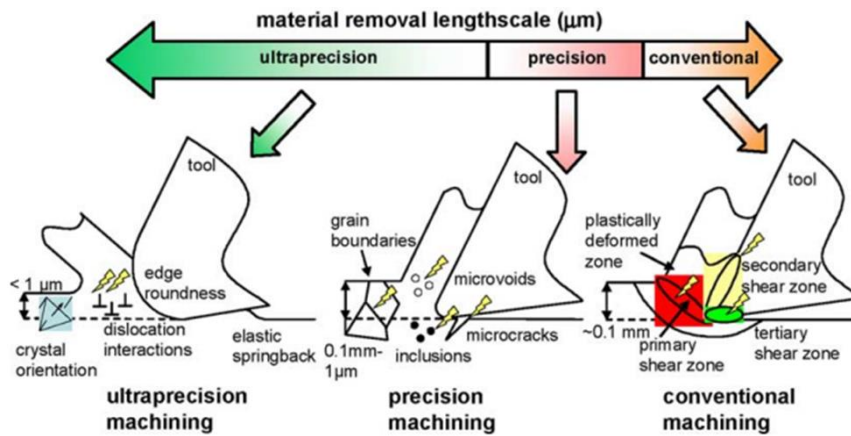


Figure 9: Detailed comparison of cutting processes [41].

The resulting chip variation across the swept arc of the cutter is shown to be a consequence of the different levels of elastic recovery of each material grain. This has been hypothesised that burrs are formed at the grain boundaries of different grain sizes, resulting in fluctuations in surface roughness and encouraging vibration [42, 43]. Therefore in process planning of micro products attention is given to the structure of the micro material, which cannot be achieved by merely downscaling the conventional machining processes, in order to meet the accuracy requirements and minimising burr size [44]. Material properties that reflect on micromachining characteristics are summarised as follows [45]:

- Impact of material mechanical properties on size in comparison to macro scale.
- Interaction between the material and cutting tool in the cutting zone and the separation, deformation, physical and chemical decomposition.
- Grain size and the influence of interfacial friction that results in dislocation of grains, particularly in mechanical material conversion.

The chip formation in microscale machining starts at zero thickness, where the ploughing effect between the tool rake face and the material surface is dominant, until the sweep angle of the cut is equal or greater than the minimum chip thickness value. This is when the material removal

process takes place in the form of chip formation. Elastic recovery at the tool-workpiece interface and the nonhomogeneity of the process due to the microstructure of the material is one of the influential factors in single-phase materials to achieve continuous chip formation during the surface generation [46]. In micromachining, elastic recovery directly affects the minimum chip thickness, and material with a higher rate of elastic recovery demand for larger sweep angle to provide the minimum chip thickness. Therefore, the ratio of tool edge radius to undeformed chip thickness becomes critical [47].

2.3 Evaluation of cutting conditions in process planning

As outlined in the introduction, the aim of this section is to review the methodology used in the evaluation and optimisation of cutting conditions during process planning.

2.3.1 Machining parameters

Manufacturing restrictions in tool fabrication results in a short tool life and cutting edge radius that is comparable to the feature geometries. This in combination with the size effect and burr formation in micromilling demands for a conservative selection of machining parameters. Maintaining an appropriate ratio of uncut chip thickness to cutting edge radius is critical in achieving the required machining stability and for limiting burr formation [48]. To compensate for low rigidity of the tool, high spindle speed is commonly used in micromilling with an opposing effect on tool run out and finished part accuracy [49]. To satisfy both tolerances and fabrication cost, many researchers have attempted to optimise the machining parameters (spindle speed, feedrate and depth of cut) using different optimisation methodologies; also by studying the impact of individual parameters in relation to finished part accuracy and tool life. To optimise parameters for maximising the material rate of removal (MRR) within constrains of surface roughness and tool breakage, generic algorithm (GA) is used [50]. The findings have been collected under the optimal spindle speed of 60K RPM, feed per tooth of 1.6 μm and depth of cut of 144.23 μm to be used in machining of Inconel 718. To maximise MRR at a cost of surface roughness, tool breakage is the limiting constrain in micromilling.

Similarly, GA is also used in the development of optimisation algorithm for selection of optimal parameters in machining of hardened Steel in relation to total part cost [51]. The cost is benched marked against the part fabricated using a parameter recommended by the tool manufacturer catalogue, which shows up to 59% savings was achieved. To evaluate the machining data gathered for micromilling of Titanium under different spindle speeds, feedrates and depths of cut, Taguchi based grey relational analysis is utilised. The machine performance in relation to surface roughness and burr formation indicates a lower feed per tooth which increases the burr width, while recommending feed per tooth and depth of cut of 0.25 μm and 100 μm

respectively, to be used in achieving the optimum surface quality of Titanium [52]. A similar trend of feed per tooth in relation to burr size in machining of AL2124 is reported that is different to machining of SS304 [53]. A limited use of radial depth of cut above 60% of diameter has also been reported for machining of stainless steel suggesting that the violation of the limit majorly impacts tool stability and surface performance [54]. Machining of ceramics, an increase in feed rate and depth of cut has been reported to degrade the surface roughness, while the optimum spindle speed of 22K RPM, axial depth of cut of 0.02 mm and feedrate of 4.56 mm/min have been recommended [55]. Factor analysis is used to study the machining of PMMA substrates in relation to surface roughness, and the results indicate that the most and least influential parameters are depth of cut and spindle speed respectively [56]. Also, spindle speed of 20K RPM, feedrate of 300 mm/min and depth of cut of 10 μm was recommended. The ANOVA results on the effect of depth of cut, feed rate and spindle speed in relation to appearance and size of exit and top burrs suggested that the depth of cut is the most influential parameter (percentages are 37.92%, 15.72% and 11% respectively) [52].

Even though machining parameters are optimised for a range of reviewed materials that are proved to be accurate statistically, the machining data used in optimisation have been obtained under laboratory conditions that do not mimic the true industrial environment. Also, unless the same machining parameters used in optimisation are used and similar procedure is repeated, the outcome of machining may not be as expected. Therefore, under the influence of real industrial environment is affected by noise and vibration and the machining parameters identified as optimal in literature may not be adequate.

2.3.2 Machining strategies

This section studies the approach and methodology used in the evaluation of machine tool path and layer strategy used in micromilling.

2.3.2.1 Machine layer

High aspect ratio features are one of the commonly encountered geometries found in micro products, known for their relatively low stiffness values and therefore often used as subjects in evaluation of the machining performance in micromilling [57]. Similarly thin wall structures have been used in experimental and numerical studies of machining layers in relation to cutting forces and finished part geometries. The impact of machining layers on thin walls has been experimentally observed by monitoring cutting forces during machining, following a z step layer strategy, which indicated the need for additional structural support by using a special fixture or unmachined area of the workpiece [58]. In the study of three different machining layers evaluated quantitatively in relation to geometrical accuracy (burr presence and thickness

error) for two workpiece materials, subjective choice of layer strategy to workpiece material suggested the z step and ramp strategy (shown in Figure 10) to be the optimum layer strategy for machining of aluminium and brass respectively [59]. The impact of milling technologies have been compared in relation to cutting forces and surface roughness which indicates that down-milling results in lower cutting forces and lower surface roughness, consequently improving machining stability [60, 61]. In a numerical study of a cylinder-shaped thin wall, a continuous change in feature rigidity resulted in a different degree of deformation along the feature structure that suggested the changeable impact of tool layer strategies. The starting position of the tool in respect to rigidity of geometry (start at high and end at low rigid area) has been suggested to reduce the resultant wall deformation [62]. Further advancement through compensation methodology using finite element model (FEM) of thin walls is achieved by accounting for tool and part deflection. The effect of workpiece material rigidity and tool deflection (excluding the coupling error) is compensated through the development of a dynamic model for adjustable radial depth of cut along each layer. The radial depth of cut value is updated for each layer in relation to the deformation predicted from previous layer which shows up to 86% improvement in the geometrical accuracy of a finished thin wall [63].

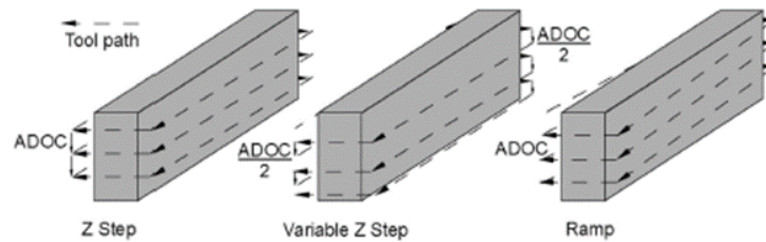


Figure 10: Different machining strategies [59]

Similarly, to compensate the error in the machining of high aspect ratio features (e.g. ribs and thin wall), an adaptive tool layer strategy unique to the stiffness of the feature structure is suggested to provide optimal structural support throughout machining [64]. Therefore FEM study of the layer strategy is further improved the layer strategy explicit to thin wall structure by studying the sequence and the depth of cut, as shown in Figure 11, to maximise support along each layer to improve geometrical accuracy [61].

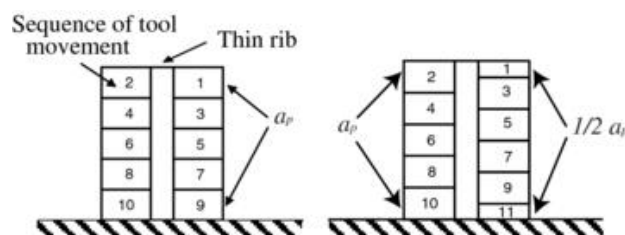


Figure 11: Demonstration of the conventional (Left) improved tool path (Right) [61].

Following the review of work in this section, an emphasis on characterising the layer strategy in relation to the rigidity of workpiece and geometry type can be observed. In addition, adequate methodologies to compensate machining error and supporting strategies are found. However, the focus of the studies found in this research were limited to improving the geometrical accuracy of the feature and no attention has been given to machining efficiency that is key to process planning. Also the main aim of tool path planning from the aspect of manufacturing. The importance of tool position in relation to high aspect ratio feature geometry was highlighted by the recommended start and end position of tool path from the highest to the lowest rigidity respectively. However, this was specifically suggested for one geometry type (cylindrical shape thin wall) that should be further investigated for other types of geometries.

2.3.2.2 Toolpath strategy

Tool path planning consists of setting position vectors as cutter location (CL) to produce a geometry. This is followed by remove/modify CL's in relation to limits of geometry; while, interpolating the desired tool path between the discrete cutter locations adopted from conventional milling. Linear and circular interpolation have been commonly used to define the intersections with a smooth line. However, the limitations with different types of interpolation methods such as large file sizes for part program data [65]; fluctuations in feed rate between segments [66]; slow processing due to large numbers of segments [67]; discontinuity and jumps between segments degrade part surface smoothness and tool acceleration and deceleration errors along the path [68] are known to vary for different geometry type which are carried over and still apply in micromilling. Similar to conventional milling toolpaths, micromilling tool paths are characterised by the type of motion, orientation, and entry and exit motion in relation to their influence on machine stability, cutting forces and the cycle time [69, 70].

In addition to the issues that are carried over from conventional tool paths used in micromilling, the difference between the machine scales is affected by the inconsistency of feed rate along tool path during stoppage and sudden changes in tool direction which leads to immature tool failure. Therefore, many researchers study the process of tool path generation to improve the accuracy of micromilling process and to better understand their influence on geometries. To restrict maximum feedrate, intelligent interpolation techniques can be applied to the curvature base tool path generation to increase the sampling rate and improve efficiency [71]. There are also other models that focus on the generation of desired tool paths in relation to particular surface finish requirements [72]. The feed direction in relation to cutting forces and surface finish in slot and side milling shows, lower cutting forces are achieved by using side milling that is favourable for machining of low rigid features. However better surface roughness using

slot milling indicates to improved machining stability that is key to reduce burr formation and avoid tool failure [73]. An intelligent segmentation method has been developed for sequencing CL along each layer using B-Spline interpolation method to compensate the feedrate limitation which reduces the overall process error [74]. To avoid the variation in feed rate and tool stoppage for smoother overall machining, circular tool paths are favoured over linear tool paths [75]. The key parameter for tool trajectory selection in a circular tool path is also identified as the tool path radius and rotation angle that influences the chip formation along the tool path. Conventional development of tool path selection by investigating the discontinuity of chip formation for circular tool paths indicates a direct relationship with tool path radius with continued chip formation at a conventional scale [76]. Similarly the impact of tool path radius for circular tool paths in relation to cutting forces and surface roughness indicates that the path radius is inversely proportional to cutting forces [77]. Furthermore in the application of dies and moulds, the machining knowledge is based on the observations made during prototyping of common features such as channels (round and square), levels and slopes; that lead to the development of a simple guide for the operator to identify and select suitable tool path [78, 79].

By utilising the existing tool path strategies and tool path planning process from conventional scale machining, experience and the methodologies developed over the years benefits the selection of tool paths strategies in micromilling. However, the issues arise from process differences in micromilling and the limited knowledge of micro tool performance while using conventional tool path strategies and therefore the response of the geometries to the machining process for stability and accuracy of needs to be further examined.

2.3.3 Tool wear

One of the key elements in mechanical material removal processes is the cutting tool that has to withstand high pressure, oscillation in machining temperatures and vibration during chip formation without any degradation or change in geometrical shape. Therefore, this section reviews the machining knowledge on micro tools in relation to wear and life as outlined by the aim of this study.

2.3.3.1 General description of wear for end mill

The mechanical material removal process is a result of a rubbing effect between a harder material, *i.e.* the cutting tool, and a softer material, *i.e.* the workpiece. Tool deterioration, which is known as wear, occurs due to volumetric loss or the geometrical properties of the cutting tool change. Different mechanisms of tool wear may arise, due to simple wear and fracture. The causes of simple wear are mainly characterised as:

1. Abrasive wear

Abrasive wear is the most common type of wear around the active edge of the tool. It can result in increased tool cutting edge radius and violation of the minimum chip thickness that transitions the material removal process to a ploughing effect when the material is shifted outside the wear grooves but is not removed. Alternatively, in cutting, the material with lower hardness is removed in the form of chips where the material removed from the surface has the same volume as that of the wear groove along active tool edge. However, the result of material cracking on the subsurface cracks affects the volume of material being removed than that of the wear groove.

2. Adhesive wear

Adhesive wear is described as the effect of the softer material being removed from the cutting surface, where due to high pressure and temperature, some of the material removed becomes welded to the surfaces of the cutting tool. Micro-joints then form that rupture as machining continues.

3. Diffusion wear

Diffusion wear occurs due to machining temperature and is caused by the adhesion of material during the cutting process. The increased temperature enables the fusion of atoms belonging to the cutting tool material to the workpiece's metal surface, which strengthens the workpiece material and degrades the cutting tool and therefore enhances wear.

4. Chemical wear

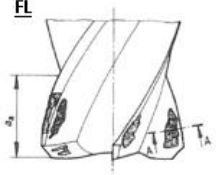
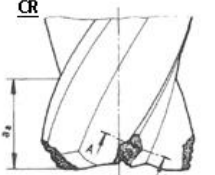
Chemical wear is a combination of corrosive and erosive wear as the rubbing of two surfaces results in the removal of oxide films from the surface of each material, thus promoting the process of oxidation. Machining results in the continuous removal and formation of the new oxide film and; in the case of the formation of hard oxide particles, the removed particles become trapped between the surfaces that enhance abrasive wear.

The effect of the above factors were described as a function of cutting temperature and machining velocity. Cutting temperature is the most influential factor since the strength of the tool material degrades as cutting temperature increases, enhancing the wear coefficient. Plastic deformation of the tool caused by tool material softening under high cutting temperature and cutting forces exceeding the hardness grade of tool material results in distortion of tool geometry. Tool fracture is usually caused by overloading the tool due to high cutting forces

which exceed the maximum strength of the material, leading to crack propagation on the surfaces and subsurfaces of the tool. Depending on the dominant wear mechanism, there are different kinds of tool deterioration defined by ISO-8688 for endmills, which are summarized in Table 1:

Table 1: Tool deterioration is defined by ISO-8688 for endmills [80]

Tool deterioration / Schematics		
1) Flank wear (VB)		
Uniform flank wear (VB1)	Non-uniform flank wear (VB2)	Localised flank wear (VB3)
VB1	VB2	VB3
2) Face wear (KT)		
Crater wear (KT1)	Stair-formed face wear (KT2)	
KT1	KT2	
3) Chipping (CH)		
Uniform chipping (CH1)	Non-uniform chipping (CH2)	Localised chipping (CH3)
CH1	CH2	CH3
4) Cracks (CR)		
Comb cracks (CR1)	Parallel crack (CR2)	Irregular cracks (CR3)
CR1	CR2	CR3

5) Flaking (FL)	6) Catastrophic failure (CR)
	

Tool life is described as the duration of machining time until the process has to stop due to the poor performance of the tool. Depending on the wear mechanism involved, the tool wear characteristics defined earlier are used as criteria to judge the moment when the tool needs to be changed. However, due to tool wear, which is a function of machining parameters, the plot of tool life as a function of machining parameters is used in the determination of useful tool life. The criteria used for the rejection of a tool in tool life testing are set out in ISO 8688-2 standard [80] for conventional milling. While the standard procedure is used in the assessment of machining variables to determine the tool life, it is experimentally derived and presented graphically using the methodology proposed by Frederick W. Taylor which is known as Taylor theory [81]. Tool life is plotted against the machining parameters, namely cutting velocity (V_c), feed rate (f) and depth of cut (a_p), where a vT curve is described as exponential. Therefore, to obtain a strain line, a logarithmic scale is used to present it in the form shown in Figure 12.

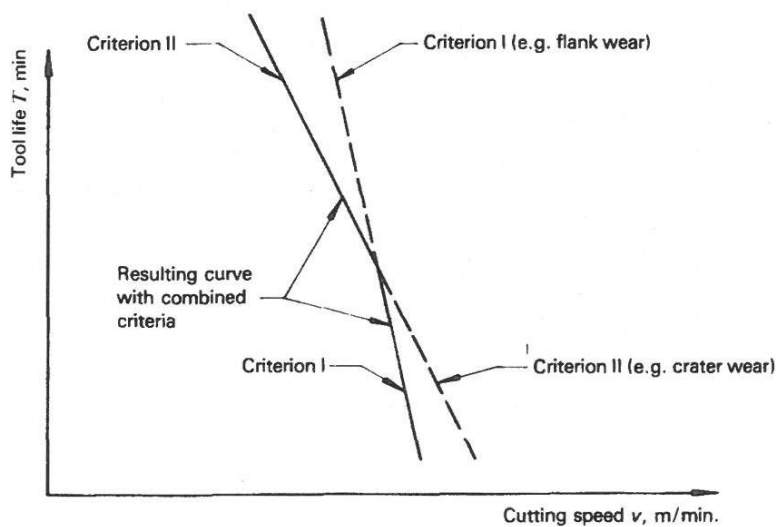


Figure 12: Set of vT resulting from the use of multiple criteria [80]

However, other criteria in the evaluation of tool life, such as finished surface roughness, cutting temperature, or burr formation may also be used to specify the end of tool life in micromachining. For simplicity, Taylor's tool life relationship can be described by the following equation 1:

$$VT^n = C \tag{1}$$

where V is cutting speed (m/min), T is tool life (min), and C is a constant. The tool rejection criteria for tool life testing described in ISO 8688-2 [80] for conventional milling need to be modified to take into account the effect of downscaling in micromachining for use in estimating the effective tool life of cutting tools.

2.3.3.2 Study of tool wear

Tool wear is a complex mechanism influenced by the properties of the workpiece and tool material. The tool is decided to be at the end of its useful life if the finished part surface finish includes any loss of dimensional accuracy. This is described as defect or a level of excessive wear, chipping, fracturing, or tool breakage which passes a critical point that results in tool failure. The miniaturization of tools featuring a diameter size less than 1 mm and a relative cutting edge radius of a few microns focus on the area of contact between the tool edge and the workpiece which results in the concentration of cutting force at the tooltip. The reduced contact point makes it difficult to directly monitor wear during machining that leads to the researchers attempting to measure the tool wear after machining.

In high speed milling of different hardness's of hardened steel using micro tools with different coatings (TiAlN and TiSiN), wear has been measured following a series of machining interruption categorizing tool wear by occurring stages of initial, stable and sharp wear [82]. Also reporting flank wear is the dominant wear mode joint with chipping and adhesion in both stable and sharp stage. The change of helix angle, cutting speed and depth of cut on tool wear in micromilling of copper suggests a reduction in cutting speed and helix angle while an increase in the depth of cut reduces the rate of non-uniform flank wear [83]. The comparison of tool life following the procedure given by ISO in relation to the range of rake face angle (0° , 90° and 45°) in slot milling of Steel-NAK80, indicating to the lowest flank wear of 0.134 mm is achieved by the tool with a 90° rake face [84]. Also reporting the tool failure after 400 mm of machining.

The impact of different microstructures (mill annealed, bimodal, fully equiaxed and fully lamellar) of Ti6Al4V on the wear rate of coated micro endmills suggest adhesion wear-causing tool coating delamination, while emphasising on the importance of material structure (lamellae result in lowest flank wear rate) on improving tool life [85]. The wear of hard carbon and nano grain diamond-coated tools in slot milling of zirconium, which has been studied in relation to cutting length and surface roughness confirmed the influence of the coating used on tools where a maximum of 66 mm and 1980 mm of machining lengths have been reported respectively. Also a remarkable average surface roughness of 30 nm has been achieved by using diamond coated tools [86]. In high speed milling of TA15 using cutting speeds of 250 m/min and 350

m/min, non-uniform flank wear with dominant notch wear mechanism for two coated tools (PCD and PCBN) suggest high cyclic stress and high temperature, leads to a reaction of the coating and encourages adhesion wear [87].

Following the desire for live tool wear measurement during machining, number of machine condition monitoring which are traditionally used in conventional milling have been adopted including acoustic emission (AE) signals. However, direct use of this measurement process is shown to be impossible due to same range as the noise and vibration in micromilling, in addition to the strong disruption by resonance frequency [88]. A procedure that is tailored for the micro end milling to filter and categorize the AE signals has been proposed where the reliability of the process is validated experimentally, and shows acceptable accuracy in the prediction of tool wear and tool life, limited to the use of new tools [89]. Similarly, tool wear monitoring using the proposed fusion of various sensors signals combined by the neuro-fuzzy method (accelerometers, force and acoustic emission sensors) have shown to provide an effective mean of tool wear monitoring for micromilling to warn the operator to minimise tool damage and tolerance violation [90]. Using a combination of force, acceleration and AE signal data in the monitoring of machining also provides a better characterisation of tool wear in high speed machining. The determination of the distribution of AE sources on the shear plane using a numerical model following a one-dimensional wave equation predicts the effect of the shear plane by quantifying the tool flank wear using the AE signal generation, as demonstrated in Figure 13 [91].

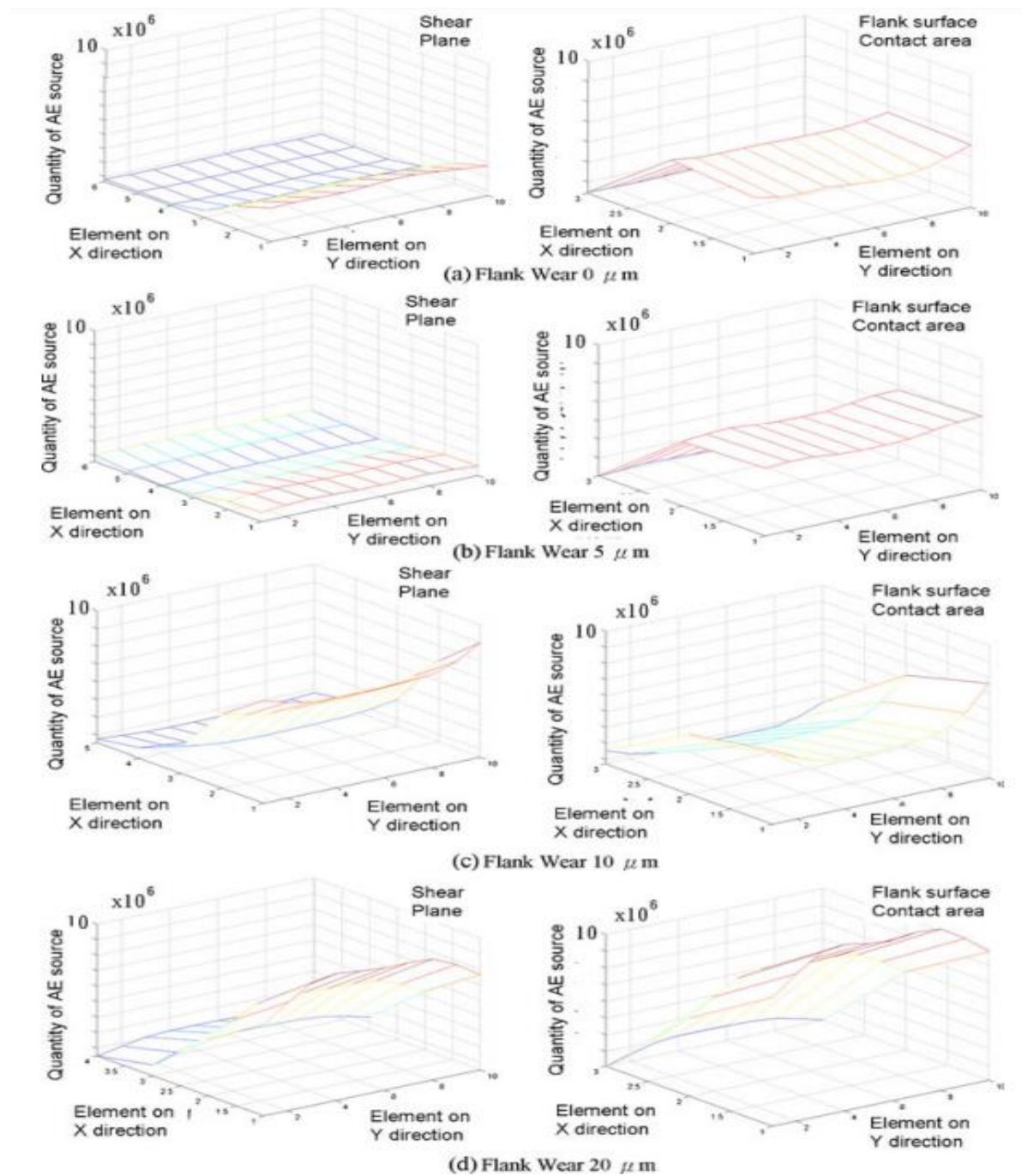


Figure 13: Effect of flank wear (a) $0\mu\text{m}$, (b) $5\mu\text{m}$, (c) $10\mu\text{m}$, and (d) $20\mu\text{m}$ on the shear plane and contact surface area [91].

The plot AE signal maps and quantifies the tool engagement area between the flank face and the material which can be used for active monitoring of tool wear while the change in plot of shear plane guides the operator in material removal process during machining. In literature, a range of wear rate and wear mode have been reported for the combination of tool and workpiece material while specific behaviour for the combination of commonly used tools and materials reviewed in this work are gathered and summarised in Table 2. These specific behaviours are valuable for machining knowledge and can be used in the development of machining

knowledge database explicit to micromilling operations for the use of operators without a prior knowledge of specific tools and materials in process planning tasks.

Furthermore, the recommendations for tool life found in terms of the limiting criteria have been evaluated experimentally and applied as the end of life in relation to specific cutting length and wear rate for specific wear type. However, in process planning for micromilling in order to complete the task of tool selection, the operator needs to be able to compare the performance of the tools following a unified criteria which have not been used in the reviewed work. Also in the evaluation of tool life following existing ISO procedure, tool failure reported by [84] indicated an inapplicable approach to evaluate boundary conditions for micro tools that need to be reviewed. It can be concluded that similar to the conventional scale, a unified methodology in the evaluation of micro tool life and standard tool performance indicator reflecting unique machinability issues for micro tools are required for the operator to be able to compare and select the cutting tool. Also, the different impact of material properties on tool wear necessitates the accurate prediction of tool life criteria that can be used by the operator to estimate the tool change interval.

Table 2: Summary of significant findings in micromilling field

Authors	Machining speed (m/min)	Tool diameter (μm)	Tool material	Workpiece material	Findings highlights
T.Ozel, et al.[92]	25, 42, 50, 62, 75, 82	635, 508, 381	Tungsten carbide uncoated and CBN coated	Ti-6Al-4V alloy	Using cBN coated tool lower machining temperature, surface roughness and tool wear. Reducing the feedrate has shown to decrease burr formation and improve surface roughness.
Irfan Ucum, et al.[93]	48	768	AlTiN, AlCrN, TiAlN + AlCrN, TiAlN + WC/C and diamond-like carbon	Inconel 718	DLC and TiAlN + WC/C-coated tools resulted in the lowest surface roughness in comparison to all other coatings tested. Feed rate and material properties of tool coating have the highest impact on surface roughness while the impact of depth of cut is statistically insignificant.
D Huo et al. [94]	31.4,78.5	500	TiAlN-coated and uncoated tungsten carbide	Fine-grained graphite	Diamond-coated tools proved to be more effective in micromilling productivity and achieved a better surface finish.
G. Bissacco et al.[95]	30	100	Tungsten carbide-uncoated	Hardened steel 58 HRC	The size effect is due to the limited scalability of the workpiece material microstructure. Cutting parameters should be selected with reference to cutting force and cutting edge radius.

H.weule et al.[96]	5	200	Tungsten carbide- uncoated	Steel SAE 1045 (Ck 45)	A prerequisite for using tungsten carbide tools is the homogeneity of the workpiece material with no internal stresses. The selection of cutting speed directly influences surface finish.
A. Iglesias et al.[97]	250	125	Steel-diamond coated	Steel SAE 1140 (Ck 45)	Due to different patterns of machining dynamic behaviour, tool selection in micromilling must be conducted with reference to D/Z ratio and machine spindle dynamic properties
G.Campatelli, A. Scippa.[44]	283	600	Solid carbide- Uncoated	Aluminium 6082- T4 alloy	Material removal rate and uncut chip thickness directly affect the quality of the finished part. In micromilling, the use of AE signals is essential to monitor the condition of machining and adjustment the machining parameter for material removal rate.
K.-D. Bouzakis[98]	100	500	Cemented carbide- TiAlN coated	Steel- 42CrMo4 QT	In a study of machining parameter selection in micro blasting, the properties of different coating materials affect the performance of the material removal process in micromilling
Kunpeng Zhu et al.[99]	80-180	500,800	Tungsten carbide- uncoated	Pure copper and steel	A new approach based on a hidden Markov model (HMM) for micromilling is proposed and validated

					experimentally, suggesting an effective method for micromilling tool wear monitoring
Oliaei. S.N.B. et al.[100]	67-270	450-500	Polycrystalline diamond (PCD)	Silicon	<p>Large negative rake angle results in an increase in compressive stress in the cutting zone.</p> <p>Effect of depth of cut can be compensated for by increasing the feed rate.</p> <p>A large clearance angle reduces the rubbing of cut material on the machined surface.</p>
H. Rezaei et al.[28]	280	80,200	Tungsten carbide-uncoated	Titanium alloy Ti-6Al-4V w	<p>Evidence of surface and sub-surface hardening is observed, indicated by a plastic deformation zone around the tool work-piece contact.</p> <p>Downscaling of uncut chip thickness from scale results in the ploughing effect increasing non-linearly and higher burr formation.</p>

2.3.3.3 Coolant

The effectiveness of coolant on reducing tool wear and improving surface quality especially in the machining of hard to cut material is well known [101]. Therefore attention was given to the effect of lubrication and optimisation of the coolant composition to cater for cutting temperature in micromilling. The effect of three coolant compositions (Isopar-H, ethyl alcohol and distilled water), using minimum-quantity coolant (MQC) in micromilling of thin wall structures, have been compared with dry milling which shows 10.4% decrease in surface roughness for walls machined when using a coolant [101]. Ethyl alcohol is found to be the better choice of composition to be used. Similarly, the impact of vegetable-oil-based-dispersed-graphene in the machining of titanium alloy in relation to forces, temperature, surface hardness and surface roughness using Gray relational analysis and MQC has been compared to dry machining which shows significant improvement of 18.13%, 13.59%, 8.36%, and 24.82% respectively [102]. The impact of adding various nanoparticle additives of mainly four types, metal, metal oxide, metal sulfides and carbide, in cutting fluid have shown to triple the heat transferability of the cutting fluid by the principle of heat transfer using an additional solid [103]. The comparison of cryogenic, flood cooling and MQC in relation to resultant thrust force, tool wear and surface roughness in machining of Ti-5553 alloy results in up to 30% reduction in thrust force and lowers tool wear reported for tools that use cryogenic cooling [104]. However, MQL results in better surface roughness that is preferred in micromilling due to the difficulty of the secondary finishing process. A similar comparison of traditional flood cooling with pneumatic mist jet impinging cooling (PMJIC) in relation to tool life and material rate of removal in machining of Ti40 alloy indicates a high-pressure jet capability to break the thin skin of steam around the cutting zone, improving cooling efficiency and directly improving tool life is favourable in micromachining [105]. From the comparison of the work in literature, commonly Titanium alloys have been used for the evaluation and comparison of lubricants where PMJIC is recommended for micromilling due to its high efficiency and capability to break the thin skin of steam around the cutting zone.

2.4 Overview of process planning methodologies

The fundamentals of process planning of the mechanical material removal process can be divided into several categories that involve shaping a block of raw material into the desired product. Each process relies on the performance of the previous process, with interrelated subprocesses. Given the variety of product shapes and the design demands involved in many machining processes, the determination of the best method and sequence of the machining process is still highly dependent on human skills. The tedious and time-consuming human

decision making steps in process planning links the design stage to the manufacturing stage as demonstrated in Figure 14.

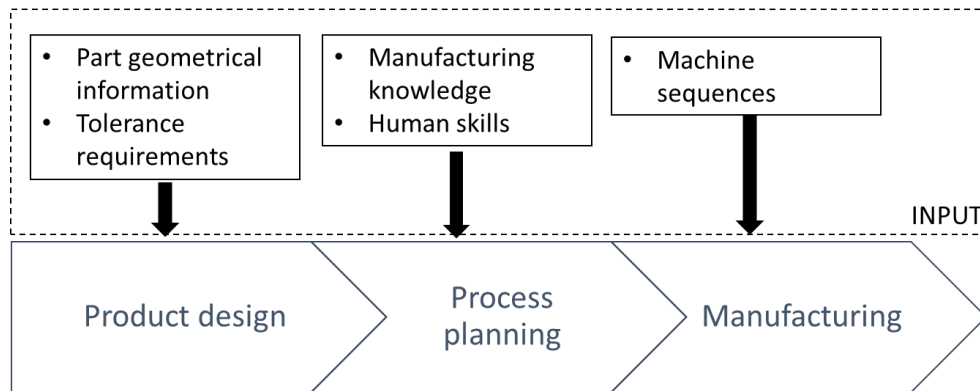


Figure 14: Link between process planning stages and the required inputs

In order to fulfil the designer intentions at the manufacturing level, product design represented by CAD model must be reinterpreted to a list of features found in part design before it can be linked to sets of machining processes and corresponding parameters to fabricate the part. Two widely used approaches in the design of products are governed by feature and solid modelling. To manually extract the features from the basic topological and geometrical information formed within the CAD stage, labour-intensive manual feature recognition relies on the user knowledge to identify and explicitly define the feature. Therefore, this area has been heavily automated by the introduction of automatic feature recognition (AFR) to increase productivity. Automatic feature recognition (AFR) uses a matching definition of the feature defined explicitly within the domain knowledge base. It also plays an important role in the automation of machining in terms of the elimination of human engagement. This benefits the manufacturing process by saving a significant amount of time and human resources while communicating the relevant information to ensure the functionality of the desired part without restricting design creativity. Boundary representation (B-rep) is a common system used to extract and identify the unique topological and geometrical characteristics of machining features in the classification of features for commercial CAM systems. CSG uses sets of Boolean operators and 3D solid primitives to specify the feature, whereas the B-Rep of the solid model is made up of information about the faces, edges and surfaces of the model, including topological information, to define the relationships between these features. The four main algorithms used in automatic feature recognition are as follow [106]:

(1) The graph-based approach utilises a feature template graph containing attributes of the convexity or concavity of edges, faces and orientations defining on the explicit primitive

template of the feature. This method benefits from an intelligent rule-based system for generating part feature vector tree and extraction of manufacturing features limited to the comprehensiveness of the domain database that requires an extensive feature pre-processing in construction of feature library. Due to its unique vector tree, the algorithm used to match with templates in the feature library made of vector tree templates proven to be more efficient and have more advantages due to the inclusion of new user-defined features each time the cluster of faces is not recognised. Another limitation of graph-based approaches is the inability to detect the feature intersection while excluding information such as dimensions or tolerances of feature surfaces that is essential for the process planning stage [107].

(2) Syntactic pattern recognition uses descriptive language with grammar sets as rules to define a particular pattern. The descriptive language is used to translate the geometrical feature extracted from the part into sets of strings that then run through stages of rule checks known as grammar checking, if a matching string is found within the database then the identified shape will be the outcome; otherwise, the shape is unknown. The shortcomings of this method arise from the restrictions of its syntactic representation which limit it to 2D parts even though this method is not affected by geometrical changes in the part feature [108, 109].

(3) The volume decomposition approach break into the convex hull and cell-based methods where both methods share the same basic steps in identifying the overall removable volume by comparing the part features with the blank and then utilising the graphical comparison of the part with the feature database using if-then rules with features within the database. The cell-based method breaks down the features through co-plane and subdivides them into sub-features, which are then matched graphically by searching the database. Although the cell-based approach improves the identification of the features for the AFR process, each feature will form a cell. In machining of a complex part, several cell formation increases the computation time where lack of secondary algorithm to merge the feature to be machined on the same surface are reported [110, 111].

(4) The hint-based reasoning system uses the orthographic projection of the parts inputting the 2D graphic representation of an engineering drawing projection. This then undergoes the two stages of profile search and feature completion where the volumes of the cavities are allocated to the 2D contours detected. For a feature that could not be detected by the system, the feature is subdivided for interpretation utilising isometric view analysis. This system benefits from the extraction of features forming the part without relying on the feature database library; however, a disadvantage is that there may be multiple duplicated features while small features may be missed by the feature recognition system. The constructive solid geometries (CSG) method is

adopted for use in feature recognition due to its unique graphic representation of features, including the small-scale variations in part design that are ignored in B-Rep-based feature recognition. However, the inefficiency of information provided by part design representation and incapability of existing feature recognition system to output advance surface and geometrical information required for characterising the features limit the use of the method relying on manual input in feature extraction at the process planning stage.

Furthermore, advances in computer-aided design (CAD) and computer-aided manufacturing (CAM) have significantly enhanced the computer-aided environment, while computer-aided process planning (CAPP) automates the bridge from design to manufacturing. The development of CAPP allows the integration of design and manufacturing, and the main elements of this process have been the core subject of research in macro-scale machining over the past few decades [112-115]. Several tools have been developed to support the corresponding elements of process planning. The primary organisational steps of knowledge structuring and logical reasoning are used to describe the data architecture of manufacturing information in CAPP [115]. These elements are categorised into two types of planning, macro and micro process planning. Macro process planning involves the selection of manufacturing resources, operations and sequences, while micro process planning consists of the choice of machining parameters, and setups and tool path determination. The task of process planning is shown in Figure 14 is to ensure that manufacturing requirements are met, that the finished product is made to the correct specifications and the design tolerance is achieved.

Methods used to determine the steps required in the process are based on the geometry of the part concerned and process capability and can be characterised as variant and generative approaches. A variant approach is a method adopted from the original manual in the process planning stage that assumes that similar features require a similar process plan. The process plan retrieved from the database includes sets of predefined machining stages based on group technology (GT). Variant coding systems establish a group formation, which includes all the features that require similar machining steps and procedures. Each part group will form a matrix that is stored in the database. In process plan generation, the feature of each new part is extracted and the code of the matrix is searched for in the database to retrieve the process plan for machining operations followed by modifications made by the process planner in detail plans based on part specification. At this stage, if the process plan for the part family was not available, one will be manually created and saved in the database for feature reference [116]. Figure 15 presents the variant CAPP approach.

The variant approach can be developed further through standardisation of product data (STEP) representation to provide specific application protocols and to change the structure of physical files in the logical software layout [117]. Algorithms are developed to optimise the retrieval of process plan data so as to improve the efficiency of the method [118], while further optimisations are made to the algorithms in order to best utilise the resources available [119]. Many researchers have focused on the development of data to accommodate new features in previously generated process plans and new manufacturing requirements such as high precision parts [120, 121].

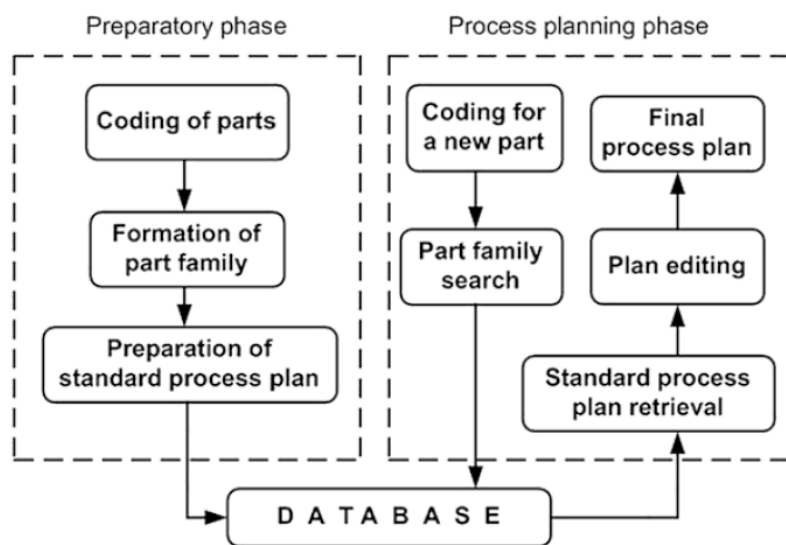


Figure 15: Variant CAPP approach [116]

Meanwhile, the generative approach in CAPP involves an automated process planning system that develops a process plan from scratch for each new part shown in Figure 15. This method utilises a rule-based decision-making mechanism to generate the process plan. Therefore, it benefits from consistency in planning in comparison to the variant approach and a process plan can be created for a part that has not yet been specified in the variant database. For the generative method to work, an advance part geometry database is required that includes information about part shape, feature geometrical dimensions, tolerances, surface conditions and process capabilities and conditions. The functionality of the database for generative CAPP relies on in-depth information about part features and materials, where the accuracy of the process plan depends on the availability of information from real-life case studies for specific machine tools and combinations of materials.

It is clear that the accuracy of both methodologies used by CAPP heavily relies on the accuracy of information input to the system range from the quality of feature information to extensive

process knowledge of material and tools gathered in relation to the specific manufacturing process (e.g. micromilling).

2.5 Summary of gaps in knowledge

In the review of process planning, the suitability of process plan has been shown to rely on the accuracy of input into the system in relation to part feature data and the comprehensiveness of machining data and knowledge used in decision making to produce the process plan datasheet. This literature review shows that substantial attention has been given to the optimisation of cutting parameters and the development of compensation methodologies to improve accuracy and efficiency for micromilling. However, following the in-depth analysis of the findings the following gaps are identified:

- The limitation in the integration between CAD and CAM with a deficiency in transferring high-level information makes process planning a key stage to identify and extract feature data (e.g. surface roughness and tolerance) required for solving tasks within process planning activities. Furthermore, in the interpretation of micro features, advanced knowledge (e.g. aspect ratio) is required from the operator. Therefore, a systematic approach to identify and extract the geometrical information with consideration should be given to micro feature to ensure the suitability and accuracy of input to the process planning system.
- Even though optimisation of machining parameters have been achieved for a wide range of material and tool combinations, machining data for almost all the studies reviewed in this work were obtained under laboratory conditions that do not mimic the true industrial environment. Therefore, the optimum machining parameters identified may not be acceptable under the influence of industrial environments, such as noise and vibration.
- Tool paths are commonly used in micromilling which are designed for prolonged conventional tool life. However, no data has been found on their impact on micro tool performance in micromilling. Therefore, the impact of conventional tool path on micro tool life and performance must be investigated. In the optimisation of machine layer strategies for low stiffness features (thin wall), the focus was limited to improving only geometrical accuracy and neglecting the machining efficiency that is key in process planning. Therefore the machine layer strategies need to be further developed including both efficiency and geometrical accuracy. Also, similar to many optimisation methods developed for the selection of machining parameters found in literature, only a few approaches were found for selection of tool path and machine layer strategies that require further development for micromilling.

- The short life and immature failure of micro tools lead to a review of many studies characterising wear and evaluating tool life in relation to a range of independent variables for wide combinations of tool and material. Therefore the estimated tool life and wear rate can only be expected if similar machining conditions and environments are provided. Therefore similar to standardised tool life procedure used in conventional machining (ISO 8688-2 for evolution life of endmills), the same procedure must be developed and get adopted for micro tool life testing if the accurate and comparable tool data are to be produced. Furthermore, to be able to compare the tool and material performance in relation to machining limitation/capability, a quantifying machinability value is required for the operator and designer to select the suitable tool and material. The selection of criteria and procedures used in obtaining a global value should follow a standard method and procedure if a meaningful machinability index is to be calculated.
- Review of literature in this study could not identify an assembly of protocols or unified approach to process planning for micromilling. Also, the knowledge of machining constraints and criteria for process monitoring were generally found in high technical articles with limited access that cannot be utilised by operators easily. An expert level of understanding of micromilling was required in interpretation before it could be utilised in process planning. Limiting the application of the micromilling process and therefore identified as the gap between the fundamental and industrial applications of micromilling process.

It can be concluded that most of error and inefficiencies in micromilling, source from the lack of a methodical approach to process planning and standardisation of procedure in gathering of machining data and process knowledge used in the individual task which, reflects on the machining process reliability and part accuracy. Therefore, a standard procedure for process planning in micromilling is required for widespread use of this application.

Chapter 3. Research approach and experimental procedure

3.1 Experimental setup

3.1.1 Machining setup

The experimental work has been carried out on a standard Hurco precision CNC machining centre (VM10) to ensure that the results are industrially feasible. A high-speed spindle (NAKANISHI -HES810) was retrofitted to the main spindle shown in Figure 16. An ultra-precision collet was used to clamp the microtool and to control the spindle run out below $1\mu\text{m}$, the machining centre had a single axis positioning accuracy of $5\mu\text{m}$, and the experiment designed to compensate for positioning error as specified in the experimental detail planning in section 3.2. As spindle error has been shown to have a significant impact on surface roughness [49], the main spindle was set on mechanical lock throughout all experiments, thus, limiting spindle and sideway error to vibration and the run out of the high-speed precision spindle.

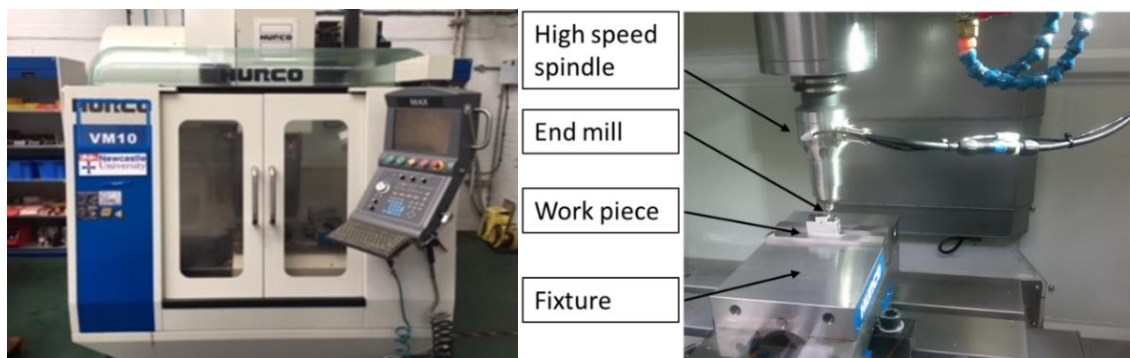


Figure 16: Hurco CNC-VM10 (left), Illustration of the experimental set-up (right)

3.1.2 FE model setup

The FE model of thin wall structure was developed using Ansys (Workbench, v15.0) in conjunction with Inventor (Autodesk, Professional 2015). Static structure analysis was applied to a parametric model of thin wall structure for simulation of feature deformation. For simplification, cutting forces along both the X and Y direction was applied using nodal force at a contact point between tooltip and workpiece interface, under the assumption that a tool with a perfectly sharp edge was used. The side faces of the workpiece were fixed along all directions, to mimic the material clamp position, while probe sensors were defined across the face of the thin wall, as demonstrated in Figure 17.

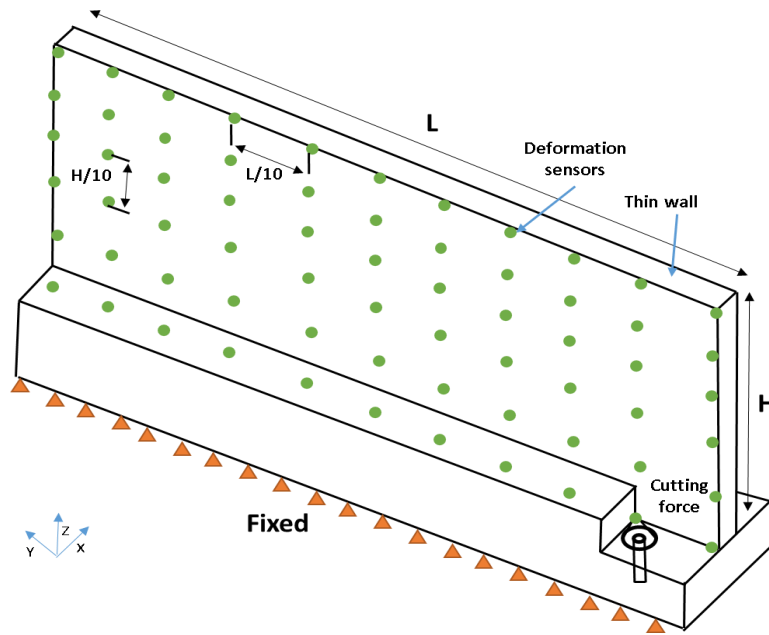


Figure 17: Predefine boundary constrains on thin wall model

The workpiece geometry was meshed with quadrilateral elements with an average size of 50 nm in order to maintain a good simulation precision and to ensure practical computer time and power. The physical properties of the workpiece material were selected from the material data library, as summarised in Table 3.

Table 3: Material properties of Aluminium 6061-T6

Physical parameter	Aluminium 6061-T6
Density ρ (kg/m ³)	2.7
Thermal expansion coefficient. (10 ⁻⁶ °F-1)	1100-1205
Thermal conductivity, λ (W/m°C)	167.3
T_{melt} (°C)	582 - 652

T_{room} (°C)	24
Poisson's ratio	0.3
Specific heat, Cp (J/kg°C)	896
Elastic modulus, E (GPa)	68.9

Whilst the plasticity was described by Johnson-Cook strength constitutive model, it is recommended by [122] that constraints for material deformation, hardening and the effect of strain rate should be included. The failure model is described by equation 2 [123]:

$$D = \sum \frac{\Delta\varepsilon^{-pl}}{\bar{\varepsilon}_f^{pl}} \quad (2)$$

Where $\Delta\varepsilon^{-pl}$ is the equivalent to the plastic strain increment and $\bar{\varepsilon}_f^{pl}$ is the failure strain. Failure strain is described by equation 3 [123]:

$$\bar{\varepsilon}_f^{pl} = (d_1 + d_2 e^{d_3 n}) \left[1 + d_4 \ln \left(\frac{\dot{\varepsilon}^{pl}}{\dot{\varepsilon}} \right) \right] \left[1 + d_5 \left(\frac{T - T_{room}}{T_{melt} - T_{room}} \right) \right] \quad (3)$$

Parameters $d1-d5$ are Johnson-Cook damage model constants, $\bar{\varepsilon}^{pl}$ is the mean plastic strain, $\dot{\varepsilon}$ is an equivalent strain, T is the deformation temperature, T_{room} is the room temperature and T_{melt} is the material melting temperature [124]. The yield stress is expressed by equation 4 [125].

$$\sigma^- = [A + B(\varepsilon^{pl})^n] \left[1 + C \ln \left(\frac{\dot{\varepsilon}^{pl}}{\varepsilon_0} \right) \right] (1 - \theta^m) \quad (4)$$

Where σ^- is the equivalent stress, ε^{pl} is the equivalent plastic strain rate, ε_0 is the reference strain rate, and θ^m is the homologues temperature and A, B, C, m and n are constants. A is a constant representing yield stress of the material under reference condition, B is strain hardening constant, C is the staining coefficient of strain rate, m is the thermal softening coefficient and n is the strain hardening coefficient. The damage constants (d1-d5) and other constants used for Aluminium 6061 identified by Johnson-Cook was obtained from published literature, as summarised in Table 4.

Table 4: Johnson-Cook material constants for Aluminium 6061-T6 [126]

<i>Damage constant</i>	<i>A</i>	<i>B</i>	<i>n</i>	<i>C</i>	<i>m</i>	<i>d1</i>	<i>d2</i>	<i>d3</i>	<i>d4</i>	<i>d5</i>
<i>Value</i>	324	114	0.42	0.002	1.34	0.077	1.248	1.142	0.147	0
	MPa	MPa								

Cutting forces are numerically described by equations 5-7 [127]:

$$F_x(t) = \frac{R}{\tan\beta} \sum_{k=1}^k \int_{\theta_b}^{\theta_t} \{-[K_{tc} h_a(\theta, k) + K_{te}] \cos \theta - [K_{rc} h_a(\theta, k) + K_{re}] \sin \theta\} d\theta \quad (5)$$

$$F_y(t) = \frac{R}{\tan\beta} \sum_{k=1}^k \int_{\theta_b}^{\theta_t} \{[K_{tc} h_a(\theta, k) + K_{te}] \sin \theta - [K_{rc} h_a(\theta, k) + K_{re}] \cos \theta\} d\theta \quad (6)$$

$$F_z(t) = \frac{R}{\tan\beta} \sum_{k=1}^k \int_{\theta_b}^{\theta_t} [K_{ac} h_a(\theta, k) + K_{ae}] d\theta \quad (7)$$

Where $F_x(t)$, $F_y(t)$ and $F_z(t)$ are the instantaneous cutting forces acting along x, y and z axes respectively. R is the nominal radius of the tool, β is the helix angle, θ_b and θ_t are the lower and upper angles of the integration limit, K_{rc} , K_{tc} , K_{re} , K_{ac} , K_{te} and K_{ae} are cutting coefficients that vary for tool and workpiece material combination.

Whereas cutting coefficients are mathematically described by equations 8-13 [127]:

$$K_{tc} = \frac{\tau}{\sin Q_n} \cdot \frac{\cos(\beta_n - \alpha_n) + \tan\eta_c \sin\beta_n \tan i}{c} \quad (8)$$

$$K_{rc} = \frac{\tau}{\sin Q_n \cos i} \cdot \frac{\cos(\beta_n - \alpha_n)}{c} \quad (9)$$

$$K_{ac} = \frac{\tau}{\sin Q_n} \cdot \frac{\cos(\beta_n - \alpha_n) \tan i - \tan\eta_c \sin\beta_n}{c} \quad (10)$$

$$K_{te} = r\tau_s \left(\frac{2\delta_0}{\cos(\delta_0)} + \pi \sin\delta_0 \tan\delta_0 \right) \quad (11)$$

$$K_{re} = r\tau_s (2(3\sin\delta_0)^{0.5}) \quad (12)$$

$$K_{ae} = K_{te} \sin(\beta) \quad (13)$$

Where K_{rc} , K_{tc} , K_{re} , K_{ac} , K_{te} and K_{ae} are machining coefficients, ϕ_n is the normal shear angle, β_n is the friction angle, η_c is the chip flow angle, i is the inclination angle, τ_s is the shear stress and δ_0 is the stagnation angle. Considering the accuracy of such models is affected by the accuracy of cutting force coefficients derived for the corresponding cutting tool and parameter [128], cutting forces used as input to the numerical model were measured experimentally (Appendix A1.2) as summarised in Table 5.

Table 5: Measured cutting forces in machining of Aluminium 6061-T6 using 1 mm Tungsten Carbide tool

Depth of cut (mm) / Cutting forces (N)	F_x	F_y	F_z
0.1	4.9	1.8	2.8
0.2	9	2.6	3.1
0.3	14.3	3.1	4.6

3.2 Experimental planning

3.2.1 Tool life

The experimental procedure recommended by ISO 8688-2 for tool life testing was used to determine the life of uncoated tungsten carbide (WC) endmills with a nominal diameter of 1 mm. The response of cutting conditions listed in Table 6 on tool life through slot milling was measured for a block of titanium alloy Ti-6Al-4V (Grade 5). The schematic diagram of the slot milling is shown in Figure 18.

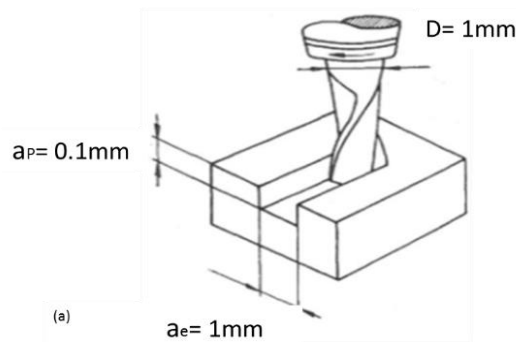


Figure 18: Schematic diagram of slot milling

A bar of 20 mm rectangular cross-section (minimum of 10 times the diameter as recommended by ISO and preferred 20 times) was selected as the workpiece. The top surface of the block was face milled before the machining was carried out to ensure the flatness of the top surface and consistent depth of cut throughout machining. Total flood cooling, using a 10 to 1 ratio of water to oil (Hysol MB 50) was used to reduce the machining temperature. The parameter response in relation to flank wear (VB), volumetric change, and tool edge deterioration and tool diameter deterioration was recorded at 60 mm intervals. Furthermore, the machining parameter response to the average surface roughness and resultant width of the slots was measured at 4 mm intervals along the bottom surface of the slot. A list of machining parameters used in this experiment is shown in Table 6.

Table 6: Cutting conditions

Tool No.	Spindle speed (rpm)	Cutting speed (m/min)	Feed rate (mm/min)	Axial depth of cut (mm)
1	30,000	94	100	0.1
2	40,000	126	100	0.1
3	50,000	157	100	0.1
4	60,000	188	100	0.1
5	70,000	220	100	0.1
6	60,000	188	50	0.1
7	60,000	188	150	0.1

3.2.2 Study of thin wall structure

For the experimental study of high aspect ratio feature, Aluminium 6061-T6 was used to study the response of layer strategies, radial depth of cut (example shown in Figure 19) and milling technology in relation to accuracy and efficiency. Thin wall structures were dry milled using uncoated tungsten carbide tool (WC) endmills with a nominal diameter of 1 mm. The cutting parameter used for the individual experiment is summarised in Table 7.

Table 7: Summary of cutting parameters

Experiments	Spindle speed (rpm)	Feedrate (mm/min)	Axial depth of cut (mm)	Radial depth of cut (mm)	Milling technology	Layer strategy	Tool path strategy
Machine Layer	60000	100	Variable	0.5	Up milling	Variable	Lace 0
Radial depth of cut	60000	100	0.1	0.5	Up milling	Step	Lace 0
Milling technology	60000	100	0.1	0.5	Variable	Step	Lace 0

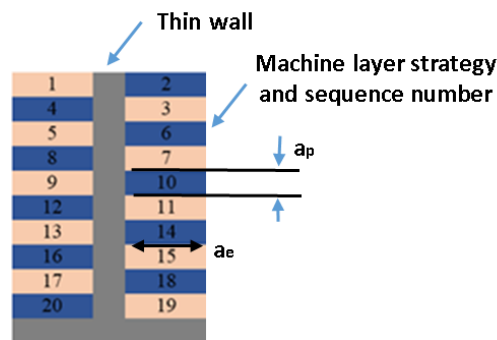


Figure 19: Schematic of the machine layer strategy “Step”

3.2.3 Study of tool path strategy

In this study, the response of five tool path strategies (Lace 45°, Lace 0°, Lace 90°, Concentric and Waveform) on the performance of micro end mill (1mm uncoated tungsten carbide tool (WC)) was indirectly measured in relation to surface roughness, geometrical accuracy and efficiency. The cutting conditions were fixed (summarised in Table 8) with the schematic of tool path strategies demonstrated in Figure 20.

Table 8: Machining parameters used in the experimental comparison of machining tool paths

Spindle speed (rpm)	Feedrate (mm/min)	Axial depth of cut (mm)	Radial depth of cut (mm)	Milling technology	Layer strategy	Tool path strategy
60000	100	0.1	0.5	up milling	step	variable

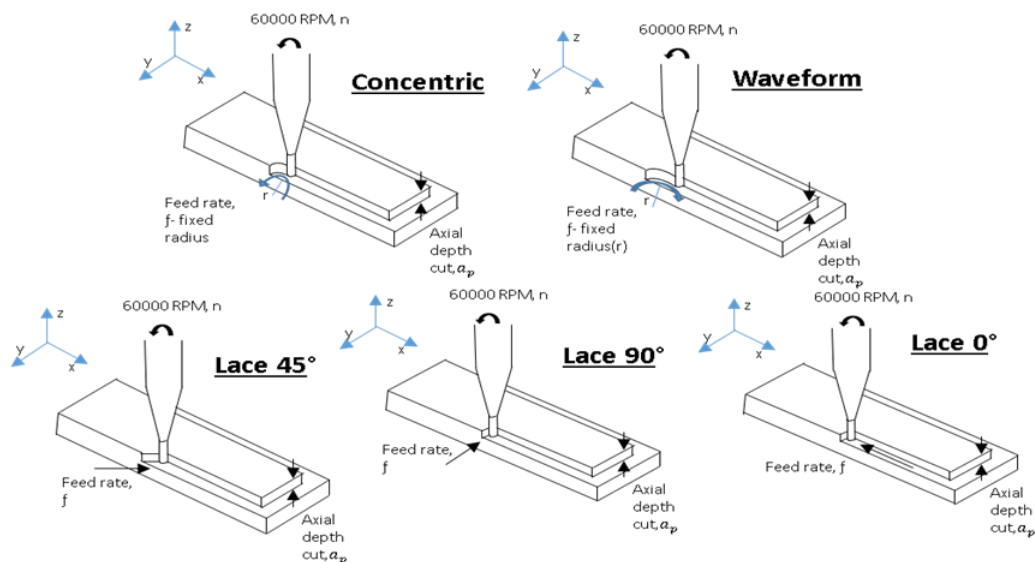


Figure 20: Schematic diagram of strategies used in this experiment

The path used in the concentric strategy involved a circular movement of the tool, using a fixed diameter tool path as the tool merged in and out of the material. The waveform strategy used variable circular tool path radius up to triple tool diameter as the tool comes out of the material. The Lace 0° path followed in the parallel to the finished geometry, with the material removed from outer to inner, layer by layer. Similarly, lace 45° and lace 90° followed toolpaths tangent and perpendicular to the finished geometries respectively. In both the lace 45° and lace 90° strategies, the path began at one end of the feature following the desired geometry until all excess material had been removed from outer to inner.

3.3 Methodology

This section reviews the methodology for the measurement of tool wear, part geometrical accuracy and machined surface roughness used as dependent variables throughout this study.

3.3.1 Tool wear

Commercially available two flute uncoated tungsten carbide endmills from Rainford Precision Machines Limited were selected from a single batch to reduce manufacturing error and to enable the visual comparison of tool deterioration in terms of different machining parameters. Tool wear was measured in relation to flank wear (VB), tool diameter deterioration and cutting edge radius where non-contact measurement method using SEM was used to capture images of tool geometry before and after the experiments. Image J processing software (Image J, 1.X) [129] was used to take measurements of tool geometry from the SEM images where measurements were repeated three times and the average value was recorded.

The measurement of cutting edge radius was performed by placing a circle of best-fit on the SEM image of the tool edge (shown in Figure 21) and tool diameter measured by inserting a line with each end matching that of the tool edges as shown in Figure 22.

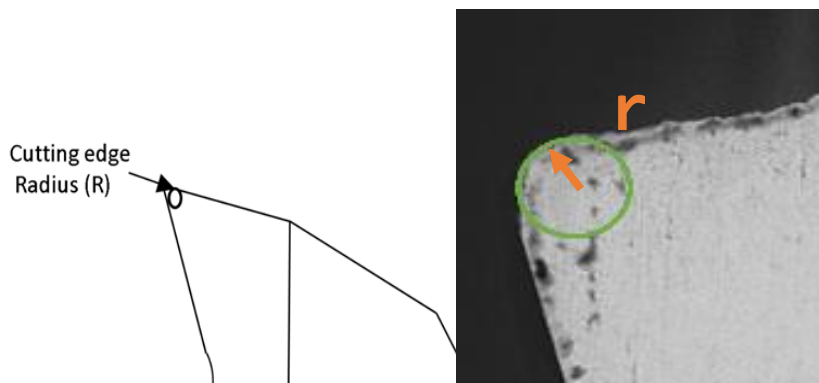


Figure 21: Schematic diagram of the cutting edge radius (left), SEM image of tool edge (right)

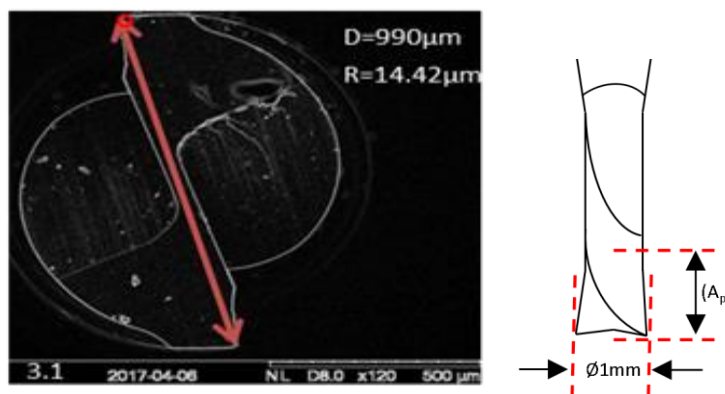


Figure 22: Schematic diagram of tool (left), SEM image of Tungsten carbide tool endmills from the top (right)

Flank wear, described by ISO 8688-2 as the loss of tool material across active tool edge, is categorized into uniform wear (VB1), nonuniform wear (VB2) with an irregular width on the active cutting-edge, or localized wear (VB3) developing on a specific part of the tool, as shown in Figure 23

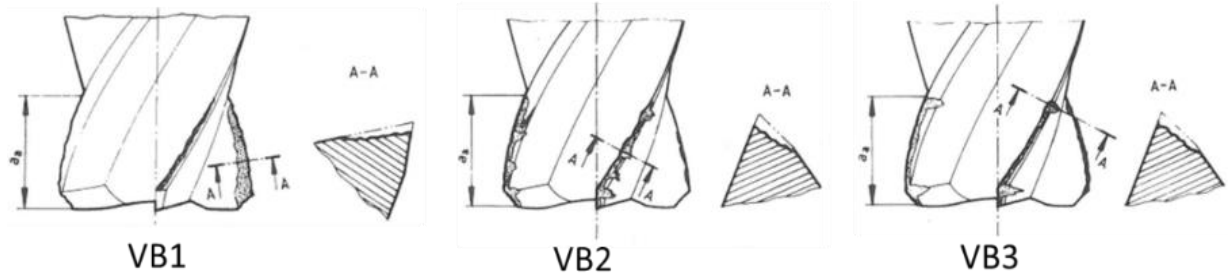


Figure 23: Schematic diagram of typical flank wear modes [80]

Therefore SEM images of the tools were processed using the sketch of a line to mark the tool edge position when the tool was new and the wear land width were measured at 0.01 mm intervals with the mean value was recorded, Figure 24.

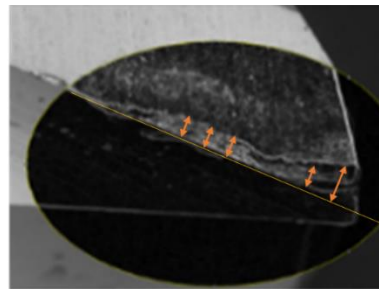


Figure 24: Processed SEM image of tool wear land width

Furthermore, tool volumetric change as a result of abrasive and adhesive wear was measured indirectly using a microbalance. To ensure complete removal of machine lubricant and debris from machining, tools were cleaned ultrasonically in isopropanol and dried using nitrogen. A precision balance with a single cell weighing system and shockproof construction was used to measure the weight of the cutting tools throughout the experiment. Before the weighing process, the balance was calibrated to reduce the machine error with measurements taken in triplicate and the mean recorded.

3.3.2 Geometrical accuracy and burr height

Similarly, the geometrical accuracy of samples was assessed using SEM images and further processed using Image J processing software (Image J, 1.X) [129]. Where the overall deflection angle and the maximum deflection of the thin wall were measured by inserting a line of the best fit tangent to the finished edge in relation to the second reference line inserted

perpendicular to the base surface. Maximum deflection and the deflection angle were measured from the top edge of thin walls (in comparison to the normal), and also the web thickness was measured across the top, middle and bottom of the thin wall web is shown in Figure 25

Figure 25. Following the burr type categorisation and methodology by Chern [130], the width of the primary side burr at the tool exit side was measured by processing the top SEM image of thin walls using a sketch of a line across the width of the largest burr, as shown in Figure 26.

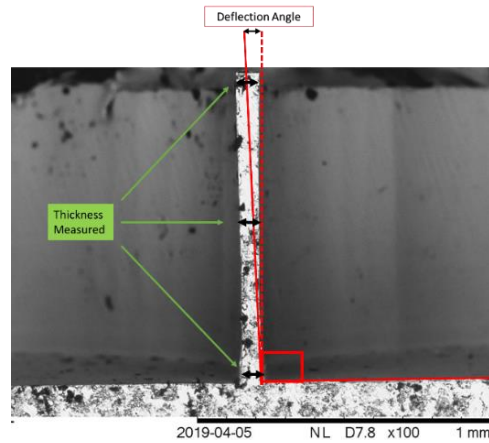


Figure 25: Example of an SEM image processed using Image J

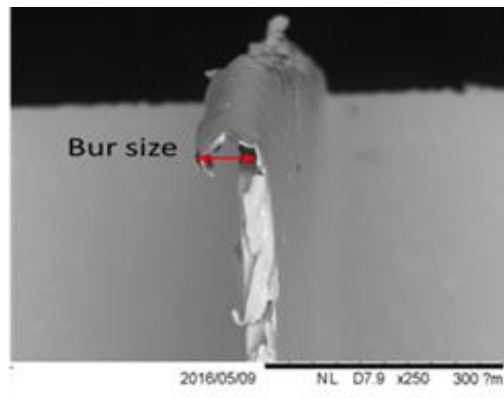


Figure 26: Example of measurement of thin wall deflection and burr size

3.3.3 Surface roughness

The surface roughness of the test piece was measured using optical 3D measurement techniques where the sample geometry was first 3D-scanned and further processed using Measurement Suit® software (Bruker, 2017) for area based roughness measurements according to ISO 25178. In the evaluation of samples with slots, the bottom surface topography was analysed, where the surface roughness was measured across the length of the slots using vertical scanning interferometry at 20x magnification. The mean average-values were recorded. Similarly, when

evaluating samples with thin wall geometries, the average mean value of side face surface area was measured and is shown in Figure 27.

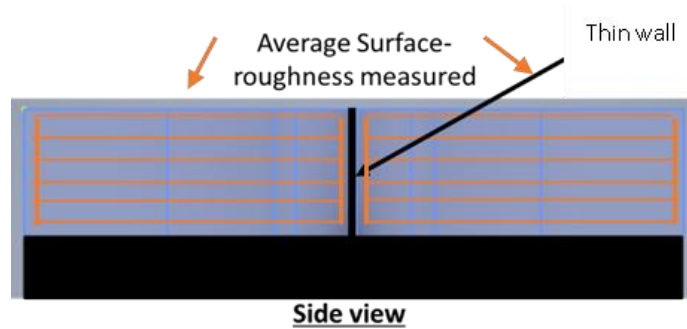


Figure 27: Map of evaluated finished surface area

3.4 Equipment

In this research, nanoscale instruments were used to quantify the experimental output. This section reviews the equipment used in the evaluation of machining performance.

3.4.1 Hitachi scanning electron microscope (SEM)

All geometrical measurements were taken using the Hitachi TM3030 (Figure 28) with rapid imaging surfaces up to 60000x magnification (up to x240000 using digital zoom), a spatial resolution of 100 nm and a depth resolution of 10 nm. The two-beam energies of 5/15KV enabled flexibility in terms of sample types. This instrument is equipped with a Bruker Quantax 70 energy-dispersive X-ray (EDX) system that facilitated the analysis of elemental distribution on the surfaces and features exist on the sample.



Figure 28: Hitachi TM3030 SEM and Bruker Quantax 70 EDX

3.4.2 Alicona InfiniteFocusSL

The Alicona infinite focus SL shown in Figure 29 provides non-contact, optical three-dimensional images, based on a focus variation surface profilometer. This instrument features a lens with a magnification of 20x, a vertical resolution of 50 nm, and minimum measurable roughness of 0.15 μm . Furthermore, the consistent high lateral and vertical resolutions are 1mm and 50 nm respectively. The 3D models are achieved through variations in focus that combine the small depth of focus of an optical system with vertical scanning to generate topographical information from focus variation. This instrument was utilised to obtain values of the surface roughness of the experimental samples as well as in the verification of changes in the cutting edge flank of the micro tools. Measurement Suit[®] software (Bruker, 2017) was used to measure the surface roughness and to obtain dimensional measurements of the 3D models developed through the scanning of experimental samples.



Figure 29: Alicona infinite focus SL optical 3D profilometer

3.4.3 Kistler Dynamometer

A Kistler MiniDyn 9256C2 force sensor was used to measure the cutting forces in this study, comprised of four 3-component force sensors, each containing three crystal rings sensitive to pressure in the X, Y and Z directions. The charge signals from the sensor are passed to a multi-channel amplifier type 5080, converting them into voltages translated and plotted by Dynoware[®] software (Kistler, v3.2.0). The workpiece was clamped on the mini-dynamometer, as shown in Figure 30.

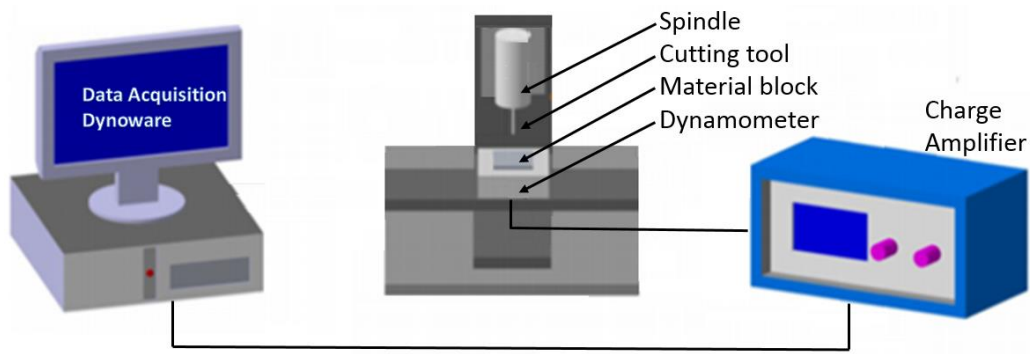


Figure 30: Dynamometer experimental setup

3.4.4 High speed air spindle

The ultra-precision high speed HES810, a single piece motor and spindle construction with an electric drive and ceramic bearing capable of a continuous power output of 350 W, an output torque of 3 Nm over the speed range of 20,000-80,000 rpm and spindle accuracy of 1 μm . High cutting velocity enables the use of tools with smaller diameter shown in Figure 31.



Figure 31: NE211 Series control unit (left), High-speed spindle NAKANISHI -HES810 (right)

3.4.5 Precision scale

Sartorius Semi-Microbalance-R200 D was used for weighing up of tools with a weight capacity up to 205 gm, readability of 0.1 mg and it is equipped with an environment protection glass for a higher degree of repeatability, as shown in Figure 32.



Figure 32: Sartorius Semi- Microbalance R 200 D

3.4.6 Micro end mill

Micro flat, uncoated tungsten carbide (WC) endmills were used in this experiment with a nominal diameter of 1 mm and nominal tool shank diameter of 3 mm. Table 9 presents the geometries of the selected micro end mill tools used in this experiment. Figure 33 shows the schematic diagram of tool geometry.

Table 9: Micro tool geometries used in this experiment

<i>Tool Geometry</i>	<i>Uncoated</i>
<i>Tool diameter (mm)</i>	1
<i>No. of flutes</i>	2
<i>Helix angle (degrees)</i>	20
<i>Rake angle (degrees)</i>	0
<i>Clearance angle (degrees)</i>	17
<i>Tool edge radius (μm)</i>	1.1

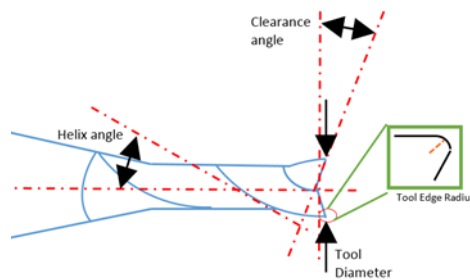


Figure 33: Schematic diagram of Tungsten carbide tool geometry

Chapter 4. Tool wear and tool life prediction in micromilling

4.1 Introduction

The poor performance of micro tools due to their small size and unpredictable wear leads to excessive tool change that effects machining productivity. This is also influencing the accuracy, repeatability and reliability of the machining operation. Since micromilling deals with 1mm tools or less, the strict set of conditions proposed in ISO 8688-2 for the purpose of estimating tool life are impractical; however, the terminology used to describe both the tool wear and machining procedures are still applicable as the wear of micro-tools can be compared with other tools. The criteria detailed in ISO 8688-2 for tools to be classified as the end of their life varies for each case depending on the machining condition, material properties, surface roughness and tool geometry and dimension. Therefore this chapter experimentally investigates the tool wear in micromilling of Titanium Ti-6Al-4V to evaluate the propagation of flank wear and tool deterioration with machining time. Critical wear as to when tools cease to produce satisfactory surface quality and geometry size in the evaluation of tool rejection criteria is also identified.

The tool rejection criteria determined in this chapter are applied as limits to plot tool life as a function of cutting speed necessary for when making comparisons of cutting tools, workpiece and machining parameters at both the design and process planning stage.

This chapter contributes to machining knowledge used in the process planning stage for tool selection and evaluation of optimum cutting speed and tool change interval. Changes to the recommended procedure and condition stated in ISO 8688-2 to predict tool life for precision endmills, applicable to laboratories and factories are proposed. Use of the new procedure is essential to achieve reliable and comparable tool performance data for the comparison of cutting tools and workpiece material.

4.2 Experimental Results and Discussion

4.2.1 Flank wear

Figure 34 and Figure 35 illustrate the impact of cutting speed and feed rate respectively on tool flank wear during slot milling with a constant depth of cut.

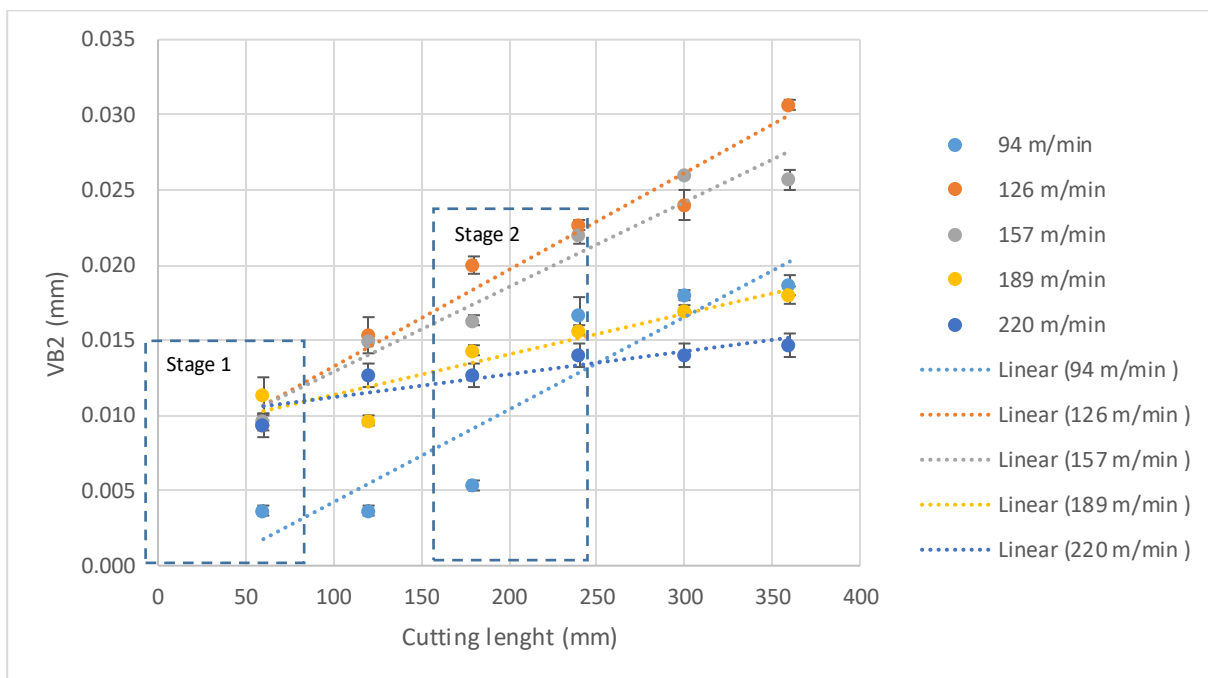


Figure 34: Average width of flank wear land (VB2) recorded for different cutting speeds.

Error bars represent standard deviation.

Figure 34 suggests that within the first 60 mm of slot milling, the lower cutting speed of 94 m/min results in a slower wear rate at stage 1. Whereas the average width of wear land is measured to be 4 μm that is more than 50 % lower than the value measured when using higher cutting speeds. For the tool using the cutting speed of 94 m/min, there is a gradual increase in wear land width up to 180 mm of machining length with a steady material removal process suggesting a controlled wear rate. This is followed by a sudden jump in wear land width which indicates a transition point before the wear rate recovers to a gradual increase. The plot of localized flank wear in Figure 35 suggests the transition point is as a result of 39 μm localized

flank wear that results in the progressive expansion of wear land between 180 mm and 240 mm of machining length and thereafter levels off.

The progressive development of wear land observed for cutting speeds of 126 m/min to 157 m/min indicate the frequent occurrence of localized wear confirmed by fluctuation observed in measured VB3 as indicated by Figure 35. Frequent localized flank wear is observed as the cutting speed increases and therefore progressive wear land was expected for cutting speeds up to 157 m/min. However, the trend line of VB2 points toward an inverse effect in wear land development as cutting speed increases. Therefore an increase in cutting speed for micro tool shows a reduction in the flank wear rate even though frequent localized flank wear is observed in the plot of VB3. The conclusion can be made that higher cutting speed reduce the influence of localized flank wear in development of wear land.

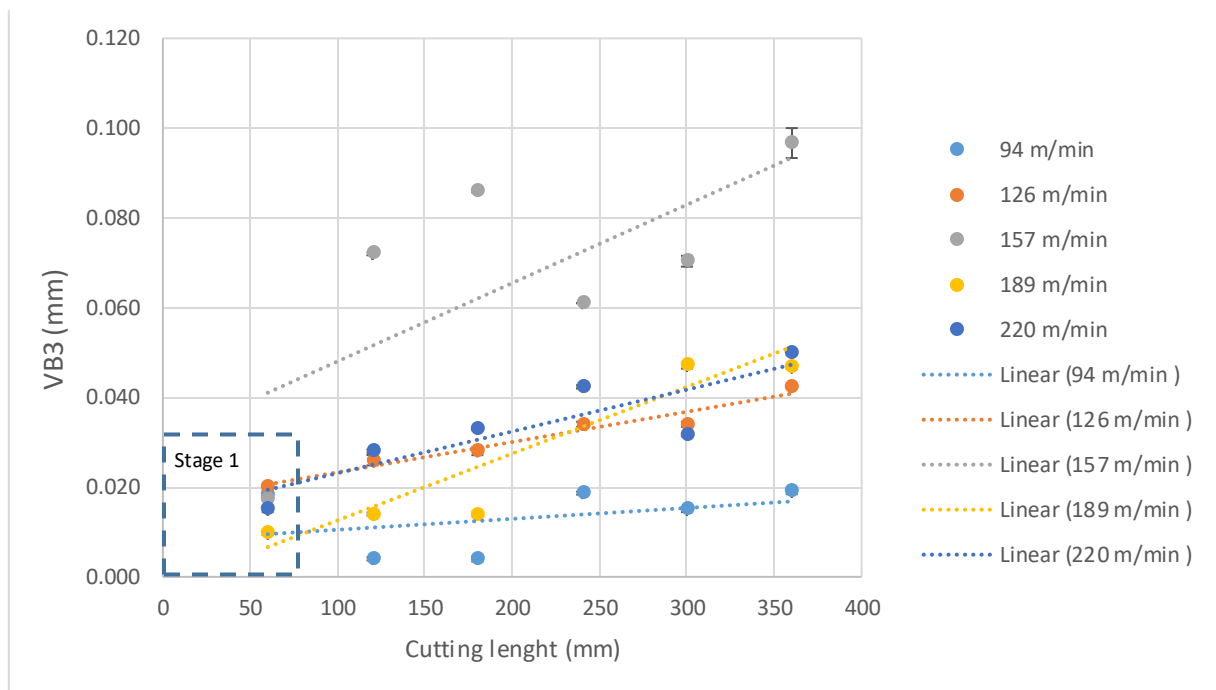


Figure 35: Localized flank wear land (VB3) recorded for different cutting speeds. Error bars represent standard deviation.

Furthermore, a sudden change to the progressive rate of wear land development from cutting speed of 94 m/min up to 189 m/min suggests that in high speed machining there is a niche range of cutting speed. This encourages localized flank wear and significantly increases the material wear trend that must be avoided to improve machining reliability.

Given the sudden changes in wear rate that leads to machining instability and immature tool failure, reduced localized flank wear and gradual development of wear land are the desirable characteristic for reliable flank wear rate. From the observation of flank wear rate, low cutting

speed shows to prolong the tool life by reduced initial flank wear at “stage one” when a new tool is used while adoption of higher cutting speed for the remaining tool life is preferred in micromilling. High cutting speed also shows to minimizing the influence of localized flank wear and sudden transition in the material removal process that often result in tool failure in micromilling.

Similarly, the impact of feedrate on the flank wear was measured and is displayed in Figure 36 and Figure 37.

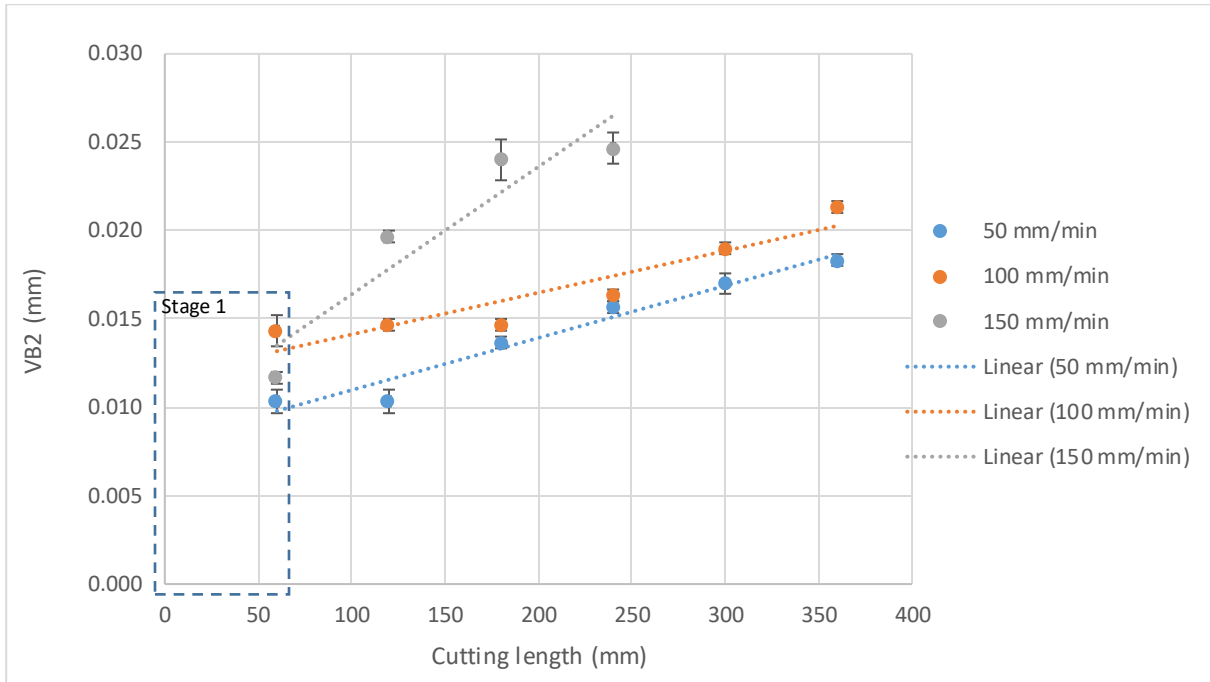


Figure 36: Average width of non-uniform flank wear (VB2) recorded for different feed rate. Error bars represent standard deviation.

The initial progressive development of wear land at stage 1 for a range of feed rates tested shows a rapid wear rate. The small gap between measured wear land width for the tool using both the lowest (50 mm/min) and highest (150 mm/min) feedrate show a similar initial wear rate of 10 to 14 μm . The slope of trend lines in Figure 36 indicates the progressive development of wear land as feedrate increases. The comparison of the trend line for feed rates of 50 mm/min and 150 mm/min shows a substantial reduction in the development of wear land (VB2). The rapid progress of wear land width up to 0.025 mm for the tool using feedrate of 150 mm/min cause a tool failure after 240 mm of machining while localized flank wear up to 0.06 mm was recorded in Figure 37. The wear measured as a result of using a medium feedrate (100 mm/min) suggests that flank wear is encouraged, however, the trend line for VB2 in Figure 36 points towards an improved rate of VB2 in comparison to the other trend lines. Higher progressive

wear rates at speeds of 50 mm/min and 150 mm/min highlight a transition point that suggests an optimal feed rate range for a specific material type and cutting speed to maintain steady machining operations.

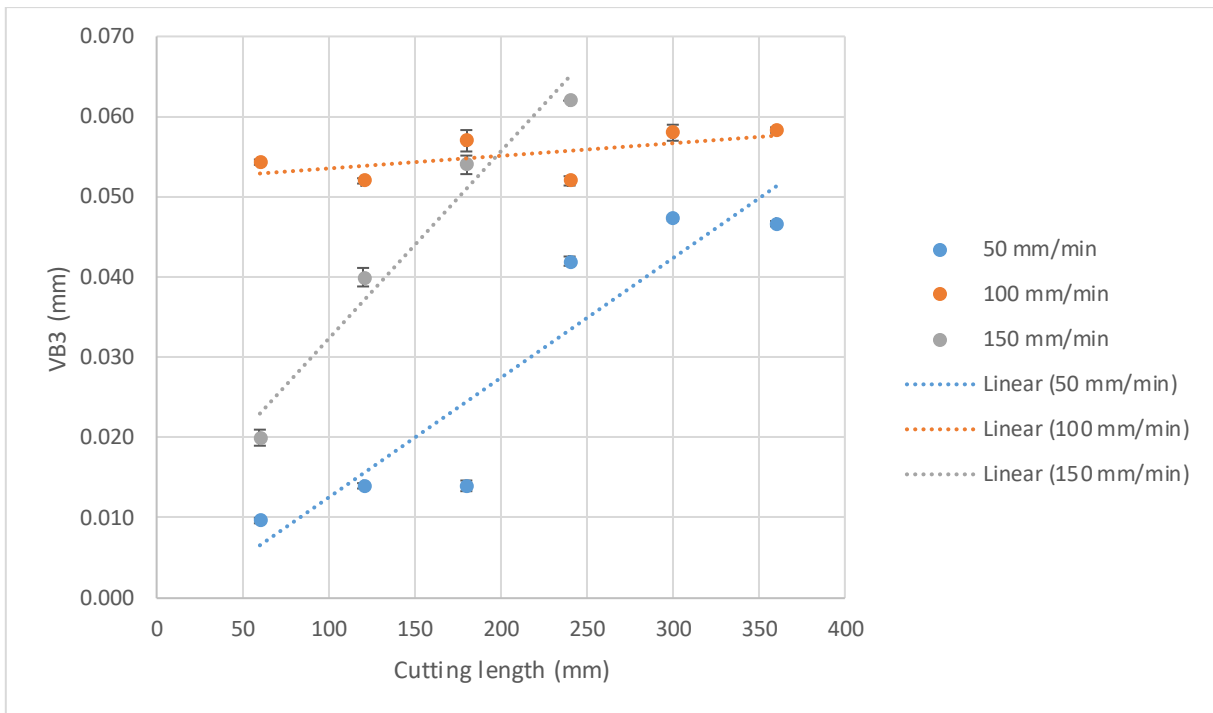


Figure 37: Localized flank wear land (VB3) recorded for different feed rate. Error bars represent standard deviation.

The analysis of flank wear data suggests that high cutting speed and low feed rate are preferred in micromilling as a lower feed rate results in reduced localised flank wear (VB3). Also, high cutting speed minimises the impact of VB3 in the development of VB2 and therefore provides a predictable and controlled flank wear rate.

4.2.2 Tool diameter reduction

The impact of cutting speed and feedrate on the deterioration of tool diameters was measured and used to plot Figure 38 and Figure 39. Figure 38 shows for the initial 60 mm of machining rapid abrasive wear resulted in insignificant tool deterioration where the wear rate reduced for cutting speeds of 94 m/min and 126 m/min. Transition in the initial wear rate can be seen as the lower tool diameter reduced from 999 μm to 993 μm for a cutting speed of 220 m/min as opposed to the reduction to 990 μm as result of using 157 m/min. The close gap between the plot of tool diameters measured as a result of using 188 m/min and 220 m/min suggests that cutting speed above the critical value decreases the impact of cutting speed on tool diameter deterioration. A minimized transition point in the wear rate is observed for cutting speeds of 94 m/min and 126 m/min, after 120 mm of machining; with changes in the trend of abrasive wear

after 120 mm of machining. Furthermore, for the remainder of the machining operation, there is a significant tool diameter reduction rate, highlighting a transition point to an unstable material removal process resulting in rapid abrasive wear.

Although the comparison of the trend line for different cutting speeds suggest that a cutting speed of 157 m/min results in a lower rate of tool diameter deterioration, the initial wear at stage 1 shows sharp abrasive wear up to 990 μm followed by a gradual wear rate that is desirable in micromilling. After 360 mm of machining, the reduction of tool diameter as a result of abrasive tool wear is approximately 25 % less when using a cutting speed of 157 m/min while cutting speeds above and below this value typically result in an 8 % increase.

The level up in the measured value indicates a critical cutting speed where tool deterioration can be minimized. Notably, similar levels of reduction in tool diameter using high and low cutting speeds indicated a similar abrasive wear pattern in the overall machining cycle. For high cutting speeds, there was a more gradual trend in comparison to the steep changes noted for the lowest cutting speed. This results in a sudden transition to wear rate which is not favourable in micromilling. The transition points in wear trend can be translated to tool life criteria in indication to tool change.

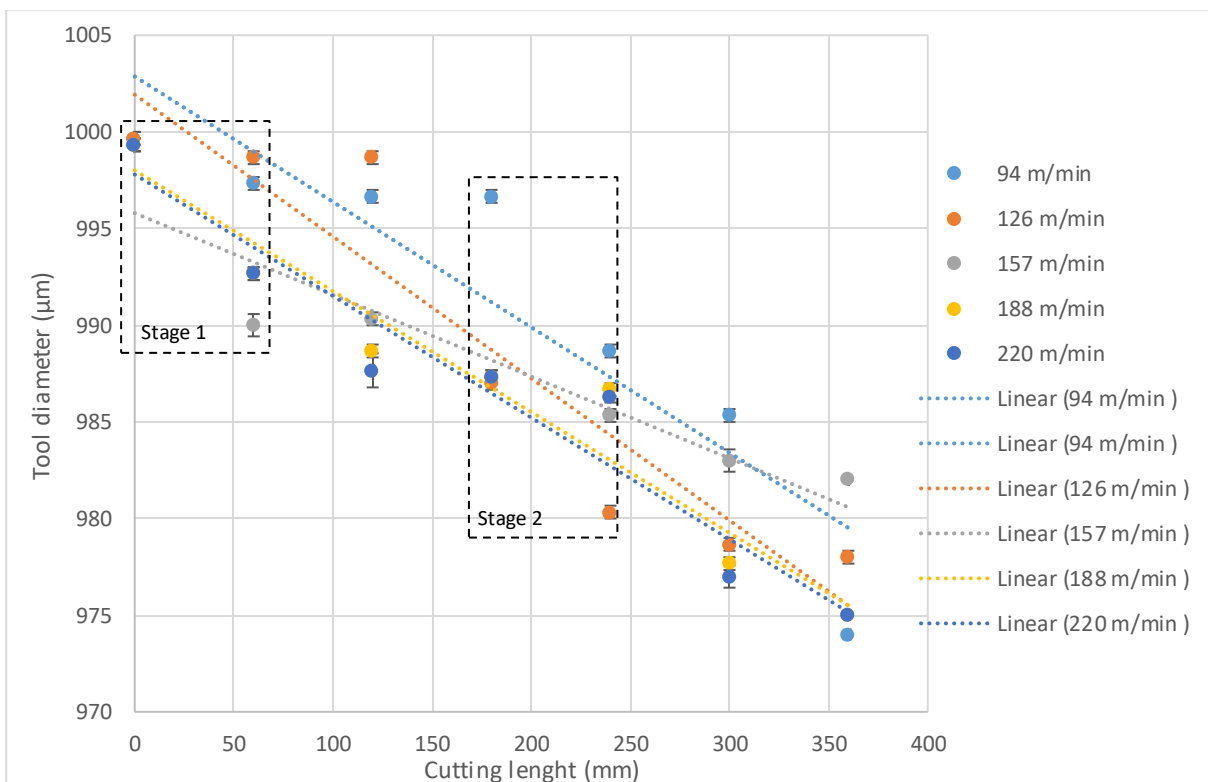


Figure 38: Tool diameters reduction for different cutting speed. Error bars represent standard deviation.

Figure 39 shows the impact of tool diameter deterioration as a result of different feed rates. A similar impact of initial rapid wear was observed for all tools up to 60 mm of machining when using a lower feedrate which significantly reduced the rate of tool diameter deterioration. The additional 7 μm reduction, as well as fluctuations in wear rate up to 360 mm of machining as a result of using a feed rate of 100 mm/min, suggest a change in wear mode where abrasive wear is no longer the main wear mode in this stage of machining with adhesive wear prevailing. Although the lower feed rate of 50 mm/min shows lower initial wear in comparison to using 150 mm/min, a slight improvement in the wear trend is observed for higher feedrate of 150 mm/min. However, tool using a feedrate of 150 mm/min failed after 240 mm of machining. The wear data as a result of different feedrate suggest a change in the wear mode at different stages of machining observed by initial and secondary transition point. The lower feedrate of 50 mm/min resulted in a gradual initial transition and aggressive secondary transition while 100 mm/min had an inverse effect. Adoptive feedrate to advantage from lower initial wear rate as well as delayed transition point are preferred in micromilling where the second transition point can be used as a limiting factor in tool life evaluation.

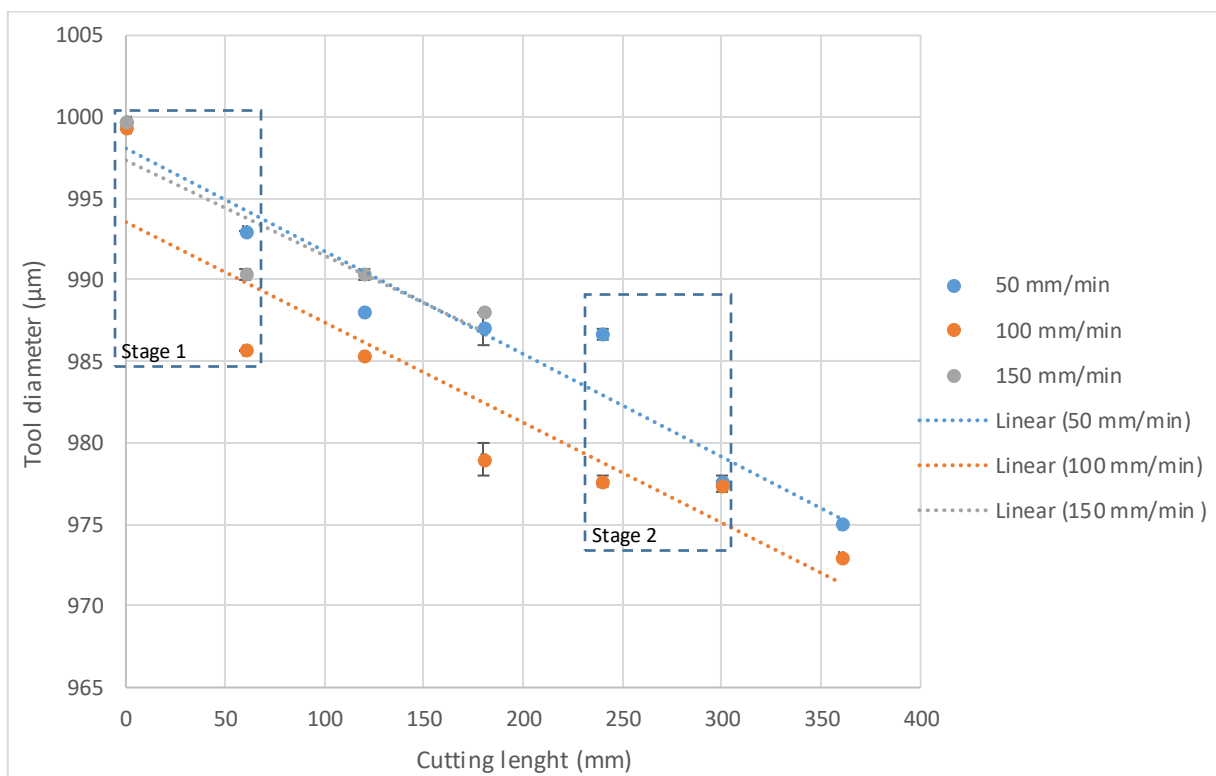


Figure 39: Tool diameter reduction for different feed rates. Error bars represent standard deviation.

In order to observe the resultant machining stability as a result of tool deterioration, attempts were made to measure the width of the machined slot to compare with the tool diameters

recorded in Figure 40 and Figure 41. Due to the common issue with the appearance of burr around the sharp edges along the slots and resultant error, resulting in the inaccurate prediction of side edges, the data plot in Figure 40 and Figure 41 didn't satisfy the accuracy required for direct comparison of tool diameters with resultant slot width. However, the trendline of the plots is compared with the trend of tool diameter deterioration as a result of different cutting speeds and feedrate.

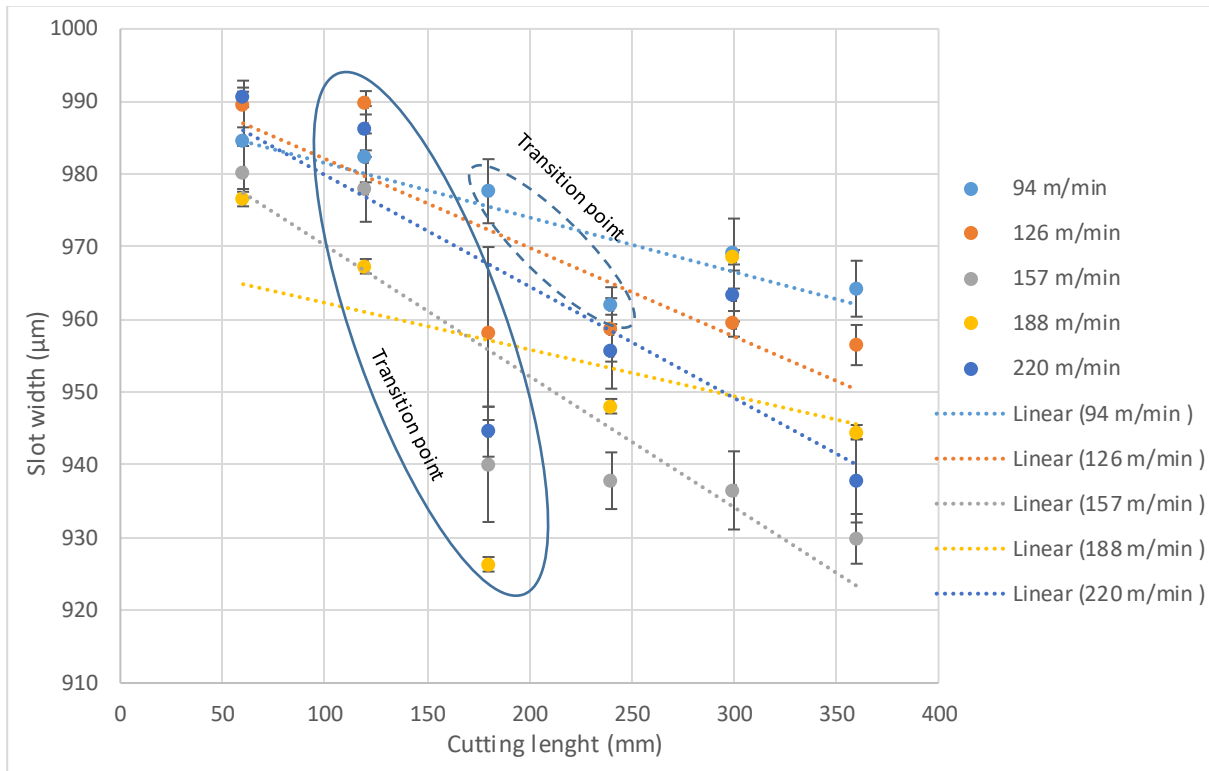


Figure 40: Measured width of the channels machined using different cutting speed. Error bars represent standard deviation.

The comparison of the trend lines for different cutting speeds suggests that a lower cutting speed of 94 m/min results in less tool run out and therefore better machining stability. The increasing slope of the trend lines suggests an increase in tool run out as cutting speed rises while early transition in machining behaviour after 180 mm of machining for cutting speed above 126 m/min can be observed. A similar transition can be observed for tools using a cutting speed of 94 m/min at next stage pass 240 mm of machining. The increase in the width of the slot after the transition points indicates the change of wear mode where the sudden jump suggests adhesive wear when the newly formed edge on the tool as a result of chip and tool welding results in wider slots width. The change in the wear mode and impact of adhesive wear is discussed further in this chapter.

Similarly, the effect of feed rate in relation to the slot width is observed where the data gathered was used to plot Figure 41.

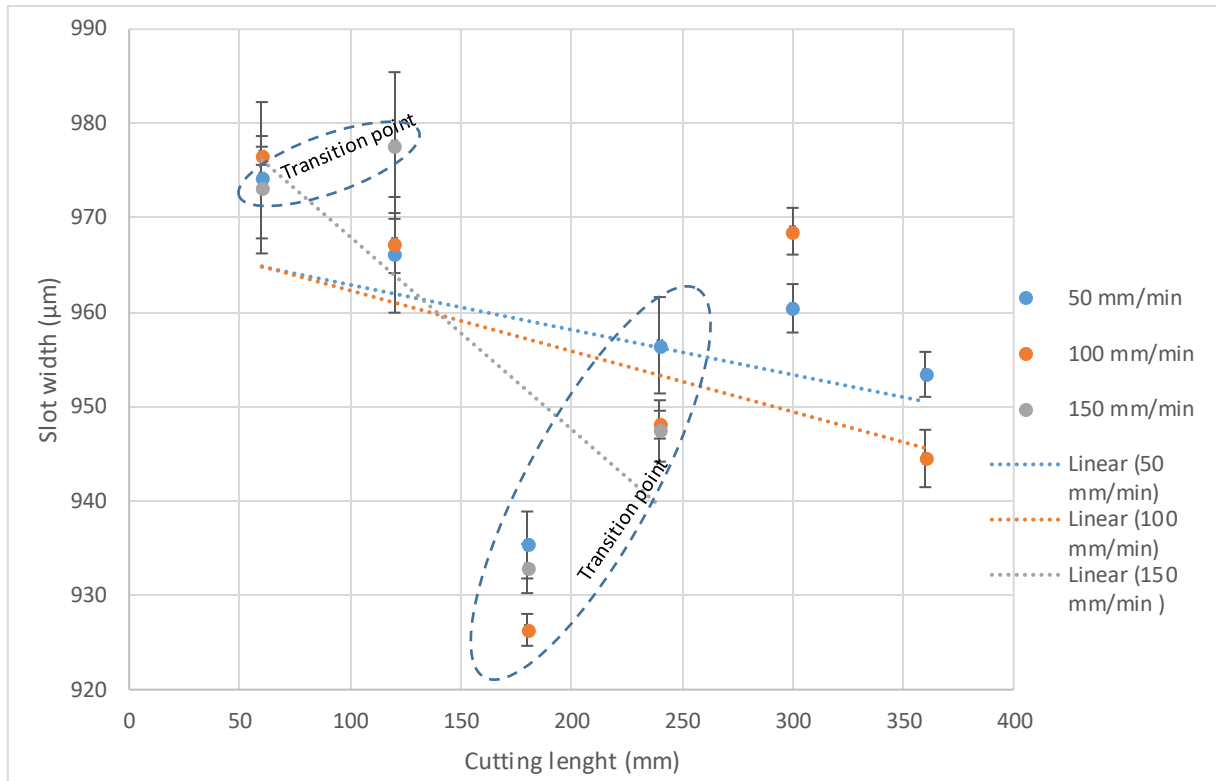


Figure 41: Measured width of channels machined using different feedrate. Error bars represent standard deviation.

The trend lines in Figure 41 for feedrates tested suggest steady machining with lower tool run out as feedrates decrease while indicating a direct relationship between tool run out and feed rate. An increase in feed rate encourages an early transition point where the wear mode changes between abrasive and adhesive, as indicated by the lower measured slots width up to 180 mm of machining, confirming the abrasive wear mode. While an increase in the width of cut up to 300 mm of machining suggests adhesive wear further discussed later on in this chapter. A similar transition pattern of initial tool wear followed by a transition point, where tools undergo rapid abrasive wear with a change to adhesive wear, is observed for the range of feedrate tested. Therefore, it can be said that feed rate has only a minor effect on the tool wear pattern.

4.2.3 Cutting edge radius

The presence of size effect as a result of the tool edge radius exceeding the minimum chip thickness requirement indicates the significance of tool sharpness in micromilling. Therefore the impact of cutting speed and feedrate on the deterioration of cutting edge radius is measured and used to plot Figure 42 and Figure 43.

During the first stage, up to 60 mm of machining, the impact of cutting speed on tool edge deterioration was shown to be insignificant, contradicting with the initial wear behaviour suggested in relation flank wear. In the second stage, up to 180 mm of machining, a significant jump in the edge radius for cutting speeds above 126 m/min and above shows a change in wear mode. Meanwhile, for the tool using 94 m/min, a similar wear trend continued up to 240 mm of machining indicating abrasive wear that continued to be the dominant wear mode.

The regular edge radius deterioration for lower cutting speeds of 94 m/min and 126 m/min throughout machining minimized changes in the wear mode resulting in controlled progressive wear. Despite the significant jump in edge radius for higher cutting speed of 188 m/min and 220 m/min, little changes in edge radius were observed up to 300 mm of machining. However, the drop in measured edge radius for tool using the cutting speed of 220 m/min indicated a change from abrasive to adhesive wear, with the formation of a temporary tool edge observed. This was further confirmed by a second transition at stage 3 after 350 mm of machining.

As the cutting speed rises, it was expected to see a direct relationship with a significant increase in wear trend featuring from multi transition points throughout machining. However, a lower progressive trend for cutting speed of 126 m/min shows a prime range of cutting speed that significantly impacts the tool edge deterioration and resultant edge radius increase up to 15 μm .

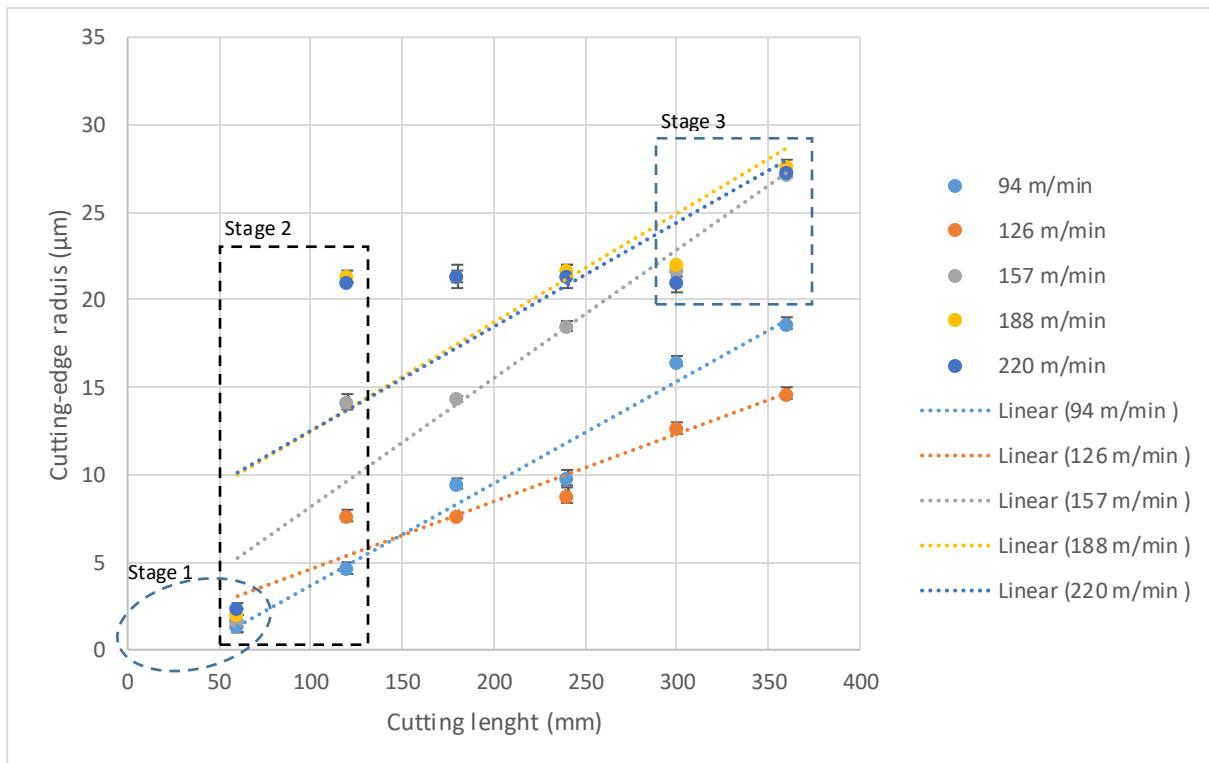


Figure 42: Tool cutting edge radius using different cutting speed. Error bars represent standard deviation.

The lower cutting speed and resultant smaller initial edge wear, improved machining stability with gradual wear rate allow a better prediction of edge radius ideal in process planning. The overall experimental results suggest that in micromilling a lower cutting speed should be used at the beginning to benefit from reduced initial edge wear, after which cutting speed could be increased to benefit from improved machine stability and gradual progress of edge wear. This could provide a predictable overall progression of cutting tool edge wear which is desirable in process planning.

Similarly, the impact of feedrate on the deterioration of the cutting edge radius was measured and used to plot Figure 43. The trend line for tool edge deterioration was shown to be proportional to feed rate as a sharper slope is observed as the feed rate rises. Within the first transition at stage 1, the higher feed per tooth resulted in a lower initial edge deterioration. However, the progressive trend of wear was observed for the remaining machining up to 300 mm when the tool failure occurred.

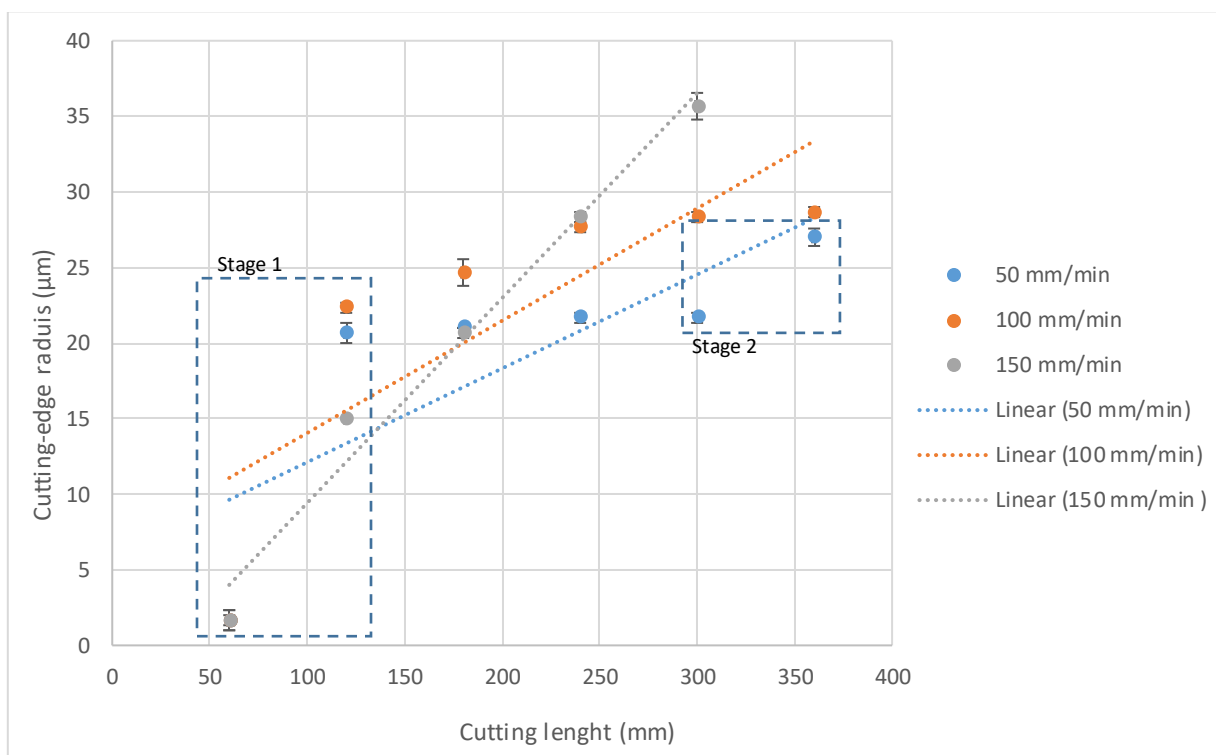


Figure 43: Tool cutting edge radius using the different feed rate. Error bars represent standard deviation.

Following an initial increase highlighted at stage 1 and subsequent levelling off, lowering the feedrate shows to have reduced the tool edge wear up to 300 mm of machining. The insignificant changes in edge radius up to 300 mm of machining followed by a transition point at stage 2 for feedrate of 50 mm/min shows the result of build-up edge followed by a sudden

change of adhesive wear across the flank face. The gradual increase in edge radius using feedrate of 100 mm/min suggests that abrasive wear dominates along the tool cutting edge and is therefore preferred in micromilling.

Feedrate shows to have a direct relationship with tool edge deterioration where the progress of edge deterioration becomes more regular as the feed rate increases. The rapid rate as a result of 150 mm/min in comparison to controlled trend as a result of 100 mm/min suggests a transition point to wear progression rate. Therefore, the optimum range of feed per tooth must be selected based on the cutting speed which results in the minimum build-up edge effect and should not exceed the limit where feedrate results in aggressive tool edge deterioration.

The accurate estimation of cutting edge radius and predictable edge deterioration is vital for control of material removal rate. The gradual wear progress suggests the dominant abrasive wear along the cutting edge, while the transition in the wear rate is a result of an increase in machining pressure due to build-up edge. The choice of a variable feed rate seems to be feasible for micromilling, as a new tool initially experiencing significant wear can benefit from a reduced wear rate by using high feed rates. Lowering the feed rates for subsequent machining can stabilize and reduce the rate of wear progression and effectively lengthen the tool life while providing the machining stability and predictable tool edge radius.

4.2.4 Surface roughness

The impact of cutting speed and feedrate on the finished surface roughness (R_a) was measured and used to plot Figure 44 and Figure 45. The effect of cutting speed, low and high, 94 m/min and 220 m/min respectively, indicated a fluctuation in measured surface roughness throughout machining intervals. Within the first stage, up to 60 mm of machining, a cutting speed of 220 m/min resulted in lower surface roughness (> 40 nm) in comparison to the resultant roughness measured for lower cutting speeds (519 nm). The lower R_a value measured as the machining progressed up to 120 mm suggests an early transition that results in the unstable material removal process and therefore rapid surface deterioration up to 240 mm of machining length. Under a lower cutting speed of 94 m/min a similar pattern was observed where the transition point occurred after 240 mm of machining, after which, a rapid increase in the rate of tool deterioration was observed.

After 240 mm of machining a significant jump marked in Figure 44 as stage 2, highlights the change in material removal process where the signs of the impact is proportional to cutting speed. Thereafter up to 360 mm of machining, the rate of recovery is significantly higher as the cutting speed increases. The impact of cutting speed on surface roughness shows that a cutting speed

of 188 m/min results in a better overall surface finish that features a gradual increase in surface deterioration. The machining transition at stage 2 indicates a critical change for the range of cutting speed between 126 m/min and 188 m/min, where after this point unstable machining results in rapid surface deterioration. The transition point and key stages identified for surface roughness can be used as a limiting factor in the evaluation of tool life.

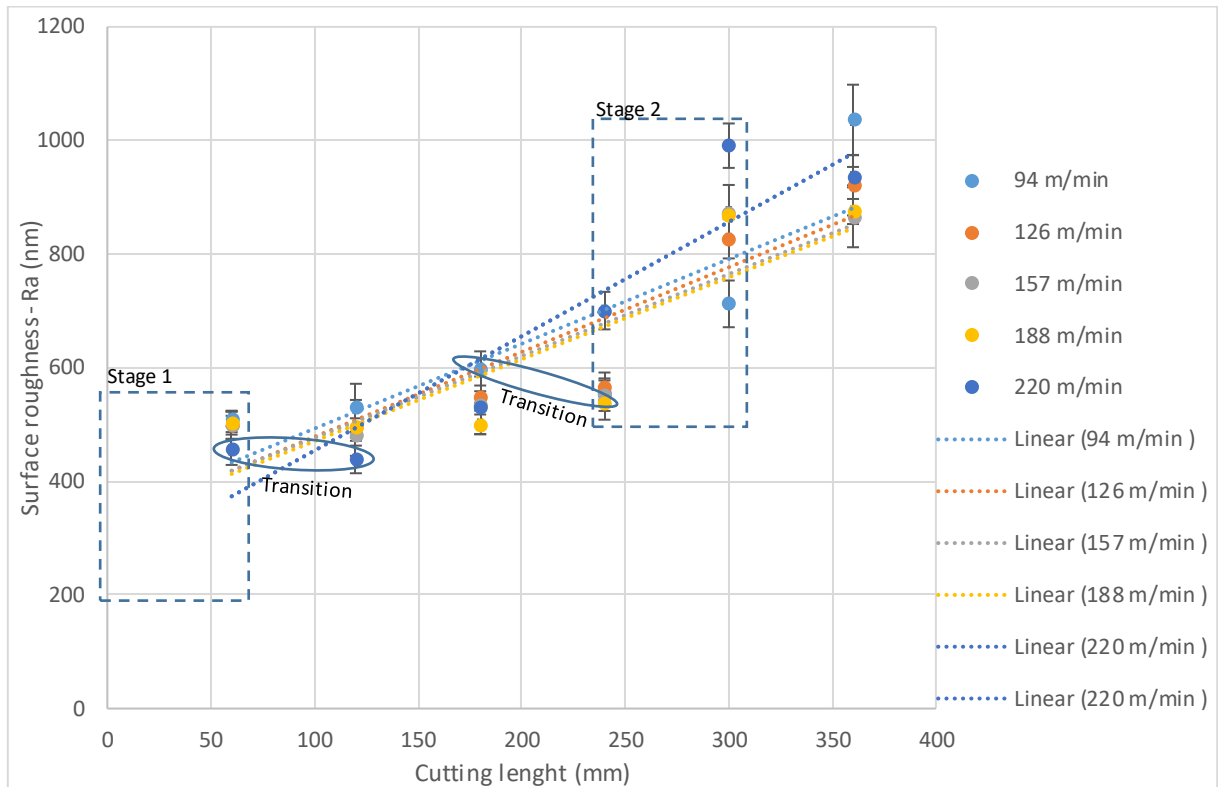


Figure 44: Measured surface roughness for different cutting speeds. Error bars represent standard deviation.

The impact of feed rate on the surface roughness was similarly measured, with the mean value of surface finish for feed rates of 50, 100 and 150 mm/min shown in Figure 45.

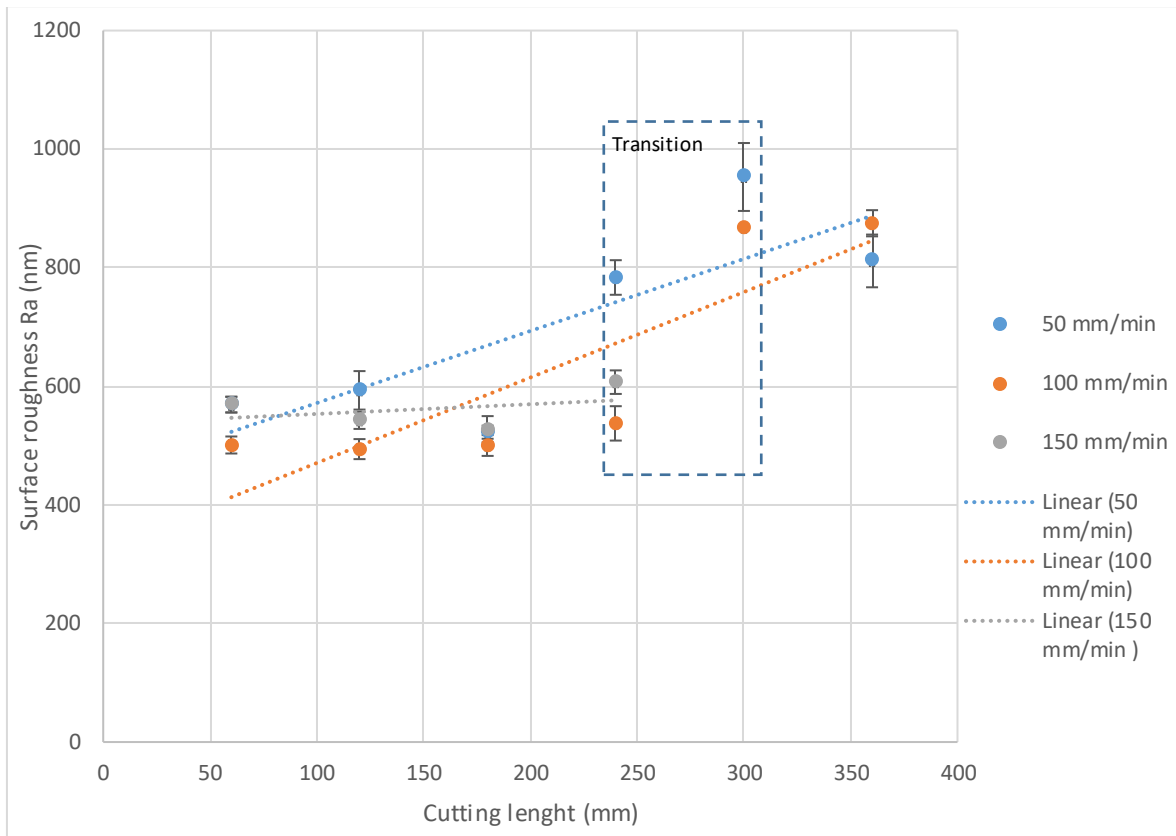


Figure 45: Measured surface roughness for different feed rates. Error bars represent standard deviation.

The impact of feed rate on surface roughness was shown to be negligible as the data recorded was close and showed a similar trend in surface deterioration. The only distinct difference after 240 mm of machining was a slight improvement in the surface finish as a result of higher feed rates, whilst an increase in the surface roughness value indicated a transition approaching 240 mm of machining that resulted in a variation of tool performance. A further conclusion that can be made from the trend of machining data is that there is an optimum feed rate range for individual cutting speeds; with data from the transition points suggesting the change of wear mode from abrasive wear to adhesive wear. Such transitions in surface roughness are not favourable in micromilling as secondary finishing process is not possible. Therefore, the transition point in surface roughness can be used as metrics for tool change interval.

4.2.5 Volumetric change

The transition observed for the trend of tool wear in relation to flank wear and tool diameter deterioration suggests a shift in wear mode as machining progressed. Therefore in this section, the impact of cutting speed and feed rate in relation to the volumetric change of tools was used to plot Figure 46 and Figure 49. In addition, chemical characterisation of the flank face is

qualitatively compared to tool volumetric changes as machining progressed shown in Figure 47 and Figure 48.

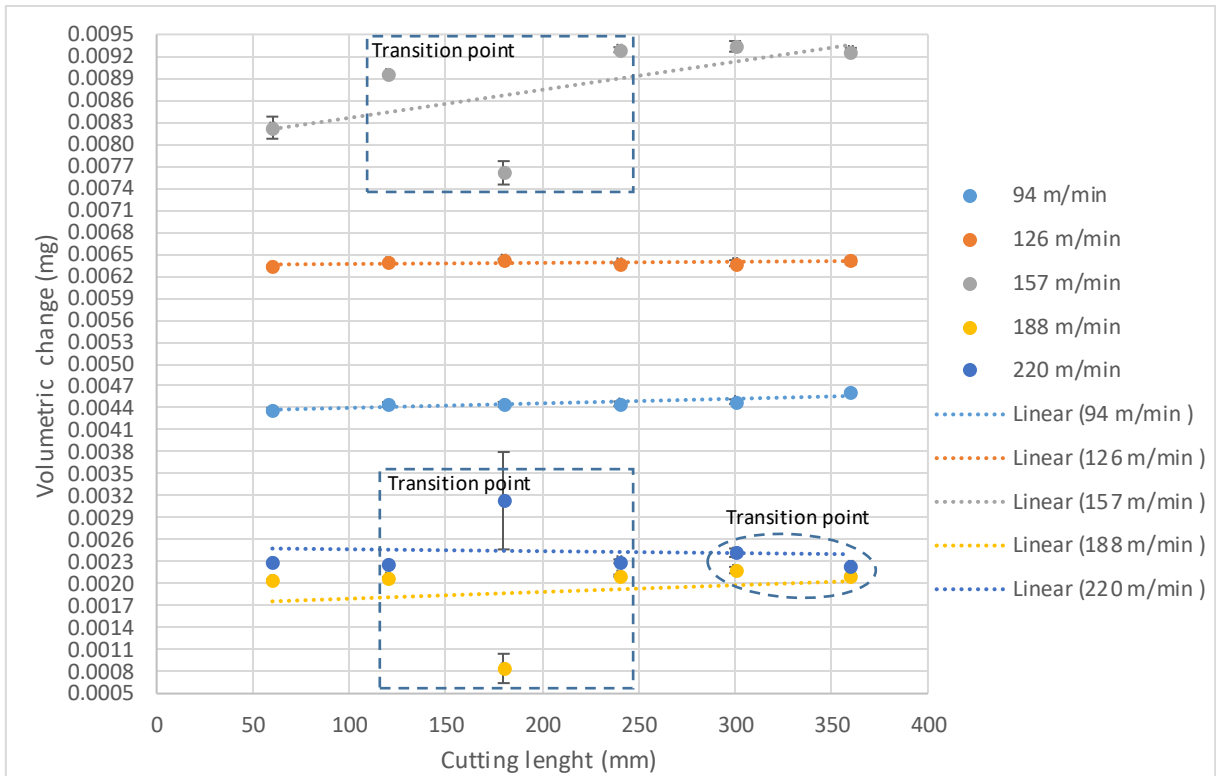


Figure 46: Volumetric change of micro-tools at different cutting speeds. Error bars represent standard deviation.

The positive trend for volumetric change of tools suggests abrasive wear is the dominant wear mode throughout machining whilst negative drops in weight indicate a switchover of wear mode to adhesive wear as machining progresses. The gradual volumetric change as a result of cutting speed of 94 m/min and 126 m/min shows, lower cutting speed result in lower tool wear dominated by abrasive wear throughout machining. However, the progressive wear rate indicated by the sharp trend line as cutting speed rises up to 157 m/min combined with the negative volumetric change up to 14 μm shows that the rate of abrasive wear was enhanced by adhesion as the machining progressed. Due to a large error in the weight measurement as well as the gradual weight change in line with earlier volumetric change as machining progressed up to 300 mm of machining the initial transition point for the wear trend using a cutting speed of 220 m/min was dismissed. However, during the second transition point, the indication of adhesive wear can be seen for cutting speeds of 188 m/min and above suggesting a delayed shift in wear mode resulted from an increased cutting speed. As a result of the associated high temperature and pressure between the tool face and material, chip welding is expected across

the flank face and tool edge, therefore, Figure 47 and Figure 48 show the chemical characterization of tool flank face for the range of cutting speeds tested.

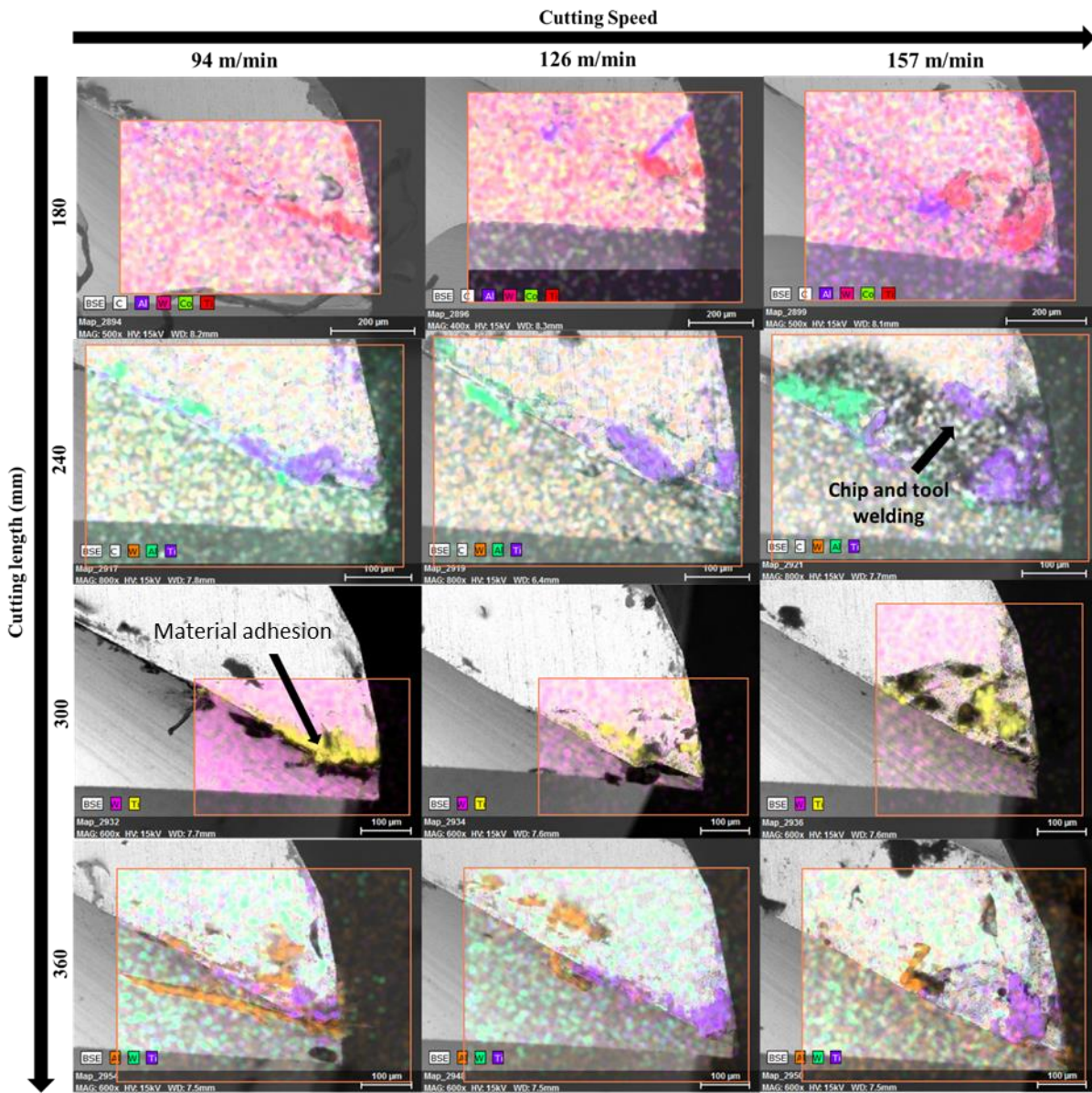


Figure 47: SEM micrographs and EDX spectra of tools for different cutting speed

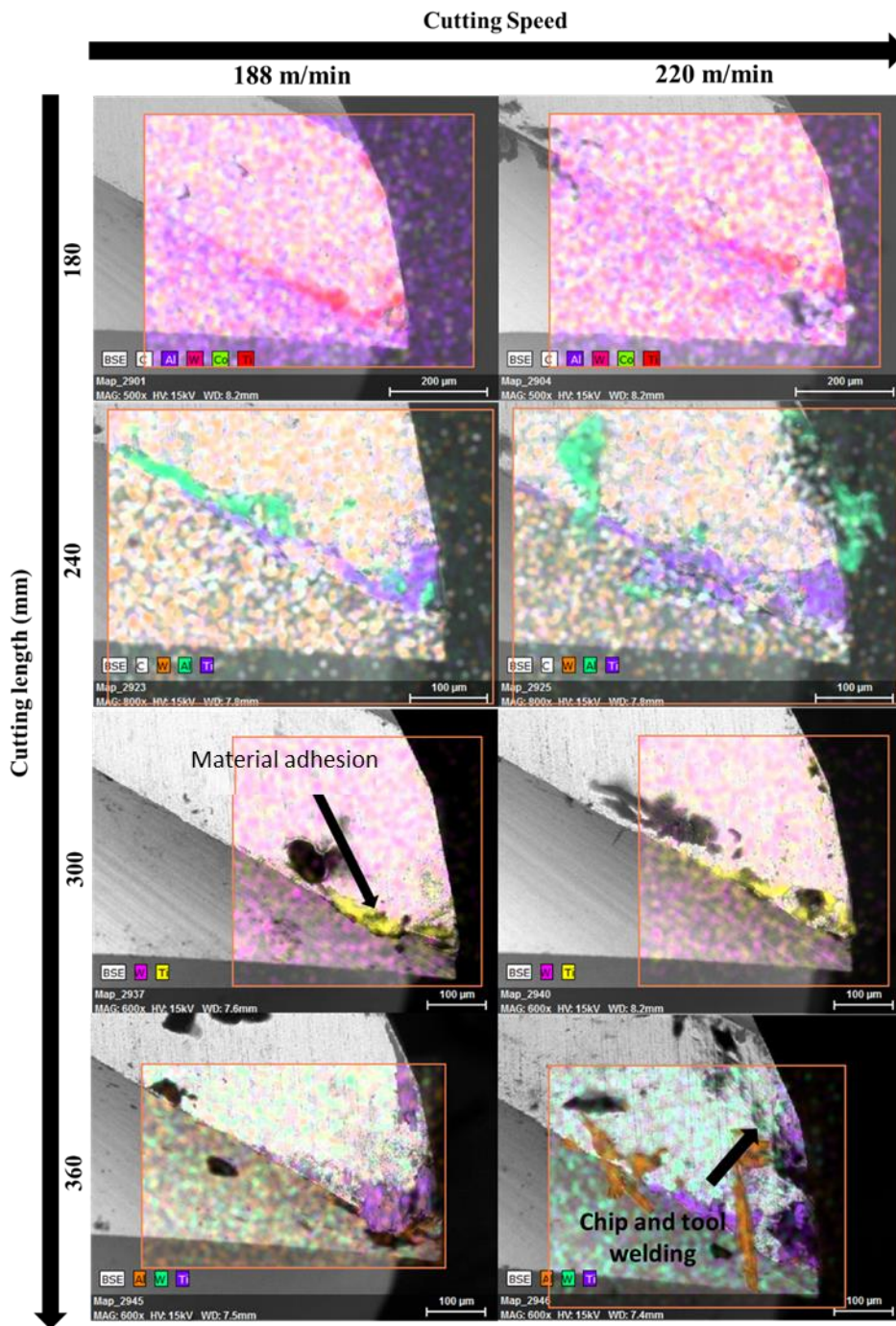


Figure 48: SEM micrographs and EDX spectra of tools for different cutting speed

The colour coding method used for material characterization for individual EDX image to identify chip welding show by the trace of workpiece material –Titanium marked as “Ti” across the flank face and along the tool edge as machining progressed. The comparison of tool volumetric change data with EDX images for each tool shows that lower cutting speeds up to 127 m/min results in chip build up along the cutting edge of the tool. The progressive wear rate for a tool using the cutting speed of 157 m/min could be due to the widespread of chip and tool welding across the flank face from early stages of machining. As the cutting speed increased, a

delay in the spread of chip welding across the flank face up until 300 mm of machining was observed whilst chip was shown to adhere in the form of build-up edge. The transition point in the volumetric change of tools, shown in Figure 46, is in agreement with the change in dominant wear mode to adhesive wear as chip and tool welding are present taking indicated by the trace of chip welding spread across tool flank face as shown in Figure 47 and Figure 48. Similarly, the impact of feedrate on the volumetric change of tool is used to plot Figure 49.

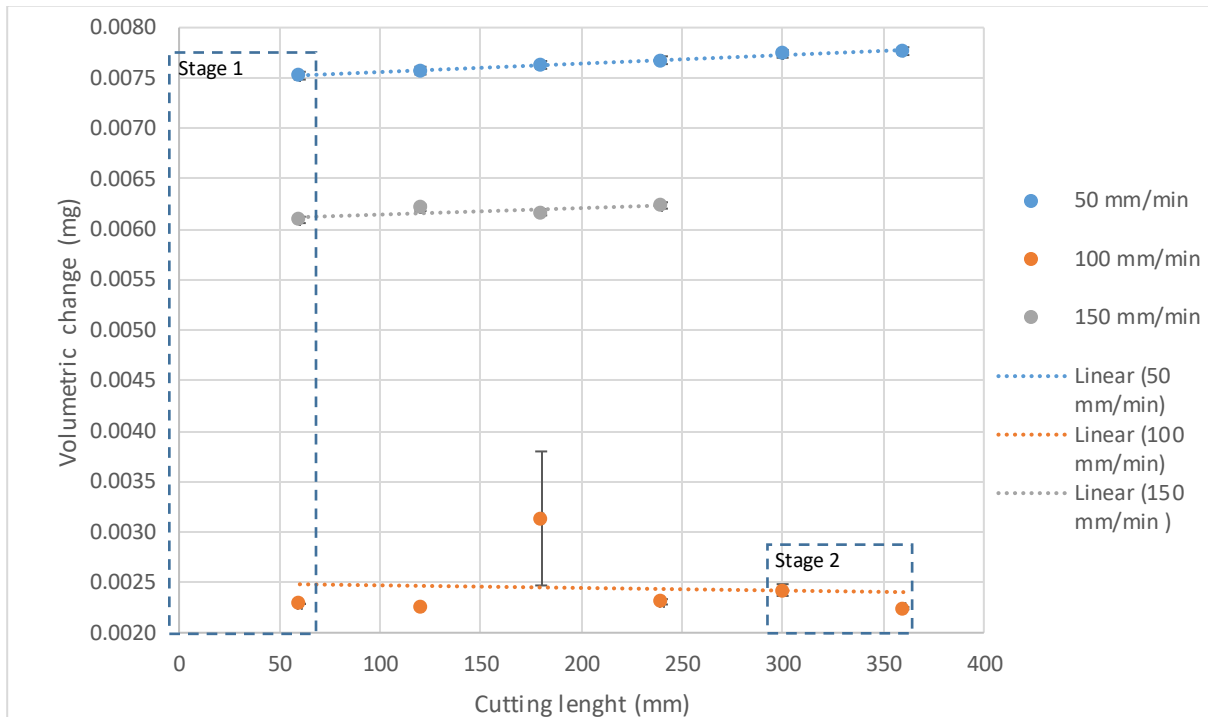


Figure 49: Volumetric change of micro-tools at different feedrate. Error bars represent standard deviation.

The volumetric data gathered for tool using feedrate of 50 mm/min suggests gradual abrasive wear indicated by the positive trend line for volumetric change rate. The increase in feed rate up to 100 mm/min resulted in a transition point after 300 mm of machining where a drop in the volumetric change to 2.5 μg suggests chip and tool welding. The jump in the volumetric change up to 3.2 μg at 180 mm of machining has been dismissed due to the large error bar and measured values for the following stages were in line with the wear trend predicted. As the feedrate was raised to 150 mm/min, a similar gradual abrasive wear was observed up to 240 mm of machining after which tool failure occurred. The impact of lower and higher feedrate shows a similar initial abrasive wear trend where tool failure, as result of using a higher feedrate, was due to the change in wear phenomena not studied in this experiment.

The observation for chip adheres and chip and tool welding by using the chemical characterization of tool edge and flank face as a result of different feed rates is shown in Figure 50.

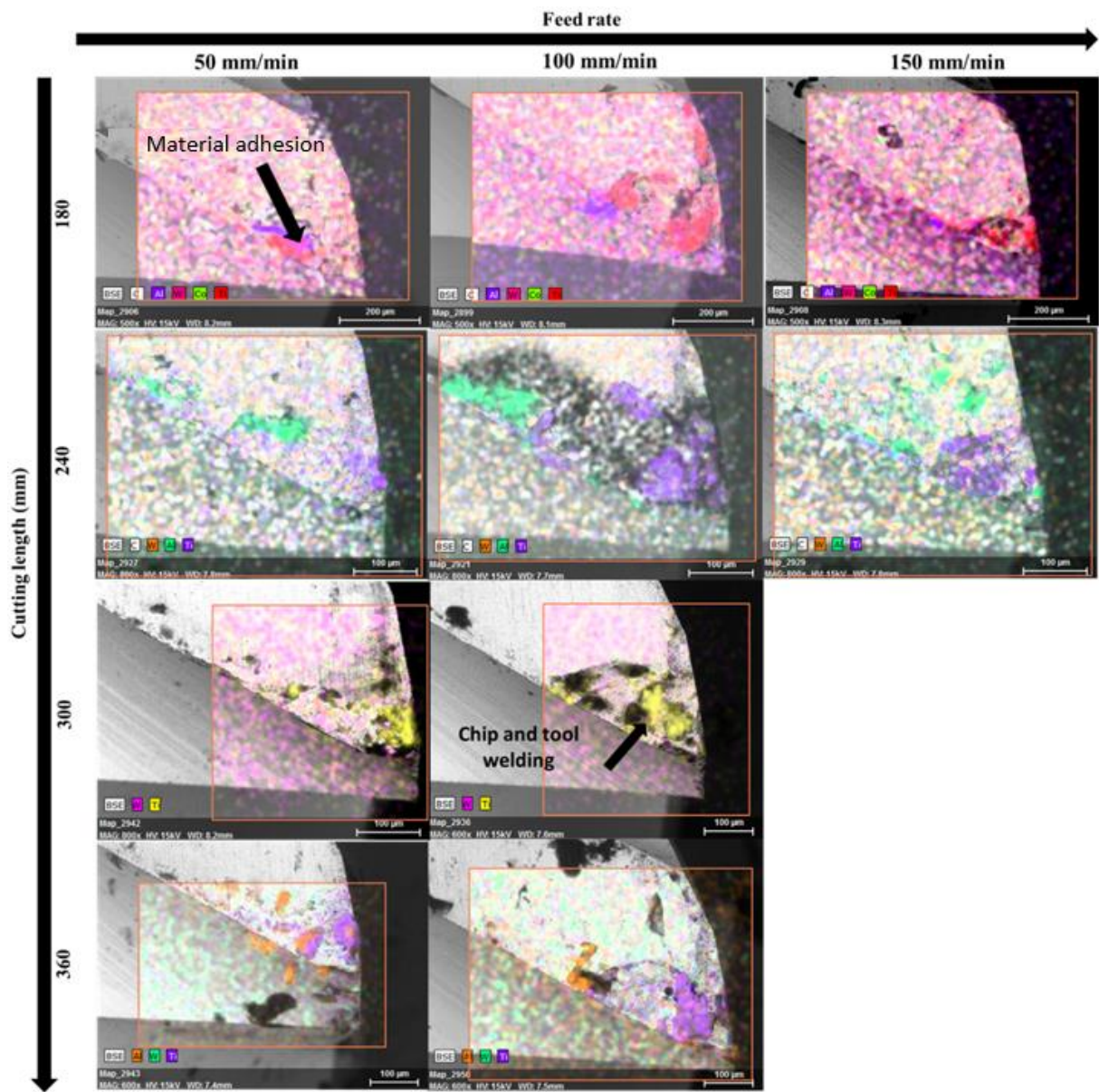


Figure 50: SEM micrographs and EDX spectra of tools for different feedrate

A lower feedrate showed a reduced trace of workpiece material –Titanium showing across the flank face of the tool (represented by colour pink, purple, yellow and purple for cutting length of 180 mm, 240 mm, 300 mm, and 360 mm respectively in Figure 50), also confirmed by the volumetric change data represented in Figure 49.

In observation of adhesive wear for tool using feedrate of 150 mm/min, a significantly lower trace of titanium was observed in comparison to EDX images for tool using feed rate of 100 mm/min suggesting that the mechanism for tool failure may not be due to a transition in the

wear mode. The fluctuation in volumetric change for tool using the feed rate of 100 mm/min fit the trend shown in Figure 50 for the appearance of chip and tool welding as machining progressed across the flank face. Lower feedrates are therefore preferred in micromilling as they benefit from a gradual trend of abrasive wear, indicated by volumetric change data, combined with a reduction in both the temperature and pressure which are associated with a corresponding adhere of chip across the flank face indicated by a reduction in the trace of Titanium.

4.2.6 Discussion of tool wear

All endmills used in this experiment exhibited a significant volume loss around tool edge and reduction in effective tool diameter. The comparison of wear in relation to different cutting speeds and feedrates show non-uniform flank wear as a result of the intense friction that occurs between the flank face and workpiece surface. Abrasive wear was shown to be the dominant wear mode for all tools where a different progression rate of VB2 and VB3, in relation to cutting speed, showed a similar wear pattern. The wear pattern of endmills in the machining of Titanium are grouped into three stages. At the initial stage when tools are new, rapid abrasive wear results in the progressive development of flank wear-VB2 despite the fact that lowering the cutting speed shows to reduce the wear progression by 60 %. The lowest wear land width of 4 μm was measured as a result of using the lower cutting speed of 94 m/min as opposed to wear land width progressing up to 10 μm as cutting speed increased.

The machining phase up to “stage two” can be described as stable machining where the trend line for flank wear shows an inverse relationship between wear land development rate and cutting speed. Following the transition point at the second stage of machining and resultant rapid flank wear at the third stage, the inverse relationship between cutting speed and wear land progression was maintained indicating a lower rate of adhesive wear to the tool and therefore most stable machining as the cutting speed increased. After 340 mm of machining, the minimum wear land width of 150 μm was measured for tool using the cutting speed of 220 m/min whilst the maximum wear land width of 310 μm was observed for tool using the cutting speed of 126 m/min.

The multi-stage wear pattern observed for flank wear shows a good agreement with machining performance reported for hard to cut materials such as hardened steel [82]. The transition points in flank wear trend are as a result of adhesive wear across the flank face where the impact of build-up edge and chip adhere along the cutting edge are negligible on the progression of flank wear. In machining of titanium, the failure mode for tools is believed to be chipping where in

the literature other failure modes such as micro cracks and notch wear are reported. However, no evidence was found to suggest that failure modes other than chipping occurred in this study [87, 131]. The dominant wear mode was identified as abrasive wear where multi-stage wear rates show demand for variable cutting speed and feed rate subject to tool condition and machining stage. When the tool is brand new, the selection of lower cutting speed reduces the initial progressive flank wear, thereafter as machining continues, a higher cutting speed decreases the impact of adhesive wear and eases the progress rate of wear land. Consequently, using a variable cutting speed in micromilling may well result in predictable wear behaviour which is critical for the evaluation of tool life.

The effect of tool wear in relation to tool diameter and cutting edge radius shows a multi-stage reduction rate for all tools, where a significant reduction in tool diameter and increase in cutting edge radius was observed. At the initial stage, when tools are new, lowering the cutting speed showed to significantly reduce the reduction rate which further resulted in a second stable stage of machining until the transition point at stage 2. Up to this point, it could be said that there is a direct relationship between the reduction rate and cutting speed. After the second transition in the third stage, rapid tool diameter reduction is observed where no link between cutting speed and reduction rate can be found. The comparison of direct tool measurement with the method used in the measurement of slot width suggests that slot profile does not accurately describe the tool diameter reduction. Hence, a direct measurement of tool diameter is recommended to be used in micromilling. After 360 mm of machining both the lowest and highest decrease in tool diameter were measured; 18 μm for cutting speed of 157 m/min and 26 μm for cutting speed of 94 m/min. Whilst a cutting speed of 220 m/min results in the highest rate of tool diameter reduction. Similar tool performance is reported in the investigation of micro machinability of copper where the percentage tool diameter reduction dropped by half when high cutting speed and low feedrate are selected [132].

Similarly, three stages in edge radius deterioration are followed from tool diameter reduction wear behaviour. Where, the inverse relationship between feedrate and tool edge deterioration rate suggest reduced feed rate and therefore increased chip per tooth, improving machining stability. The direct link between cutting speed and the initial increase in edge radius is observed; as well as, the deterioration rate during stable machining shows that lower cutting speed is favoured in micromilling. The gradual deterioration of tool edge radius carried out to the third stage of machining, for lower cutting speeds of 94 m/min and 126 m/min, suggest resultant stable machining that increases the reliability of data used in cutting edge radius prediction that is key to avoid the violation of minimum chip thickness in micromilling. The

sudden initial jump in tool edge radius up to 22 μm for tools using cutting speed above 188 m/min suggests, after a certain cutting speed similar initial tool edge deterioration is expected that follows by a level off in stable stage before entering the rapid edge deterioration. After 340 mm of machining, the lowest and highest edge radius measured is 14 μm for tool using the cutting speed of 126 m/min and 28 μm for tool using the cutting speed of 220 m/min respectively.

Adhesive wear is a common issue in micromilling caused by high friction between tool edge and workpiece that results in a sudden change in both wear rate and wear mode in micromilling. The trend line of tool volumetric change confirms gradual wear as a result of lower cutting speed compared to higher cutting speeds which demonstrated an inclining trend line, thus suggesting a rise in adhesive wear rate. The qualitative comparison of volumetric change trend lines with SEM micrographs of tools displays the existence of titanium that suggests chip and tool welding across tool flank face. The appearance of titanium on the parameter of wear land due to abrasive flank wear confirm the enhancement of wear rate due to chip welding.

At the early stage of machining, uniform build-up edge can be observed while as the flank wear progresses chip welding around the perimeter of wear land is observed. Reducing the cutting speed shows to significantly reduce the adhesive wear by lower chip welding across the flank face, believed to be as a result of lower flank wear land development whilst steady growth of build-up edge is observed as machining progressed. The effect of build-up edge shows a similar trend reported for micromilling of mild steel where a lower cutting speed is reported to encourage build-up edge [133].

The absence of build-up edge is preferred in the micro surface generation as surface roughness depends on the sharpness of the tool. SEM micrograph of tools shows lower build-up edge formation along the tool edge as cutting speed rises up to 220 m/min with an improvement in the trend line for the average surface roughness as the cutting speed increased, as expected. Transition points were observed in the surface profile of slot using a cutting speed of 220 m/min. It is thought that a transition point is due to chip adhere on the surface due to the degree of rubbing and burnishing that occurs along the machining surface. A similar conclusion is made by [134] suggesting that the transition point along the surface roughness are due to an adhesive effect of build-up edge on the machined surface. After 360 mm of machining, the lowest average surface roughness (0.8 μm) was measured for a moderate cutting speed of 188 m/min as a result of lower chip welding to the surfaces. The highest (1.03 μm) was due to the increased pressure and friction resulting from the low cutting speed.

Overall, machining parameters significantly affect tool wear. The wear pattern on the flank face and active edge radius are shown to overrule the material removal process. From the machining behaviour observed in this experiment, the adaptive control of machining parameters is essential to regulate tool wear rate observed across three stages of initial, stable and rapid wear. High cutting speeds and low feed rates improve cutting tool endurance by extending the period of stable machining and lowering the wear rate due to lower chip and tool welding effect and reducing the impact of build-up edge on flank wear land development.

4.3 Tool life prediction

Tool life is defined as the duration of effective cutting time after which the tool cannot deliver the machining performance that fulfils the quality standards required of the finished part. Following the recommendation of ISO 8688-2 in the plot of tool life as a function of cutting speed, limiting criteria is recognised by the transition in critical wear obtained from stable to rapid tool wear found in the plot of wear data. The maximum tool wear for each machining criteria are set out as below:

- Flank wear $> 27 \mu\text{m}$
- Tool edge deterioration $> 0.03 D$
- Average surface roughness(R_a) $> 1 \mu\text{m}$

Used as a limiting factor in the evaluation of machining time to plot the vT graph in Figure 51.

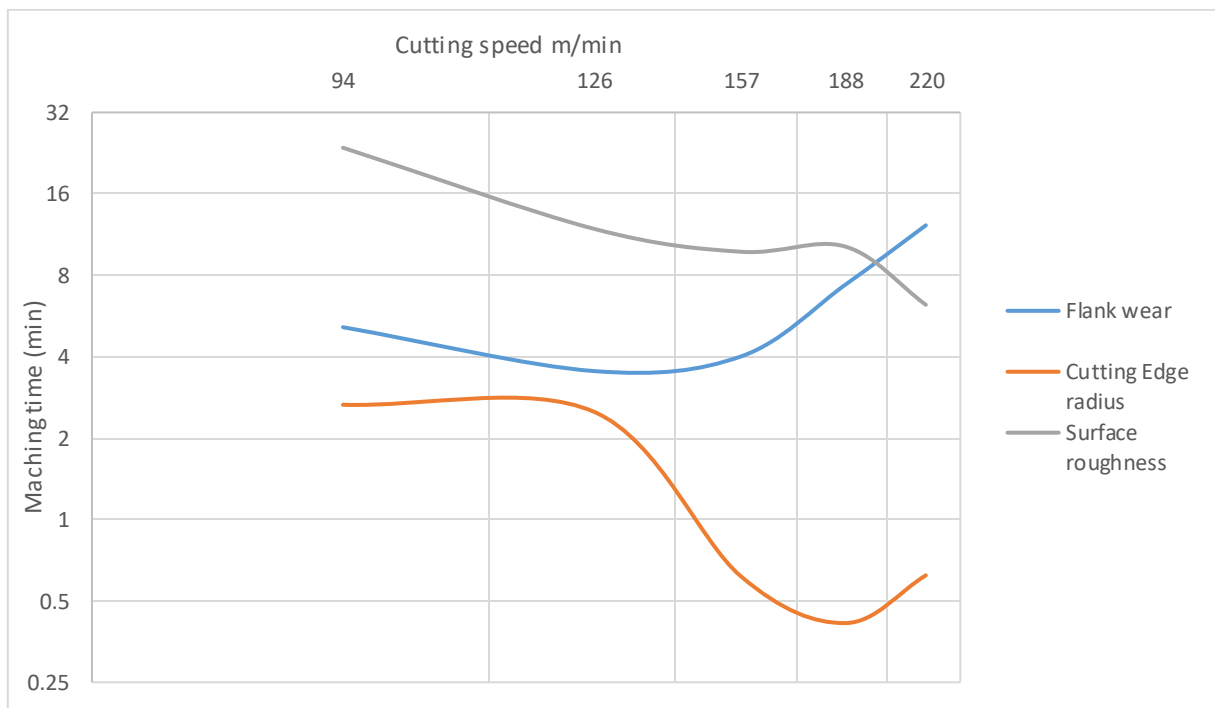


Figure 51: Set of three vT graph, resulting from the use of attributes proposed as criteria for micromilling

The plot of machining attributes against cutting speed shows the limit tool edge deterioration defines the end of the tool's useful life before other tool wear criteria are reached. The extended machining time as cutting speed increases, shown by tool edge deterioration, suggests that machining efficiency can be significantly improved if the strength of the tool edge can be improved. The rapid recovery of machining efficiency as cutting speed increases shows high cutting speeds are preferred in micromilling while maintaining an acceptable average surface roughness. Even though the plot of machining time for tool cutting edge deterioration suggests; using the cutting speed of 188 m/min and above result in lower cutting edge radius and therefore improved surface roughness was expected. The inverse effect in surface roughness trend shows the effect of increase adhesive wear rate and depreciation of surface roughness. Flank wear shows to be the second major factor determining tool life, where significant improvement is achieved by using a higher cutting speed which reduces the expansion of flank wear land. The similar trends of improvement as a result of higher cutting speed indicate that edge deterioration and flank wear are independent of each other, suggesting that higher cutting speeds in micromilling are preferred.

The plot of tool life against cutting speed plays a key role in harvesting machining data for quick selection of cutting speed and evaluation of tool change intervals. In micromilling, multi-criteria vT graphs can be used for simple and effective transfer of expected machining behaviour to the operator that improves the reliability of the machining operation. The experimental data gathered are used to evaluate the cutting speed and machining time in relation to resultant surface roughness and tool deterioration constrains, can then be transferred to industrial applications of tool selection, tool path planning, extending tool life and improving process efficiency.

4.4 Conclusion and remarks

This study has investigated the effect of machining parameters on the wear rate of uncoated tungsten carbide tools identifying the main tool wear modes, concluding with a proposal of critical wear values for the micromilling of a hard-to-cut material such as Titanium alloy. The metrics proposed are used as criteria for the estimation of tool life of micro endmills in relation to flank wear rate, finished surface roughness, and cutting-edge radius, forming guidelines to measure the effect of cutting speed on the tool wear rates. The following conclusion can be drawn:

- A consequence of the low axial depth of cut used in micromilling is the concentration of cutting forces at the tip of micro tools, which results in the rapid increases in cutting-edge radius which has a direct impact on the surface finish.
- Non-uniform flank wear is not the only dominant wear mode as machining progresses. Tool wear patterns in the micromilling of titanium suggest that the wear mode can be differentiated in three stages, with initial rapid abrasive wear at the tooltip and along the active cutting edge, then a non-uniform expansion of wear land on the cutting face, and finally combined abrasive and adhesive wear causing a deterioration in tool diameter.
- High cutting speeds and low feed rates have been shown to improve the useful tool life of micro endmills. However, low feed rates enhance the adhesive wear of the workpiece material to the tool due to non-formation of the chip at every tool evolution resulting in a ploughing effect increasing the pressure and friction between the machining surface and tool rake face, thus, increasing the machining temperature and the appearance of burrs between layers of the finished surface.
- A high cutting speed indicated a reduction in the flank wear rate, providing a stable machining environment that is favourable for micromilling. This can have an adverse effect of the selection of optimum feedrate to meet the minimum chip thickness require in micromilling.
- Due to high cutting temperature and pressure in micromilling, the chip welding across cutting face of the tool results in localised flank wear (VB3) which significantly reduces the hardness of the cutting tool. The resulting chipping effect along the flank face and active cutting edge, reduce the useful tool life and encourage premature tool failure in micromilling.
- Tool wear along the active cutting edge dictate the life of the cutting tool hence improving strength along the active cutting edge using coating can delay the tool change intervals.
- Increasing the feed rate result in less friction and rubbing effect, which is favourable in micromilling to ensure a low machining temperature consequently reducing adhesive wear that all contribute to improving the machining stability directly.
- Active, intelligent machining parameter optimiser that alters the selected machining parameter based on the pre-defined machining stage and resultant dominant tool wear mode can improve the tool life and more importantly improve machining reliability desirable in micromilling and process planning.

Chapter 5. Investigation of machining sequence for thin wall structures

5.1 Introduction

There has been an emphasis on the effect of tool path and machining layers strategy on the geometrical tolerances, machining stability and accuracy of the feedrate along the tool path when evaluating the optimum machining sequence [135]. A direct consequence of micromilling high aspect ratio-thin wall is machining vibration that consequently results in feature excitation (known as chatter), and induces feedrate variation and size effect leading to higher cutting forces and feature deformation. As such, this chapter investigates the impact of machine layers by means of simulation on the deformation of the thin wall structure in order to associate the characteristics of layer strategies with maximum deflection. Simulation results were then experimentally validated via micromilling of thin wall structures. Furthermore, the impact of commercially available tool path on tool stability was studied and compared in relation to geometry type; with the machining data gathered from these experiments being used for the development of a database including the range of tool paths and layer strategies recommended for micromilling. In reference to process objective (accuracy, efficiency and balance), an optimisation methodology for the selection of the best machining strategy for application with a thin wall structure is proposed. In process planning the selection of the optimum machining sequence is of equal importance as the selection of the optimum machining parameters,

particularly in applications with high aspect ratio feature. Subsequently, the findings from this chapter contribute to the machining knowledge and the fundamental machine sequence planning with an emphasis on the impact of geometry type in machine sequence planning for micromilling.

5.2 Simulation results and discussion

In order to further develop the existing layer strategy proposed by Li et al and Annoni et al [57, 136] displayed in Figure 52 and Figure 54 for micromilling of thin wall structures, the impact of layer strategy on the maximum deformation of thin wall was simulated. The maximum deflection was recorded as displayed below in Figure 53, Figure 55, Figure 57, Figure 59 and Figure 61 and the optimal layer sequence was recommended.

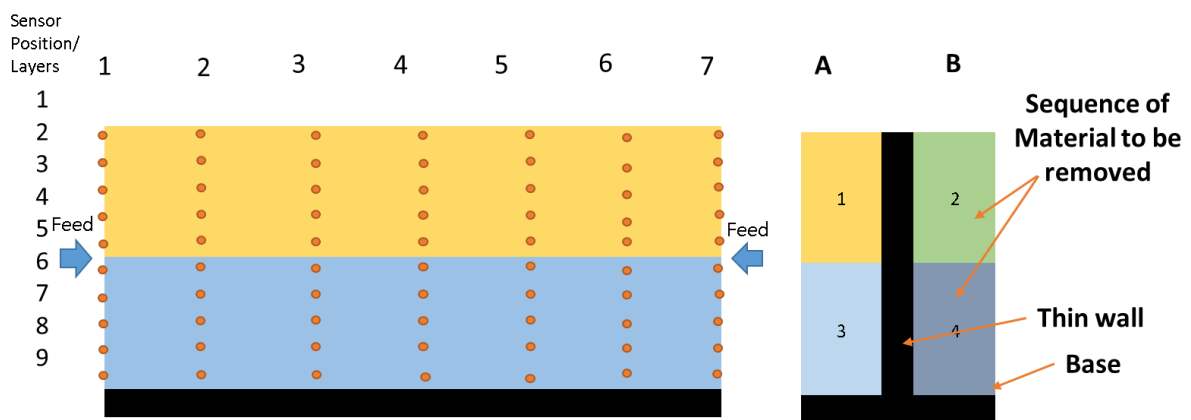


Figure 52: Layer strategy one - front and side view (right and left image respectively) of thin wall and the sequence of material removal layer overlaid by deformation probe locations.

The deformation data in the simulation of the first strategy is summarised in the 3D displacement map, Figure 53.

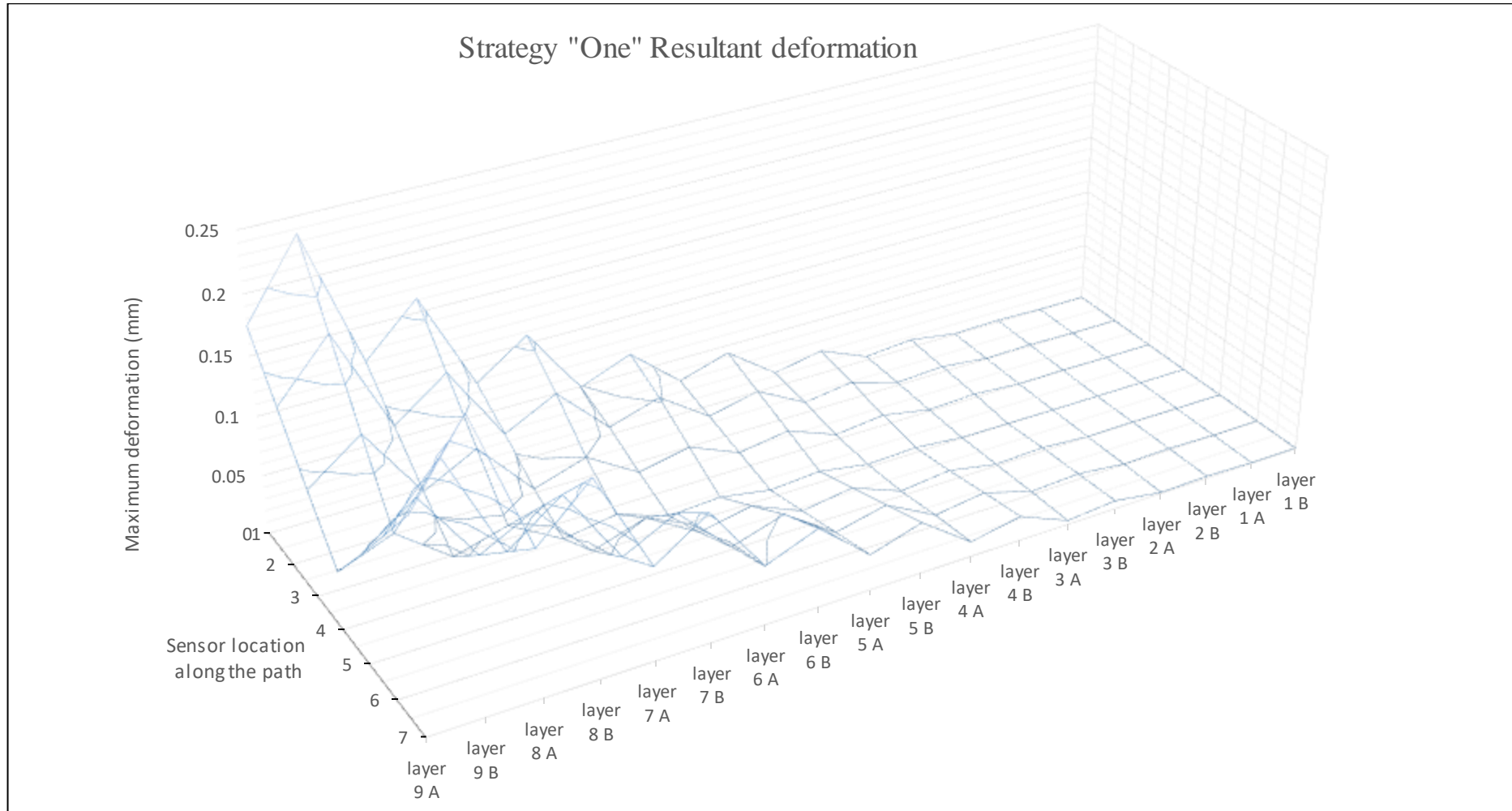


Figure 53: Maximum deflection recorded across of the thin wall structure using machining layer strategy "One"

The deformation data indicates a significant geometrical deformation as a result of the cutting forces, with the lowest at 50 μm of displacement towards the centre with progressive deformation as the cutter moves towards the edges, peaking at 250 μm . The 3D displacement map highlights where the maximum displacement occurs and therefore corresponding “weak” region where extra planning is required to determine the best strategy. The deformation trend suggests an inconsequential impact of cutting forces where up to a quarter of material was removed from the overall height of the thin wall whilst machining past this point indicated a drastic increase in geometrical deformation. The progressive deformation along the last layer reached a displacement of 250 μm as the cutter position became closer to the edges of the wall. Thus highlighting the unsuitability of this layer strategy in machining a thin wall structure. Below are drawn conclusions from the preliminary data:

- In the removal of excess material around the thin wall structure, the machine layer has an almost negligible impact on the deformation for the first 25 % of excessive material removed from the height.
- Following removal of the first 25 % of excessive material, the machining layer strategy has a significant impact on geometrical accuracy as when the cutter position approaches the weak region maximum deformation occurs.
- The layer strategies must be planned to maximise the support around the weak regions identified

The weak region highlighted by the maximum deformation observed from strategy one lead to the development of strategy two which focused on the overlapping layers shown in Figure 54. The layer strategy simulated the effect of overlapping excess material to improve the support of thin wall along the tool path. This was achieved by an initial change in depth of cut and subsequent implementation of strategy one.

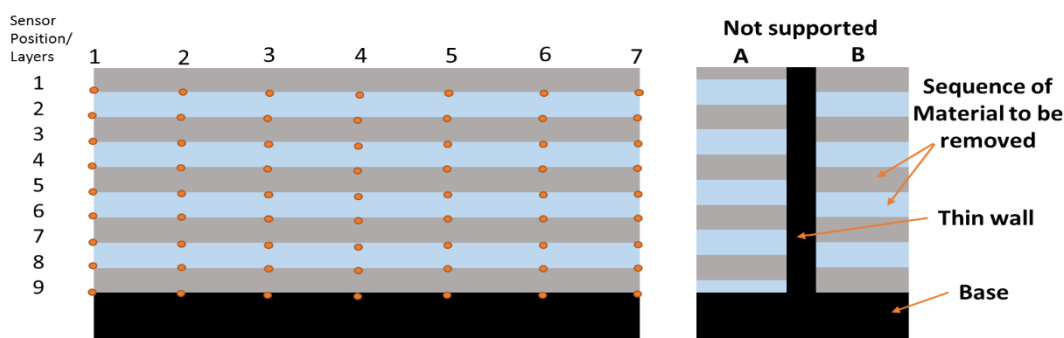


Figure 54: Layer strategy two - front and side view (right and left image respectively) of thin wall and the sequence of material removal layer overlaid by deformation probe locations.

The resultant maximum deformation of the thin wall using layer strategy two is presented in Figure 55.

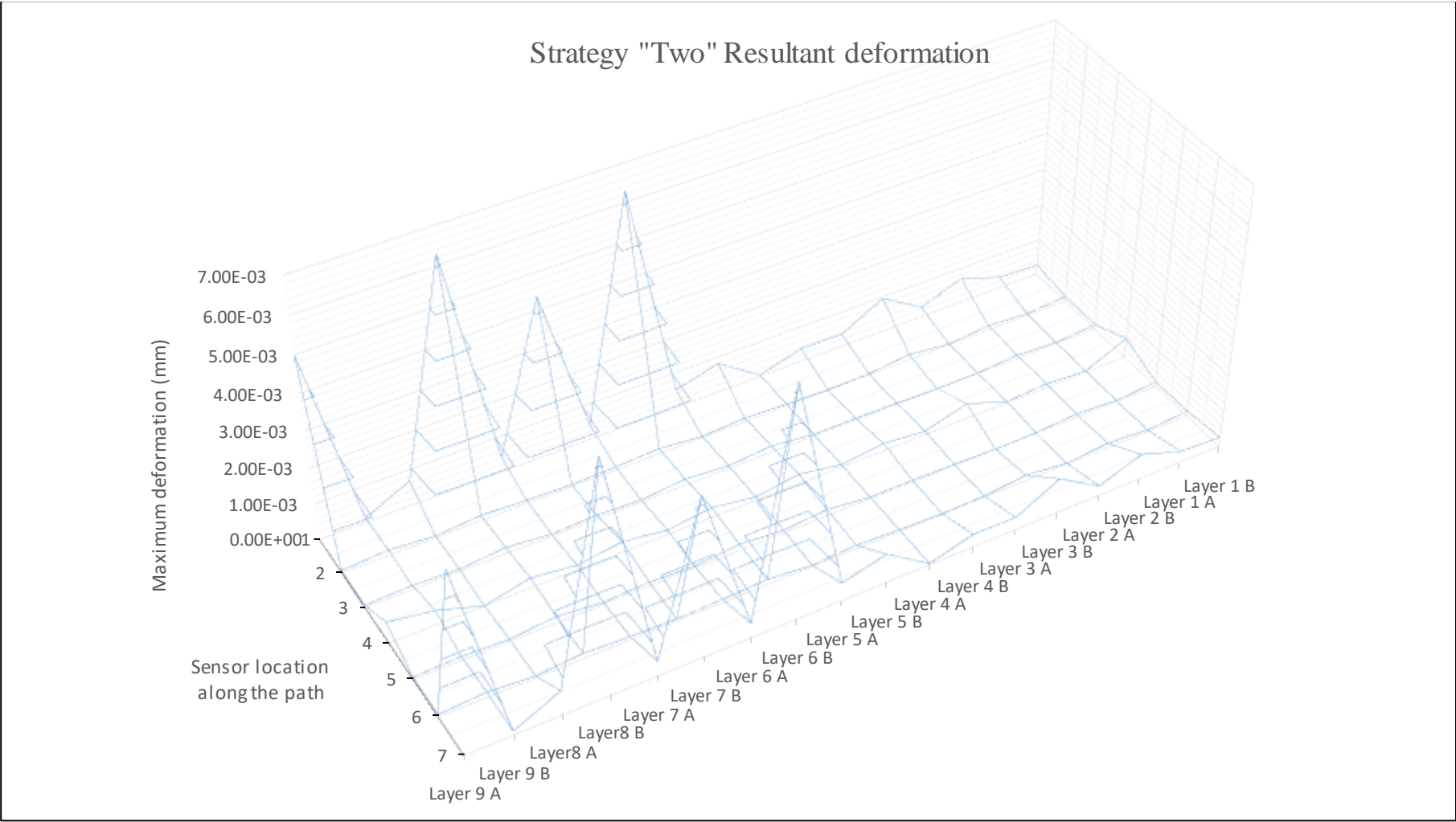


Figure 55: Maximum deflection recorded across of the thin wall structure using machining layer strategy "Two"

The deformation data shows a significant improvement, with almost no deformation recorded through all layers between sensors 2-6. Furthermore, the use of strategy two delayed the overall deformation transition point to 60 % compared to the 40 % recorded for strategy one. The peak in maximum deformation shows a dramatic drop, estimated at 7 μm , in comparison to 250 μm for strategy one. Similarly, both machining strategies showed a change in geometrical deformation rate as the tool progressed past the transition point while the resulting maximum deflection became more significant as the cutter approached the weak area identified as near the edge of the thin wall. The following observations are drawn from the simulation of strategy two:

- In machining of the thin wall using strategy two, the excess material removal up to 60 % of the overall height is shown to have an insignificant effect on the geometrical accuracy.
- A change in location of the maximum deformation can be used to track the area where more aggressive machining can be used in the proposal of adaptive machining in relation to cutter position and weak area.

In conclusion, tool layer strategies planned around the weak region identified for high aspect ratio features significantly improved the finished part accuracy.

Following the examination of strategy one and two, the trend in the deformation graphs highlighted the need to provide additional support around the edges of the thin wall in order to reduce the impact of machining. However, negligible deformation between sensor location 2-6 highlighted the areas where more aggressive machining parameters could be selected to improve machining efficiency. Given the impact of strategies one and two on the geometrical deformation, another layer strategy (strategy three) is proposed in light of the characteristics of machining efficiency and accuracy shown in Figure 56.

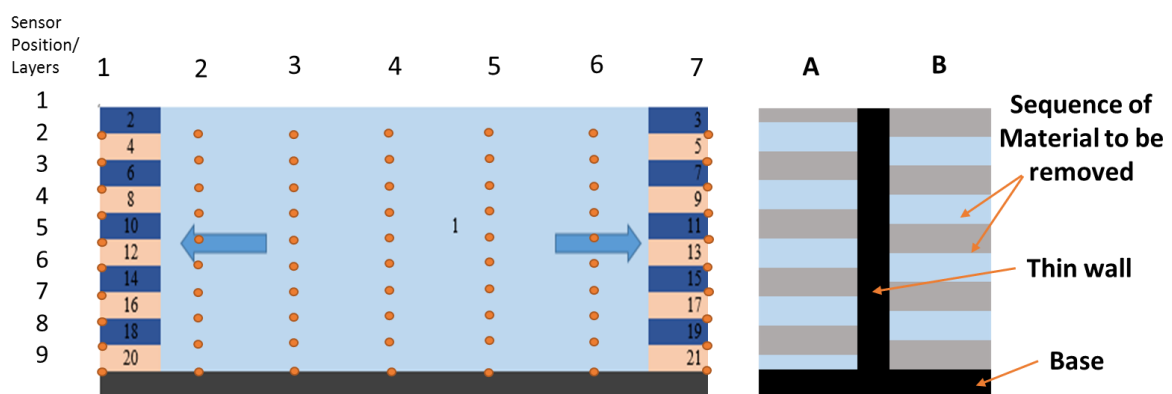


Figure 56: Layer strategy three - front and side view (right and left image respectively) of thin wall and the sequence of material removal layer overlaid by deformation probe locations.

The deformation data in the simulation of strategy three is summarised in the 3D displacement map in Figure 57.

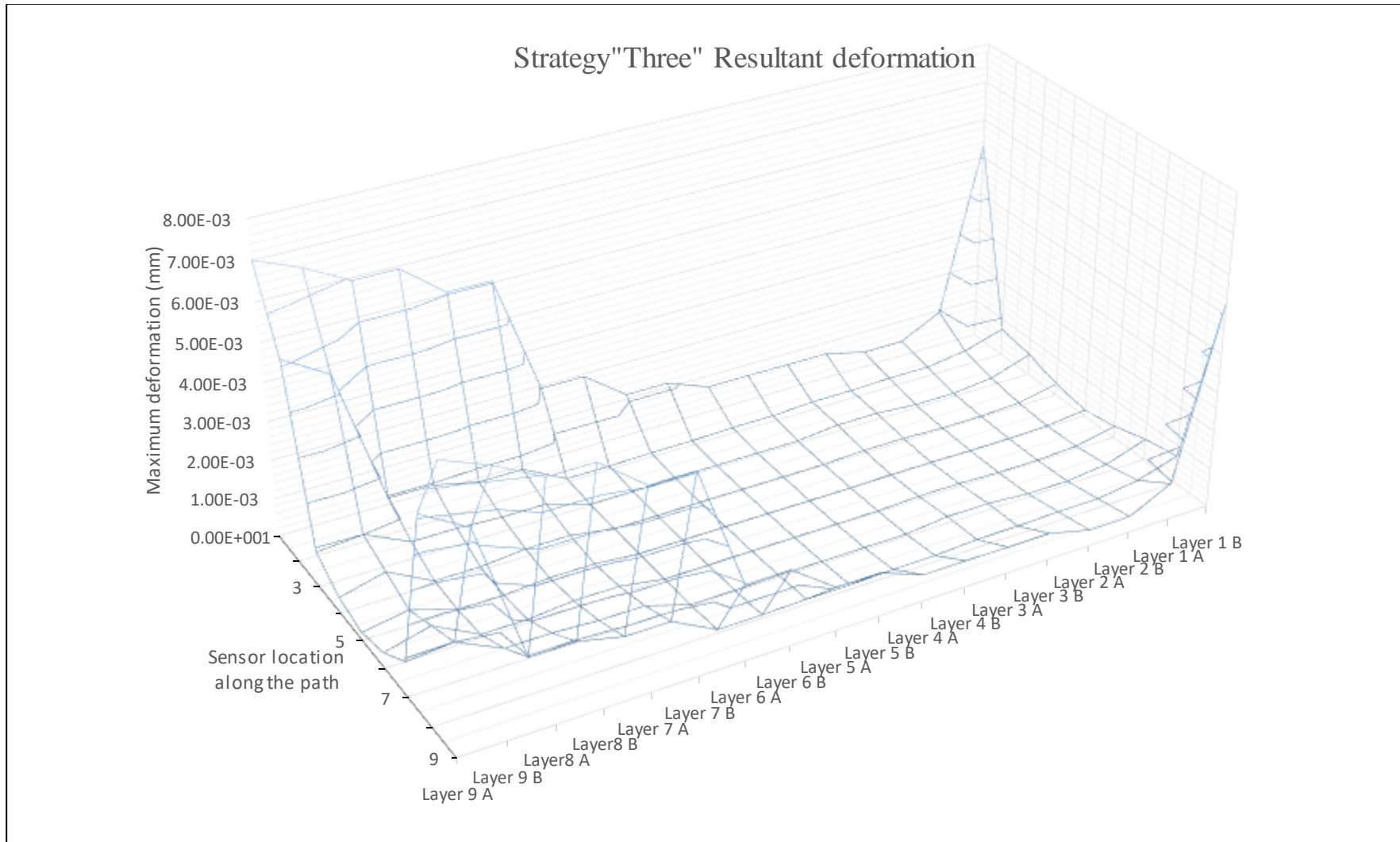


Figure 57: Maximum deflection recorded across of the thin wall structure using machining layer strategy “Three”

Implementation of strategy three led to the improvement in thin wall deformation as the transition point was further postponed until 70 % of excess material was removed, compared to 60 % and 40 % in strategy two and one respectively; after which, the rate of deformation began to increase. However, minor jumps in displacement were recorded in the remaining layers at the sensor positions on the edge of the thin wall indicating the impact of feed direction; which was pointed outwards, consequently leading to increased stress concentrations due to the resultant cutting force acting on unsupported thin wall edge.

Fluctuation in the resultant displacement along layer one indicate to the influence of the volume of supporting material near the edges; however, following the progress of the machining, the lower overall deformation trend indicated a reduction in cutting forces with improved machining stability. The following conclusions are drawn from the simulation data using strategy three:

- Feeding the cutting tool towards the edge with no excess material (to support the finished feature) must be avoided, as it has a negative impact on geometrical accuracy.
- Providing the excess material being removed supports the weak areas, increased material removal rates can be adopted to improve machining efficiency.
- The strategic selection of machining layer can be used to delay the transition point before which a higher machining efficiency can be achieved using aggressive machining parameters.

The effect of reversed feed direction using the same machining layer as in strategy three is examined and proposed as strategy four with the simulation data summarised in Figure 58.

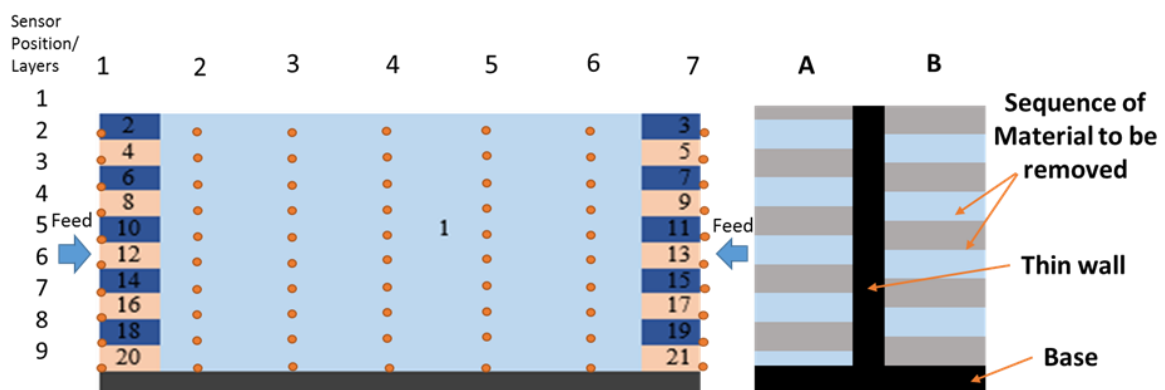


Figure 58: Layer strategy four - front and side view (right and left image respectively) of thin wall and the sequence of material removal layer overlaid by deformation probe locations

The 3D displacement graph of the thin wall using strategy four is displayed in Figure 59.

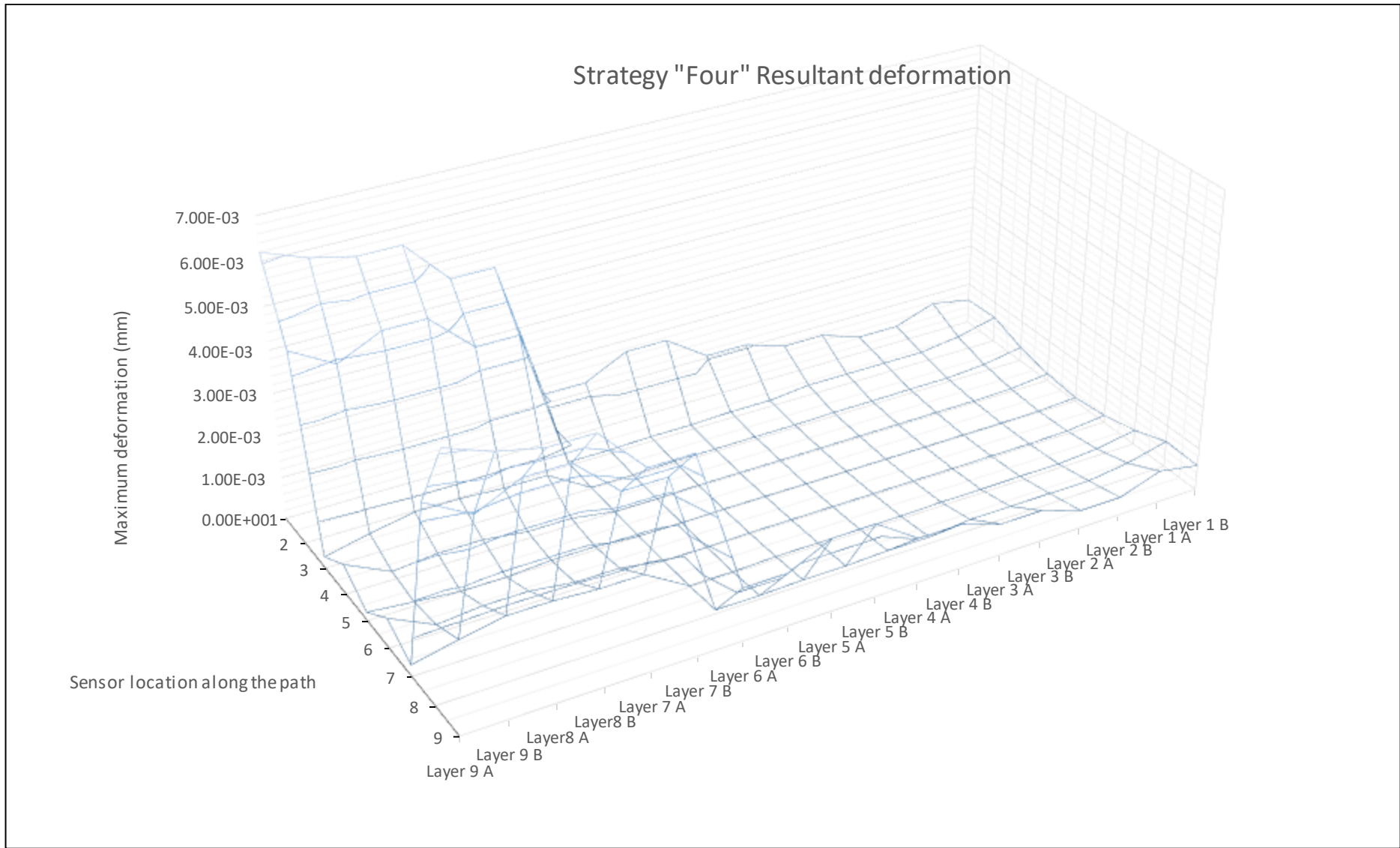


Figure 59: Maximum deflection recorded across of the thin wall structure using machining layer strategy "Four"

Similar performance was observed for thin wall deformation using strategy four as the difference between strategy four and three was the direction of feed toward the centre as opposed to outwards. The deformation of the thin wall during removal of excess material in the first layer dropped from $5\mu\text{m}$ to $0.5\mu\text{m}$ while as material removal progressed similar transition point at 70 % was observed. The impact of reversing feed direction after the transition point show to have result in lower deformation rate for remaining excess material removal layers (maximum deflection of thin wall during removal of excess material in layers 7, 8 and 9 were $4.5\mu\text{m}$, $5.6\mu\text{m}$ and $6.3\mu\text{m}$ as oppose to $5\mu\text{m}$, $6\mu\text{m}$ and $7\mu\text{m}$ respectively). Reversing the feed direction in comparison of similar machining layer strategy indicates the influence of feed direction with the offsetting effect of corresponding machining stress away from weak areas. Furthermore, lower deformation between the sensor position 2 and 8 shows the minor effect of supporting material volume around the weak area. The following conclusions were made from the simulation of strategy four:

- Planning of tool feed direction to divert the resultant machining stress away from the weak area (edge of the thin wall in this experiment) show to improve geometrical accuracy
- The volume of excess material to support weak area (around the thin wall edge) must be selected in relation to cutter end position away from the weak area

Following the conclusion made from strategy three and four new tool path (strategy five) was proposed by increasing the volume of excess material left for support to divert the endpoint of the tool path further away from the weak edge. Also, utilise the benefit of feed direction to offset the machining stress toward the centre while maximise machining efficiency by increasing the depth of cut (strategy five) in Figure 60.

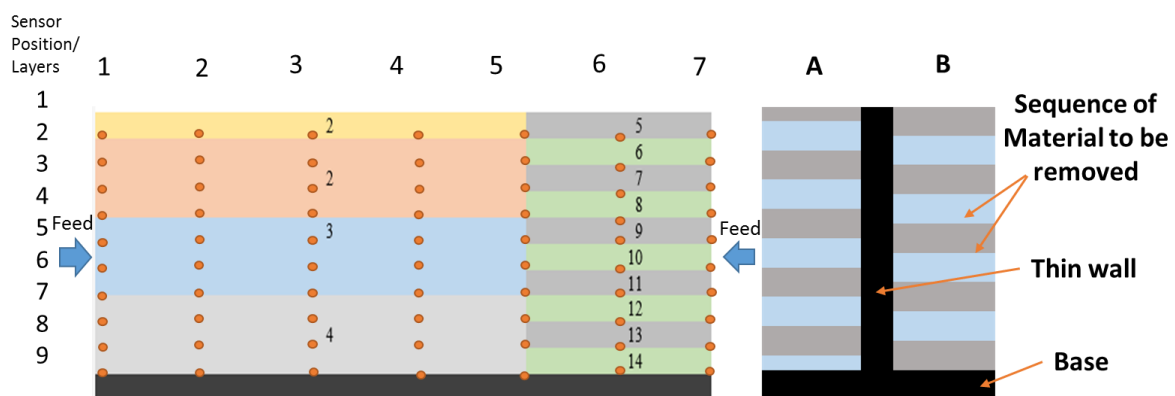


Figure 60: Layer strategy five - front and side view (right and left image respectively) of thin wall and the sequence of material removal layer overlaid by deformation probe locations

The deformation data in the simulation of strategy five is summarised in the 3D displacement map in Figure 61.



Figure 61: Maximum deflection recorded across of the thin wall structure using machining layer strategy “Five”

The comparison of maximum deflection as a result of using strategy five with strategy four indicate up to 200 % improvement was achieved (resultant maximum deflection for strategy 5, 4 and 1 were 2.4 μm , 6 μm , 250 μm). Even though the depth of cut was increased, similar transition point after 70 % of excess material was observed while reversing the feed direction towards the centre show to result in spread machining stress across the thin wall. The increase in the volume of supporting excess material in strategy to offset the tool end position away from the weak area indicated to have half the resultant deflection around the thin wall edges. Following conclusion were made from the simulation of strategy five:

- Machining layer strategy must be carefully selected in relation to maximising the support by use of excess material around the weak area of the feature to be removed at last.
- Attention must be given to tool feed direction and end position of tool path to be furthest away from the weak area (away from edges for thin wall structure).
- The transition point observed in deformation rate can be used as a set point to increase machining efficiency by use of increased machining parameters.

Following the conclusion made from the study of tool layer strategies, a new layer strategy to be used in machining of high aspect ratio feature is recommended in Figure 62 also following general observations are made:

- Selection of machining layer strategy in relation to the map of feature structure stiffness, especially for high aspect ratio features, can improve the machining accuracy as equally as the optimum selection of machining parameters.
- The transition points observed in the deformation graph for each machining layer strategy should be used as criteria to improve machining efficiency without comprising accuracy.

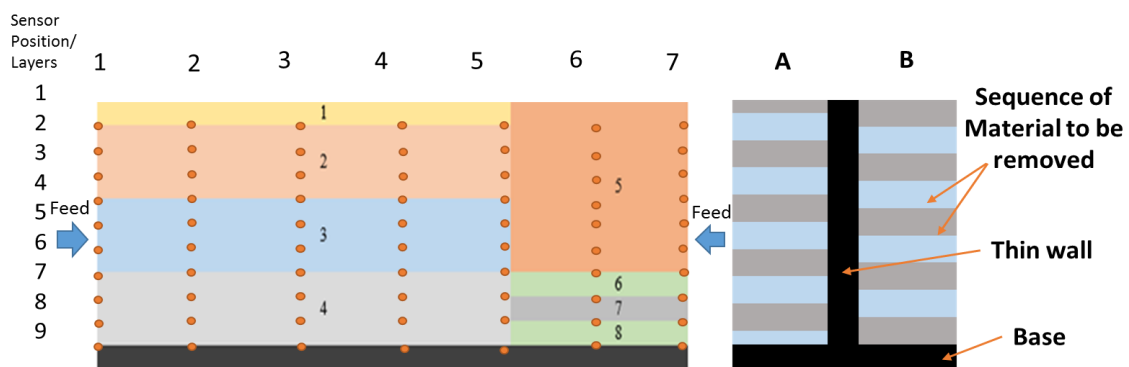


Figure 62: Layer strategy six - front and side view (right and left image respectively) of thin wall and the sequence of material removal layer overlaid by deformation probe locations

5.3 Experimental results and discussion

This section experimentally validates the impact of machining layer strategies proposed for micromilling of the thin wall structure. Also, investigate the impact of other machining sequence parameters; radial depth of cut and mill type that further characterising the layer strategy and tool path strategy that are evaluated during process planning.

5.3.1 Machining layers validation

Following the development of different machining layer strategies for micromilling of thin wall, the observation made using numerical data was experimentally validated through micromilling of 30 μm thin walls using the proposed strategy evaluated in section 5.2. The experimental tests and SEM images of the finished walls are summarised in Figure 63 to Figure 70.

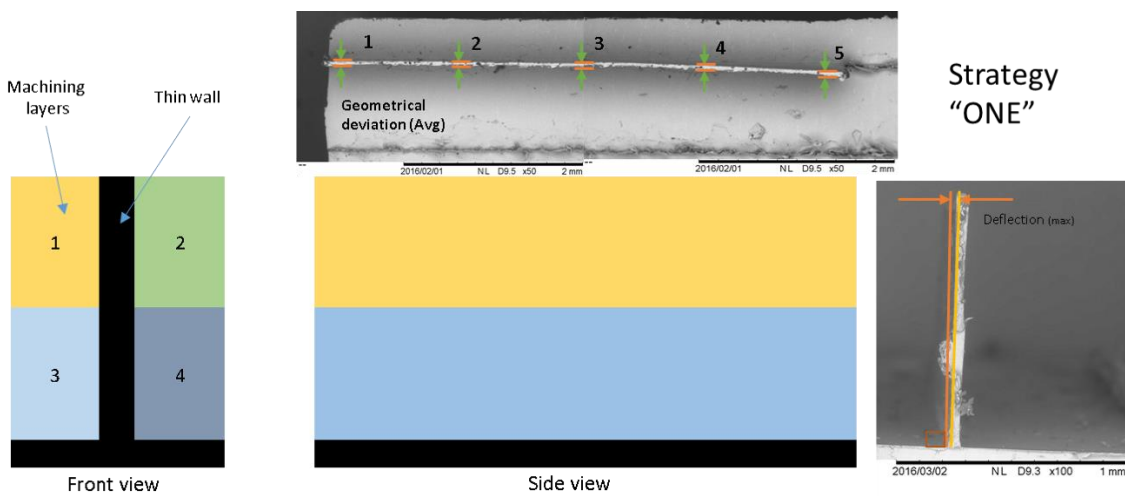


Figure 63: SEM image of the front and top view of the machined thin wall (Image on the right and middle top) using the layer strategy one (Left and middle bottom image)

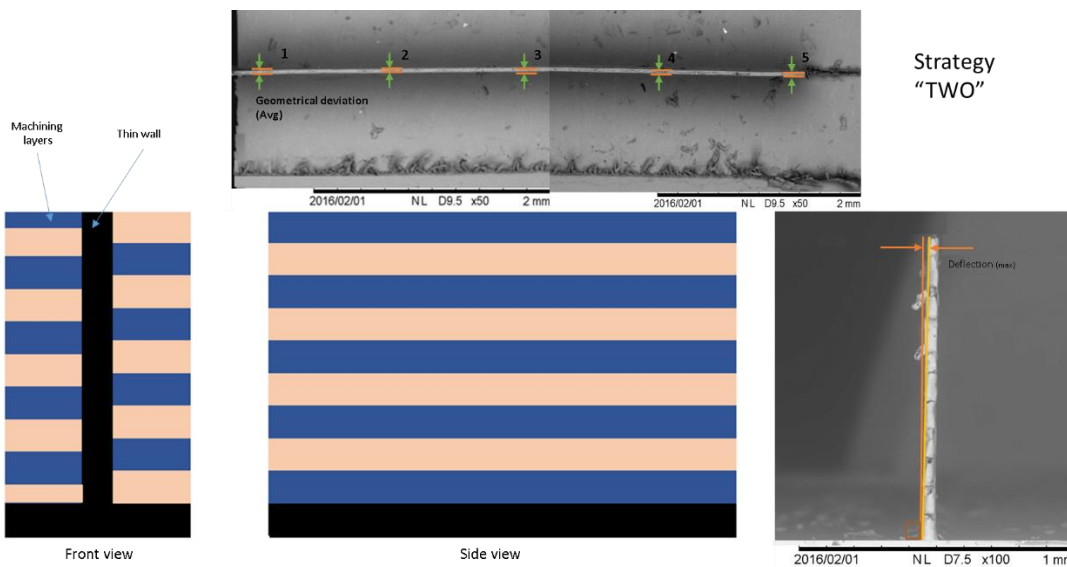


Figure 64: SEM image of the front and top view of the machined thin wall (Image on the right and middle top) using the layer strategy two (Left and middle bottom image)

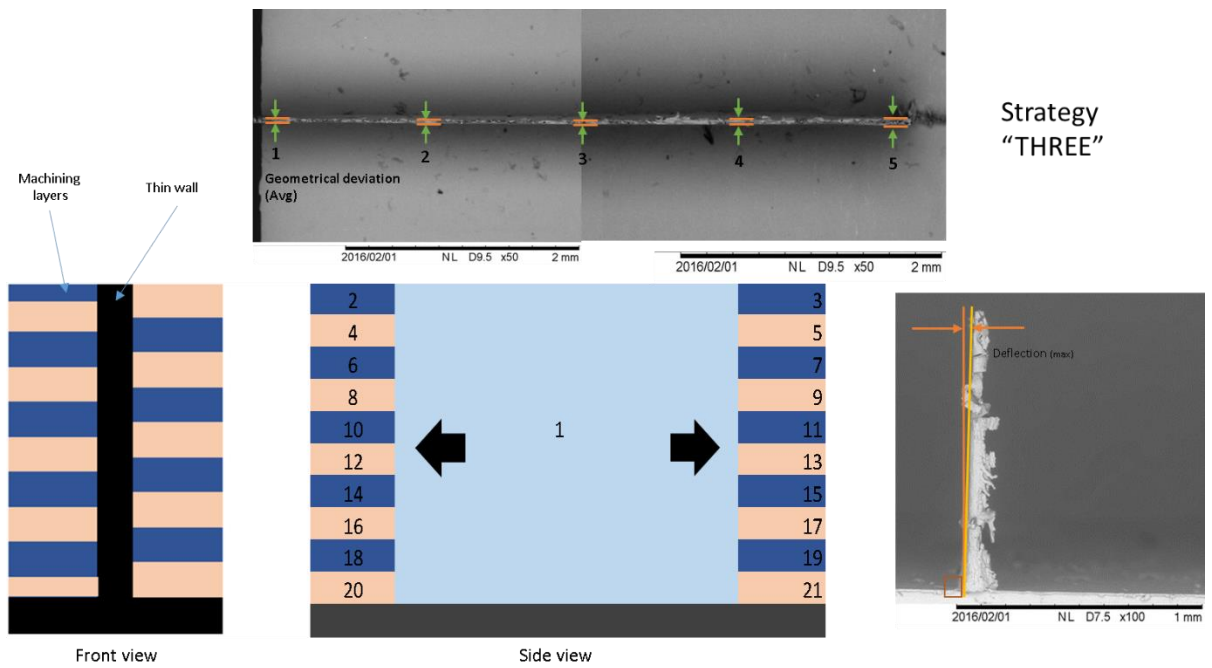


Figure 65: SEM image of the front and top view of the machined thin wall (Image on the right and middle top) using the layer strategy three (Left and middle bottom image)

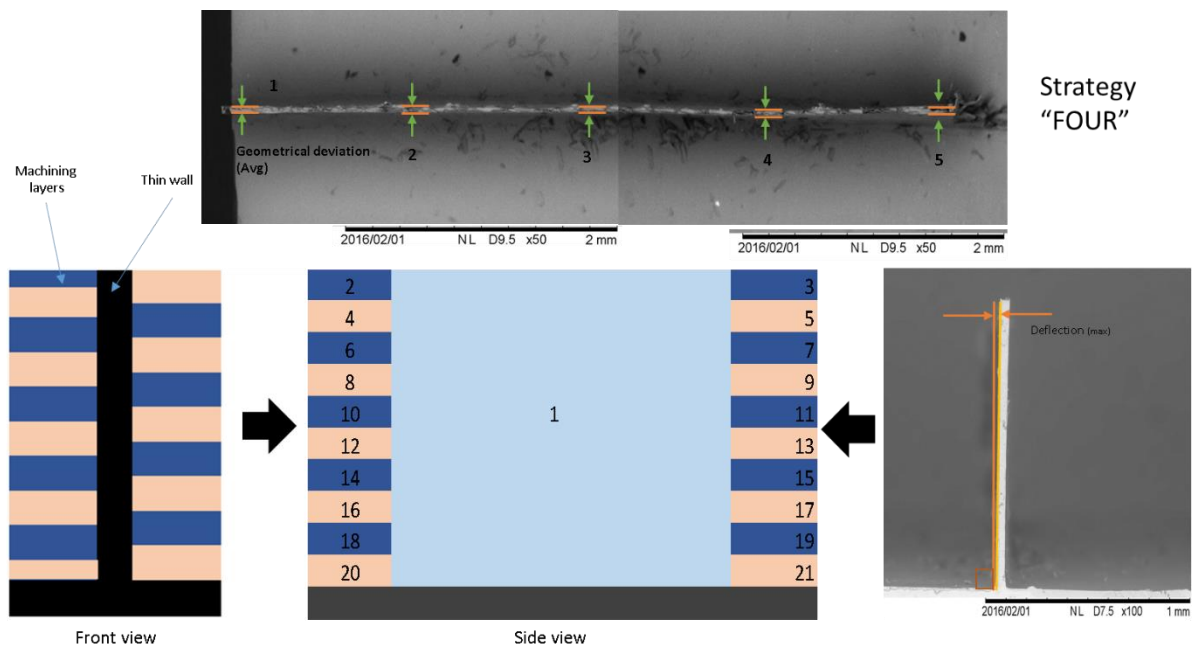


Figure 66: SEM image of the front and top view of the machined thin wall (Image on the right and middle top) using the layer strategy four (Left and middle bottom image)

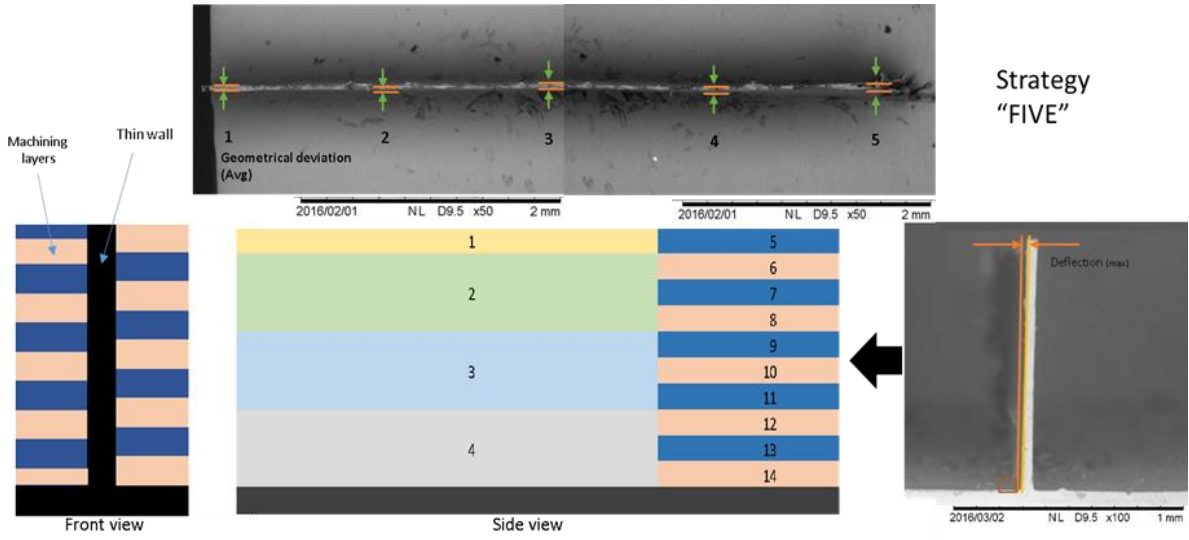


Figure 67: SEM image of the front and top view of the machined thin wall (Image on the right and middle top) using the layer strategy five (Left and middle bottom image)

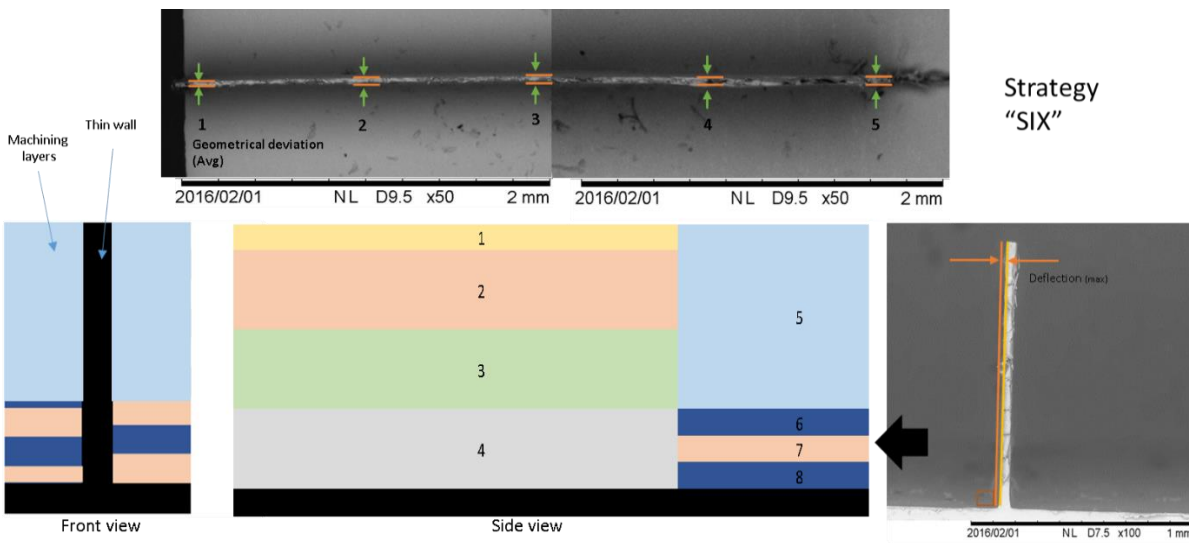


Figure 68: SEM image of the front and top view of the machined thin wall (Image on the right and middle top) using the layer strategy six (Left and middle bottom image)

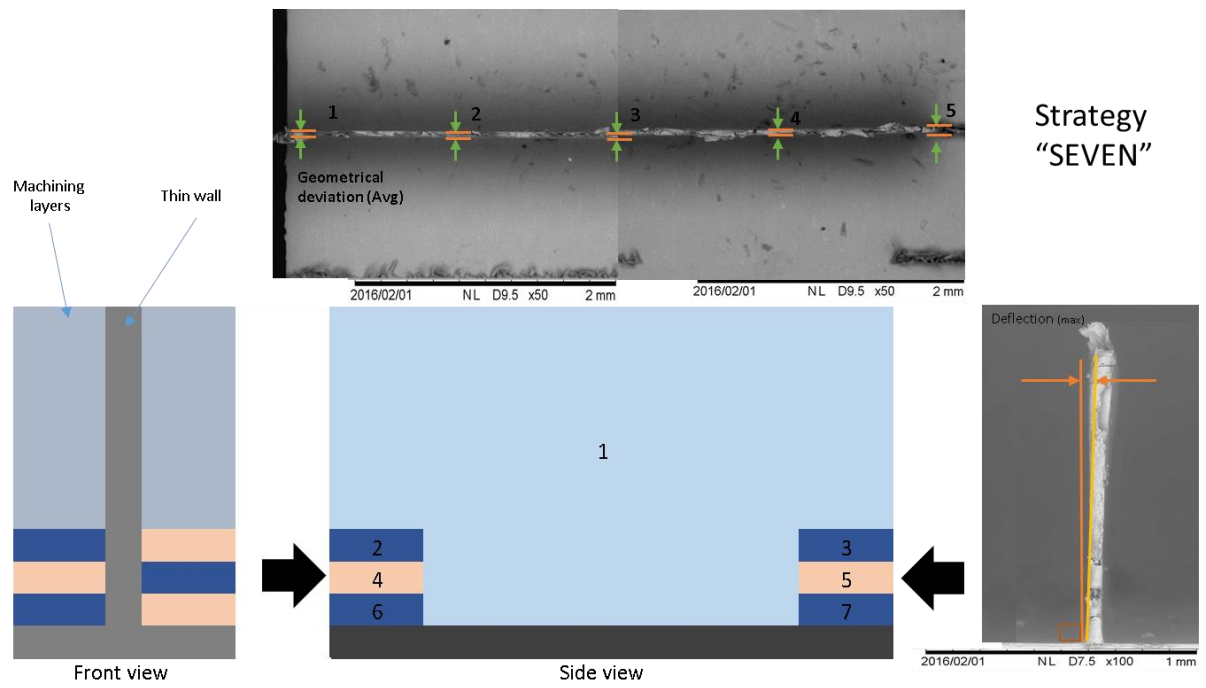


Figure 69: SEM image of the front and top view of the machined thin wall (Image on the right and middle top) using the layer strategy seven (Left and middle bottom image)

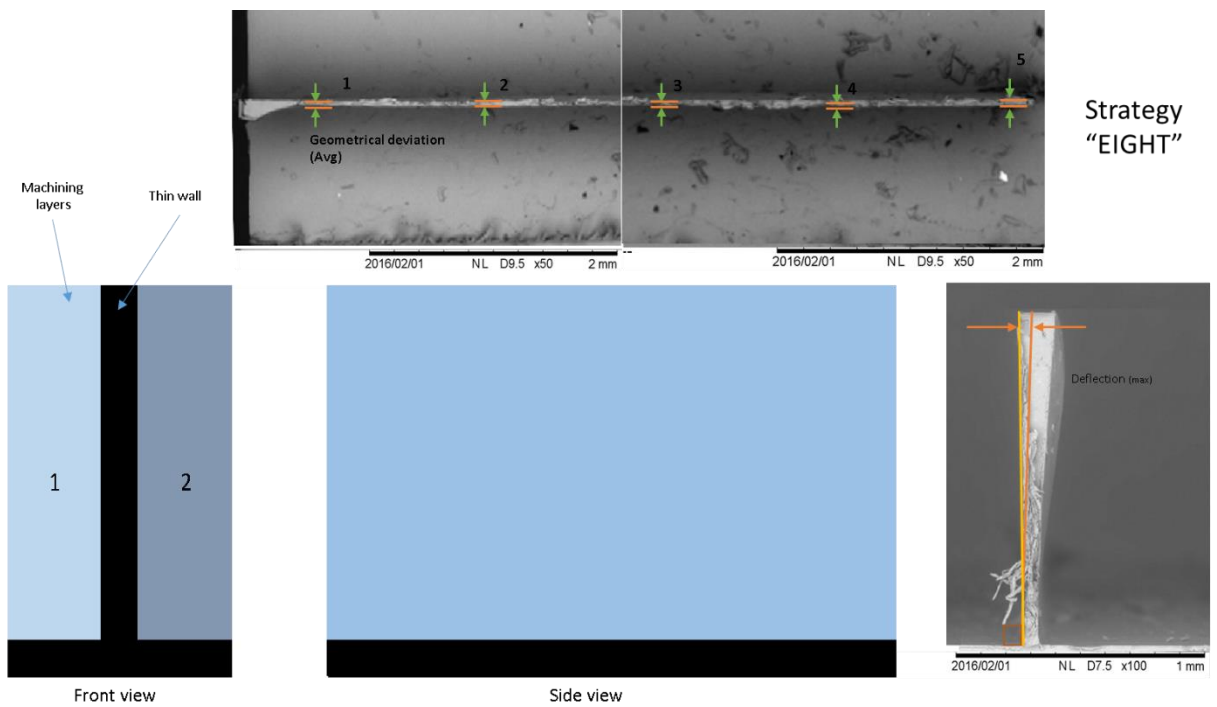


Figure 70: SEM image of the front and top view of the machined thin wall (Image on the right and middle top) using the layer strategy eight (Left and middle bottom image)

The value of measured and predicted geometrical deflection, the average deviation of web thickness and machining time are summarised in Table 10.

Table 10: Experimental data measured from SEM images of machined thin wall and corresponding layer strategy used.

Strategy No.	Mean-geometrical deviation (mm)	Max-predicted deflection (mm)	Max-measured deflection (mm)	Machining time (seconds)
1	0.008	0.023	0.068	18
2	0.003	0.006	0.042	30
3	0.004	0.007	0.043	16
4	0.003	0.006	0.039	16
5	0.002	0.002	0.039	13.8
6	0.001	--	0.011	16
7	-0.001	--	0.021	14
8	0.028	--	0.096	12

The significant impact of machining layer strategies can be observed by the descending trend of thin wall deformation as layer strategies were developed. The comparison of machining layer three and four confirm the influence of feed direction on geometrical accuracy of the thin wall. While no implication to machining efficiency is suggested machining time (lower deflection of 39 μm using strategy four as opposed to 43 μm measured for strategy three). Further comparison of deformation and machining time for strategy four and five shows, machining efficiency can be improved (machine time dropped from 16 s to 13.8 s) without impacting the accuracy through strategic planning of machining layers in relation to feature structural stiffness. The lower web thickness deviation as a result of using strategy five, featuring from larger supporting volume excess material to offset the tool end position away from the weak area (thin wall edge), indicate the importance of layer planning in according to weak areas across the structure. The negative deviation resulted from strategy seven suggests the overcut of material benefits the machining of parts with negative tolerances. However, for the part with positive tolerance, this strategy is excluded. In the comparison of strategy proposed by Li et al and Annoni [57, 136] (Strategy one and strategy two respectively) for micromilling of thin wall, the performance of proposed layer strategy (strategy 6) shows up to 8 times improvement in geometrical accuracy (Lower geometrical deviation error from 0.008 μm and 0.003 μm to 0.001 μm) and up to 200% improvement on machining efficiency (From 30s to 16s).

The trend of the geometrical deformations predicted in the numerical experiment matches the deformation data measured in the experiment; while, the numerical modelling is shown to have underestimated the maximum deformation. The error is believed to be due to the effect of machining vibration and resulting tool run out that leads to higher machining force. Therefore, the cutting force model used needs further development before it can be used as input to the numerical model for estimation of feature deformation.

5.3.2 Study of milling technology and radial depth

This section investigates the influence of other controllable variables used in the characterisation of machining layer strategy; radial depth of cut and milling type to further optimise the process in selection machining layer strategy for application with the thin wall structure. Figure 71 to Figure 73 shows the SEM images of two groups of four thin wall fabricated using a range of depth of cut (0.25mm to 1mm at an interval of 0.25) following milling technology of up milling and down milling used in group one and two respectively.

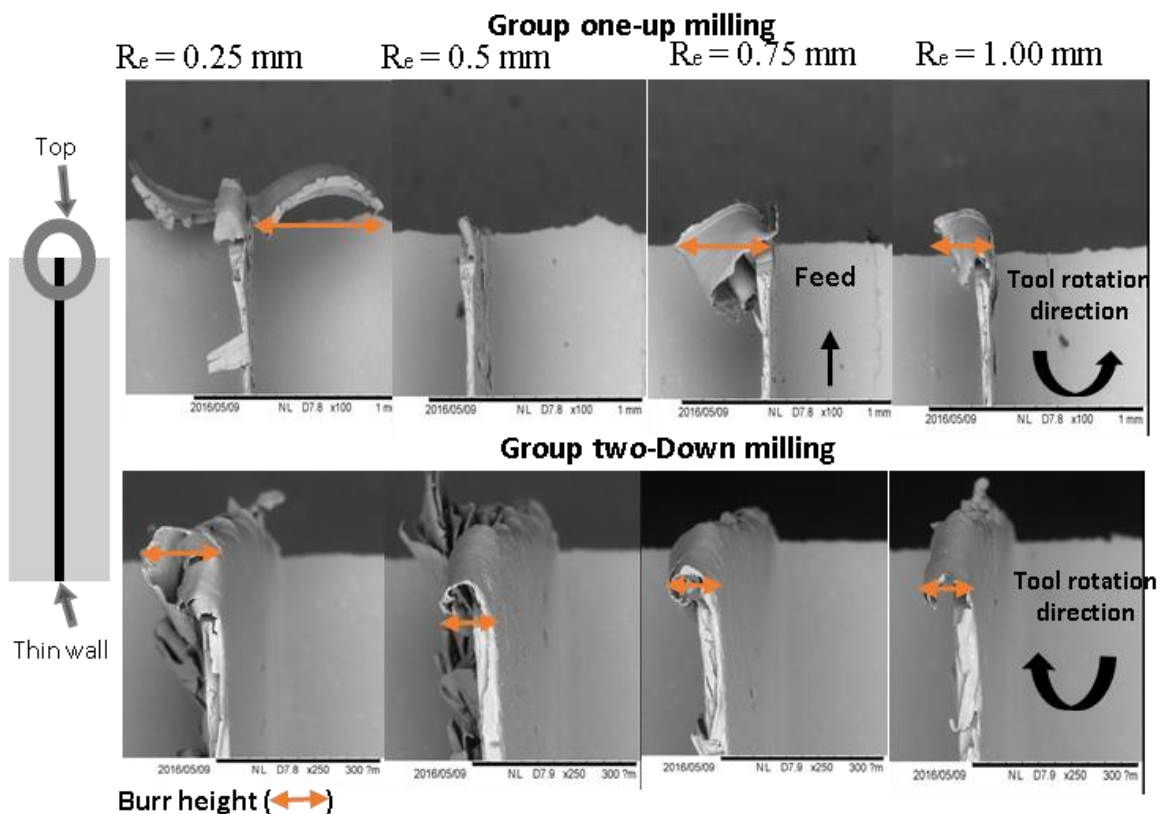


Figure 71: Top view of thin walls machined using up and down milling technology at the tool exit position

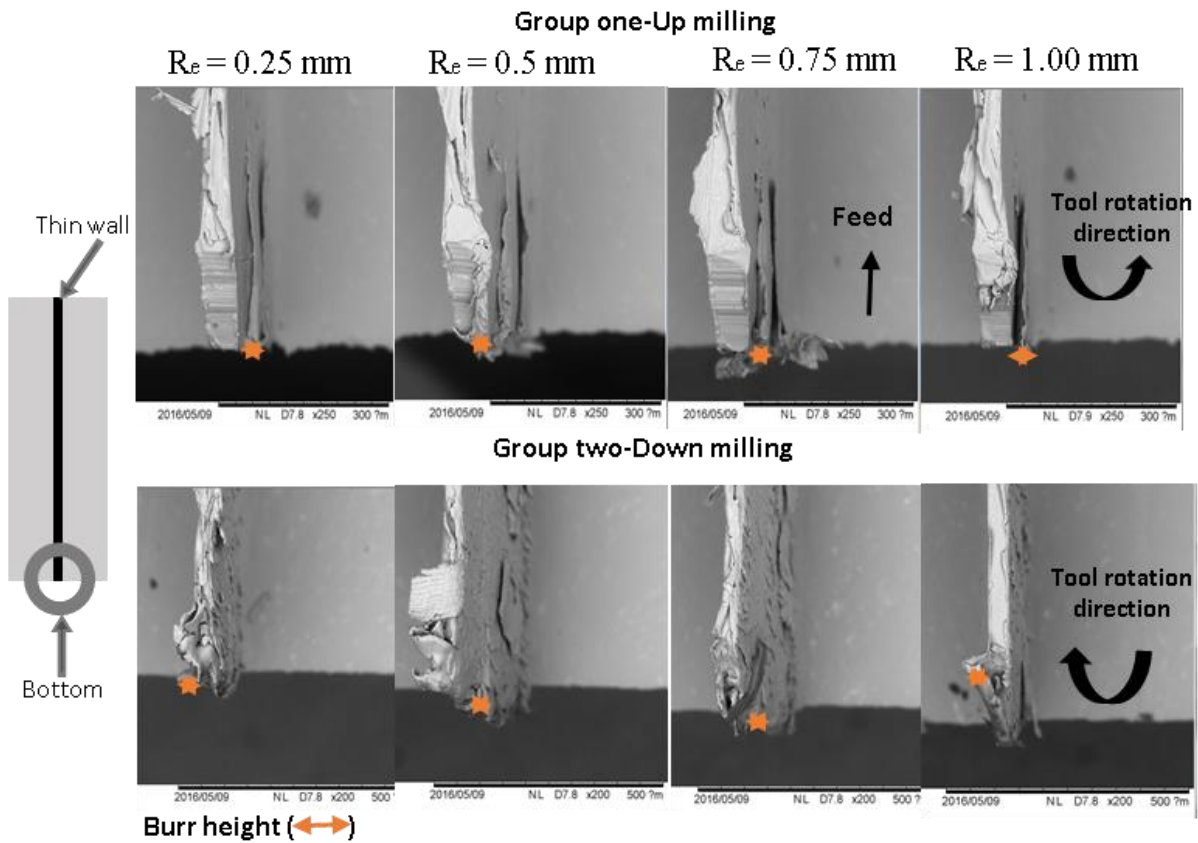


Figure 72: Top view of thin walls machined using up and down milling technology at the tool entry position

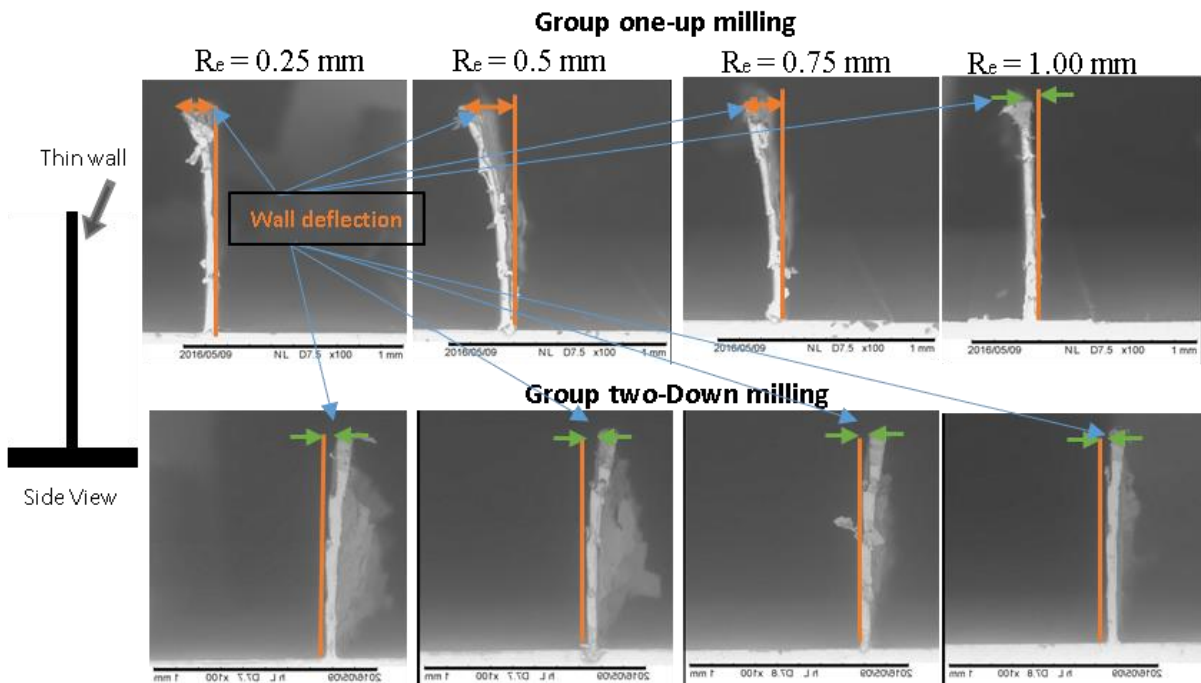


Figure 73: SEM images of side view for 40µm thin walls using up and down milling technology

The summary of the measured value for side exit burr height and maximum thin wall deflection is summarised in Table 11 and Table 12.

Table 11: Thin wall deflection measured through the processing of SEM images

<i>Deflection (μm) /radial depth of cut (mm)</i>	<i>Down milling</i>	<i>Up milling</i>
<i>0.25</i>	58	130
<i>0.50</i>	64	189
<i>0.75</i>	46	135
<i>1.00</i>	23	21

Table 12: Burr size measured through the processing of SEM images

<i>Bur size (μm)/ radial depth of cut (mm)</i>	<i>Down milling</i>	<i>Up milling</i>
<i>Exit position</i>		
<i>0.25</i>	602	275
<i>0.50</i>	35	186
<i>0.75</i>	99	158
<i>1.00</i>	142	156
<i>Entry position</i>		
<i>0.25</i>	2	15
<i>0.5</i>	23	49
<i>0.75</i>	29	73
<i>1.00</i>	17	81

The comparison of thin wall deflection in Table 11 shows a descending deformation value as the radial depth of cut increases for both milling technologies, indicating to use of higher R_e to improve accuracy. The slight increase in resultant deformation shown by increasing radial depth of cut from 0.25 mm and 0.5 mm using both milling technologies also suggest the use of half diameter as R_e value should be avoided for micromilling. A similar impact of R_e on geometrical accuracy was observed (wall deflection of 23 μm and 21 μm using down and up milling respectively) when full tool diameter was used. Therefore it can be concluded that the choice of milling technology in full slot milling is negligible. The gap between the resultant wall deflection using lower R_e indicate that choice of down milling is preferred for micromilling of a thin wall as better wall geometrical accuracy was achieved.

Similarly, the height of entry and exit side burr recorded in Table 12 shows a lower overall burr height when down milling was used confirming the preference of down milling technology for micromilling of thin wall structures. In the comparison of burr height using down milling technology, the inverse trend between the entry and exit burr shows the impact of feed direction

and tool position in relation to the weak area. Also concluded by the finding of the numerical study of machining layers in section 5.2 and verified in section 5.3.2. Therefore, it can be said that R_e has a direct impact on the accuracy of thin wall geometry while using lower R_e at tool entrance and maximising it as tool exit the material can reduce the burr formation. Considering burr appearance is due to poor machining stability, the strategy in the selection of R_e value can also improve the finish surface roughness.

The further qualitative observation made from the smoothness of geometrical edges formed suggesting, using down milling technology result in a smoother transition between each layer indicated by the reduced step height edge formation with the progress of machining layers. Also, better visibility of the wall edge was observed as R_e increased due to lower rate of burr formation for both up and down milling, suggesting the maximisation of R_e positively impacts the accuracy. In order to qualitatively compare the overall performance of milling technologies, and range of radial depths of cut; the supposedly similar thin walls were ranked from best to worst. Edge visibility and wall edge smoothness were used as criteria in the evaluation of damage scores that were used to compare the impact of milling technology and R_e . Damage scores calculated were used to plot Figure 26.

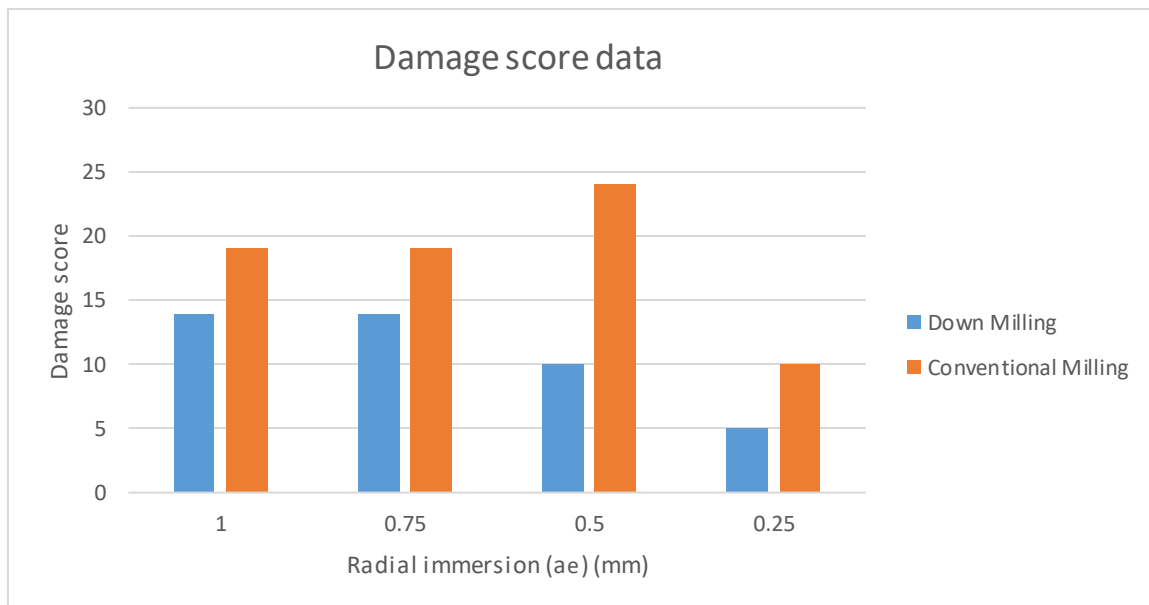


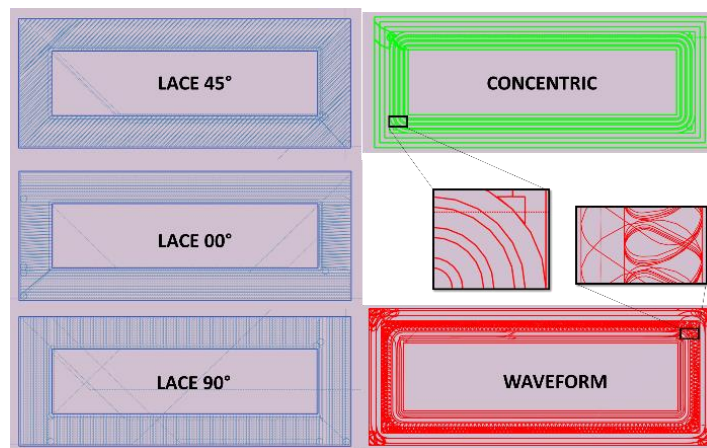
Figure 74: Qualitative damage score evaluated in relation to wall edge visibility and smoothness

While the lower overall scores value for down milling further confirms better edge formation and lower burr formation rate achieved using down milling, larger R_e show to have a negative impact on the rate of burr formation and smoothness of edges. Following the obvious choice of milling technology (down milling) in micromilling of thin wall, the finding of this study contradicted with work of others found in the literature suggesting down milling increase the

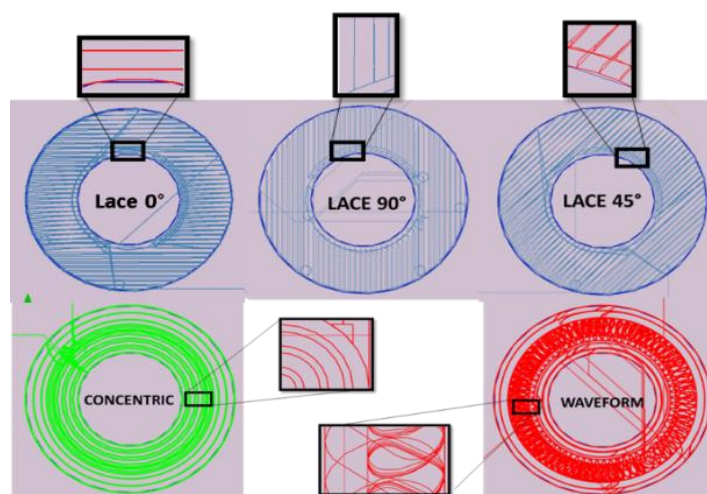
height of exit burr [132, 137]. However, this section findings agree with the findings from the observation of milling technology impact on entry burr formation that was reported to reduce the burr appearance by use of down milling [138]. The conflict of findings was believed to be due to the impact of R_e on the chatter of thin wall structure as full slot milling was commonly used in the study of burr formation for micromilling.

5.3.3 Study of machining tool path strategy

In this section, the impact of five commercially available tool paths in relation to geometry type and micro tool performance was experimentally studied. Figure 75 demonstrates the tool motion along each tool path simulated in EdgeCAM (Vero, 2016R2) while the cutter length was optimised to achieve the shortest tool path length around each geometry. Summary of experimental data obtained from machining of linear and circular geometries using different tool path strategies are given in Table 13.



(b) Circular geometries



(a) Linear geometries

Figure 75: Simulated tool motion corresponding to tool path strategies tested

Table 13: Experimentally measured data for surface roughness, accuracy and machining time

Tool path strategy	Surface roughness (R_a) (nm)		Geometrical deviation (mm)		Machining duration (min)
	Linear	Circular	Linear	Circular	Overall
LACE (0)	235	272	0.4	0.5	82
LACE (45)	296	158	0.4	-0.05	108
LACE (90)	298	369	0.1	0.1	50
WAVEFORM	181	242	0.02	0.3	99
CONCENTRIC	196	303	0.5	-0.25	76

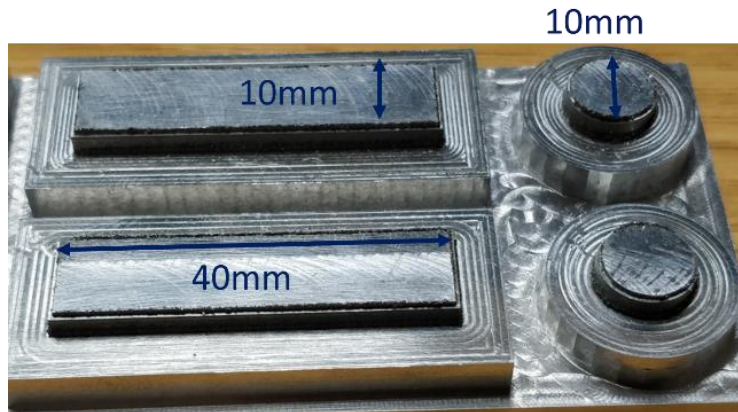


Figure 76: Preview of machined geometries using different tool path strategies

The gap between the measured surface roughness in the machining of different geometry type (circular and linear) using supposedly same toolpath suggest a change in tool performance in relation to finished feature geometry type. The range in measured surface roughness using all tool path in comparison of machining of circular and linear geometry suggests the tested strategy are better optimised for machining of linear as opposed to circular geometry. The comparison of resultant surface roughness for tool using Lace 90 strategy in comparison to the tool using waveform in the machining of linear geometry shows, choice of waveform strategy can improve the machining stability that directly influences surface accuracy by up to 150%. In addition, choice of lace 45 suggested as the least favourable strategy for machining of linear geometry (Resultant surface roughness ranked among the highest- 296nm, and highest geometrical deviation), show to have been the optimum choice for machining of circular geometries. Observation made from the resultant geometrical deviation in the machining of linear geometry shows tool strategies lace 0°, 45° and concentric strategy performed similarly leading to deviation of 0.4mm, 0.4mm, and 0.5mm in geometric accuracy respectively. The choice of strategy lace 90° show a slight improvement resulting in a smaller deviation of 0.1mm but tool using waveform strategy achieved a far lower deviation of 0.02mm (in circular geometries, the desired finish diameter was also 10mm). Experimental results summarised in Table 13 shows a diversity of deviation in geometric accuracy using different machining

strategies. The deviations for geometrical accuracy lace 0° and waveform were measured to be 0.5mm and 0.3mm respectively. Nevertheless, lace 90° resulted in a significantly smaller deviation at 0.1mm shown to be more suitable for the use of machining circular geometries. Even though lace 45° and concentric strategies led to material overcut deemed not acceptable due to positive tolerances, the lowest deviation of -0.05 was achieved by strategy lace 45 indicated the better suitability of this strategy used in combination with compensation technique such as toolpath offsetting in the machining of circular geometries. Therefore, it can be concluded that waveform and lace 45° strategies achieved the lowest surface roughness in machining of linear and circular geometries respectively. Nevertheless, the machining duration recorded for both strategy were among the highest time measured concluding machining accuracy was a sacrifice to machining efficiency in micromilling.

Furthermore, the influence of tool engagement and the machining stability were indirectly observed through the motion study of tool path strategies on surface roughness. From the observation made from tool motion study, waveform tool path shows to improve the surface roughness through the use of larger path radius at tool entering and exit from material that leads to improved machining stability in the machining of linear geometries. The contrasting surface data utilising the same strategy in micromilling of circular geometry suggests the tool motion preference at tool entry and exit radius changes in relation to geometry type. Further observation of tool approach angle and their impact on geometry accuracy using lace 0, 45 and 90 indicates the 90 degrees approach achieve better accuracy and should be adopted for tool path planning in micromilling. It can be said that the exit angle is an influential parameter in micromilling that must be selected in relation to geometry type in tool path planning. In the comparison of machining time and surface roughness in Figure 77, the waveform strategy shown to be among the highest machining duration recorded while the most efficient tool path results in poor surface accuracy.

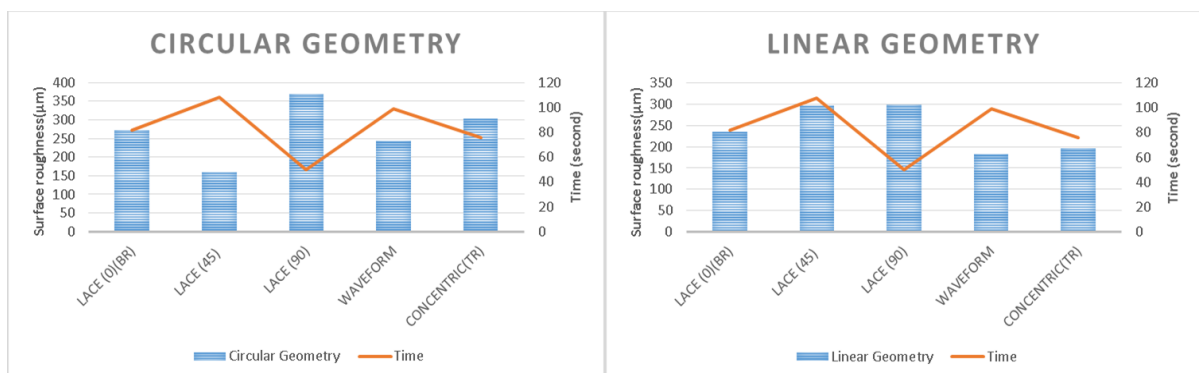


Figure 77: Surface roughness and machining time measured experimentally

Similar surface performance using strategy lace 45 and lace 90 in the machining of linear geometry shows efficiency can be improved up to 50% by the change of approach angle (from 108s to 50s using lace 45 and 90 respectively) without compromising accuracy. It can be concluded that the accumulated change in surface performance indicates the vulnerability of tool path strategy to geometry type as well as the choice of strategy on the efficiency. The comparison of machining cycle time and surface roughness value indicates to strategic selection of tool path that could benefit both machining accuracy and machining efficiency, and accuracy that was not always a trade-off with machining efficiency. In tool path planning, the selection of tool entry and exit motion in relation to feature geometry can improve machining stability.

5.3.4 Summary

The observations made in the study for the different aspects of machining sequence planning highlighted the impact of downscaling on the performance of machining and consequently the need of a different aim and approach to sequence planning for micromilling. The difficulties in achieving a secondary finishing process on micro features mandate to satisfy machining accuracy and efficiency through the process of sequence planning. Furthermore, in micromilling of high aspect ratio features, the strategic planning of machine layers in relation to part stiffness has been shown to be vital in order to achieve the tolerance requirements. In the selection of tool path strategy, attention must be given to the association of strategy with geometry type in addition to the aim of maximising efficiency. Attention must also be given to the tool motion and tool exit position in applications with low stiffness features. From the study of radial depth of cut and milling technology, minimisation and maximisation of radial depth of the cut at tool entry and exit positions into excess material are shown to improve machining stability. Nevertheless, the correct selection of down milling technology is shown to minimise burr formation and improve accuracy in micromilling of thin wall structures.

Even though the direct downscaling of conventional approach and the mature procedure for sequence planning cannot be applied for process planning in micromilling, similar process flow with explicitly applied compensation methodologies proposed in this chapter can be used for sequence planning in micromilling. The data gathered in this section fill the gaps in the systematic understanding of machining sequencing as a result of process downscaling. It also shows a demand for an optimisation methodology for tool path selection and machine layer strategies in micromilling.

5.4 Optimisation of machining sequence

The difference in objectives of machine sequence planning between both machining scales shows the importance of the optimum selection of tool path and tool layer strategy in

micromilling. In the literature review, many studies were found which focus on the optimisation of machining parameters for micromilling. However, little attention was given to the importance of machine sequence planning and no optimisation methodology was found for the selection of toolpath and machine layer strategy. Therefore, the multi attributes machining data gathered for tool path strategies and machining layer sequences in the previous sections, in combination with other findings (e.g. preference of milling technology in the micromilling of thin wall structure) were used as an input to Cardoso ranking model [139] for the optimisation of machining sequences. The model benefits from a weight system to reflect the prerequisite of micromilling process (machining stability, efficiency and accuracy) that varies based on the machining stage. The expanded Cardoso mathematical model including the additional variables to represent attributes used in the evaluation of tool path and machine layer in Section 5.3 is described in equation 14 [139].

$$f(\alpha, \beta, \gamma) = \frac{1}{(x * (\frac{\alpha}{\alpha_{max}}) + y * (\frac{\beta}{\beta_{max}}) + z * (\frac{\gamma}{\gamma_{max}}))} \quad (14)$$

where f is the score value, α, β and γ represent the process criteria with x, y and z as their corresponding wright factor respectively. Depending on the process stage, the contribution of each attribute is multiplied by the importance weight to reflect their significance defined by process requirement (the weight attributes corresponding to x, y and z are: accuracies, surface roughness and machining time respectively) and it is decided by process planner to overall machining performance. It is important to note that the accuracy of this method is limited to the number of criteria used in the comparison of tool paths and layer strategies. The weight factors used in this work for the three focused performance objectives (i.e. accuracy, machining stability and efficiency) are used in the optimisation of the machining sequences, as shown in Table 14.

Table 14: Corresponding weight factors to manufacturing aims

<i>Criteria</i>	α	β	γ
<i>Accuracy</i>	0.5	0.25	0.25
<i>Surface finish/maximum deflection</i>	0.25	0.5	0.25
<i>Machining time</i>	0.25	0.25	0.5
<i>Balance</i>	0.33	0.33	0.33

The experimental data gathered in Section 5.3 is in relation to accuracy, machining stability and efficiency where accuracy is defined as the achieved geometrical accuracy of the thin wall, machining stability is defined as the achieved average surface roughness, and efficiency is

defined as the overall machining time. All of these are used in combination with weight factors from Table 14 to calculate the individual score for tool paths and machine layer strategies, as summarised in Table 15 and Table 16 respectively. Higher scores indicate a better performance.

Table 15: Toolpath strategy scores for different weightings of each scenario

	<i>Design requirement</i>			
<i>Toolpath strategy</i>	Accuracy	Surface finish	Machining time	Balance
<i>Waveform</i>	1.22	1.40	1.28	1.30
<i>Lace (0)(BR)</i>	1.14	1.22	1.22	1.19
<i>Lace (45)</i>	1.10	1.21	1.09	1.13
<i>Lace (90)</i>	1.18	1.17	1.39	1.24
<i>Concentric(TR)</i>	1.19	1.27	1.29	1.25

Table 16: Cutting layer strategy scores for different weightings of each scenario

	<i>Design requirement</i>			
<i>Machining layers Strategies</i>	Accuracy	Machining stability	Machining time	Balance
<i>1</i>	1.17	1.14	3.36	1.20
<i>2</i>	1.93	2.81	1.30	2.20
<i>3</i>	3.05	4.24	1.72	3.24
<i>4</i>	3.08	4.25	1.55	3.32
<i>5</i>	4.71	5.92	2.74	4.57
<i>6</i>	5.25	6.13	2.93	4.73
<i>7</i>	1.98	1.63	2.03	1.56
<i>8</i>	1.37	2.30	3.87	1.89

Providing that the surface roughness and machining accuracy are individually targeted, waveform tool path strategy delivers a better performance as indicated by the highest score of 1.22 and 1.40 respectively. Also, the performance of the waveform tool path strategy in relation to efficiency scored among the top three choices for micromilling. The commonly used conventional tool path strategy (lace 0) is shown to be the least desirable tool path to be used in micromilling. When the efficiency is the focus of the process stage, lace 90 is the

recommended tool path while the choice of this strategy in relation to accuracy confirms the trade-off between accuracy and efficiency. Similarly in the comparison of machining layer strategies proposed for machining of high aspect ratio features, the machining layer six identified to be the optimum choice without a major impact on efficiency since the scores are among the top three tool paths. However, the trend of scores evaluated for layer strategy with the highest efficiency indicate the trade-off between accuracy and efficiency for the evaluated tool paths. Due to the difficulty of performing secondary finishing process on micro features, a balance of machining criteria is expected to be commonly used to indicate a waveform toolpath strategy to be used in micromilling. For the application of high aspect ratio features, layer strategy six satisfies both efficiency and accuracy requirements. The proposed optimisation model provides the selection of the best tool path and layer strategy in relation to operation importance factor selected by machining criteria for micromilling. The accuracy of the proposed model can be further improved by extending the range of available sequence strategies in the database as well as using a wider choice of process indicators such as burr formation to better capture the downscaling effect for micromilling.

5.5 Conclusion and remarks

During the study of tool path and of tool layer strategies, important results have been discovered that are useful in the advancement of knowledge in machine sequence planning for micromilling. This includes the following:

- In micromilling applications with high aspect ratio features, the strategic planning of machining layer to maximise support around the weak region using the excess material can improve the geometrical accuracy with no impact on efficiency. Excess material is recommended to be removed from the least supported to the most supported locations in the machining of linear thin wall structure as opposed to the cylindrical thin wall structures [62].
- Machine sequence planning in micromilling is as equally important as evaluating optimum machining parameters to achieve an optimal balance of performance and productivity.
- The association of tool performance with machining stability and surface roughness suggest that the tool path strategy that results in constant engagement of the tool with the material can effectively increase machining efficiency. Surface roughness has been identified as a good process indicator in comparison of tool path strategies in micromilling.

- In addition to maximising efficiency for the optimisation of tool paths strategies, tool motion characteristics along the path must be selected in relation to geometry type while machine layer strategy dictates the tool entry and exit positions.
- Accurate choice of the process indicator explicit to individual machining process is key for the proposed optimisation model where surface roughness, geometrical accuracy and machining time are recommended for micromilling.
- Accuracy is believed to be achieved at the expense of productivity. However, the optimisation of tool path and layer strategy has achieved the balance between high-performance and productivity.

Chapter 6. Process planning methodology for micromilling

6.1 Introduction

In process planning, multiple activities are undertaken during the preparation of the processes required for the fabrication of a part. In the overlap of macro and detail planning, standard methodologies in the evaluation and selection of these activities associated with common tasks of part design interpretation, manufacturing process selection, evaluation of machining sequence and selection of tools and associated tools and machining parameters, and geometric dimensioning and tolerances were developed for task of process planning that are utilised as a tool by operators and engineers [140]. However, due to the complexity and dynamic nature of machining, the overlap of detailed and micro-planning level still remains a manual and knowledge-intensive task that is undertaken by the operator with few or no explicit methods to solve the tasks within each activity [141].

Nevertheless, the kinematics of milling are similar at both scales; the impact of miniaturisation on part and tools, including part handling between processes, process monitoring and use of endmills with sub-millimetre dimensions gives micromilling a distinct feature that was neglected in the conventional process modelling making the existing guidelines impractical. Furthermore, the downscaled version of conventional milling limits the interaction of the operator during machining process that mandate to create an accurate micro plan for each

activity at the process planning stage, and necessitates the operator to have advance knowledge of micromilling processes.

Therefore in this chapter key activities overlapping between the detail and micro-planning level affected by miniaturisation were identified, and a systematic approach in solving tasks for each activity, explicit to micromilling, was proposed. The methodology proposed was recognised through the review of work by others found in the literature and the gaps studies in Chapter 4 and Chapter 5. The outline of activities undertaken to produce a process plan comprising of internal processes and data that flows in between these activities in creating a comprehensive process datasheet for micromilling is demonstrated using a flow chart. Furthermore, a deeper understanding of industrial process planning for micromilling with an application on thin wall structure is provided. The benefit of this approach was demonstrated through the fabrication of an artefact processed using the proposed guideline.

6.2 Proposal of process planning for micromilling

The standard process model proposed in this section excludes the selection of machining processes (where this study focus on micromilling) and machine tool (where comparison of machine efficiency and accuracy was excluded from the scope of this study) as the range of available tools was restricted to endmills. The remaining activities are grouped in relation to their internal process interaction that follows a typical step in process planning, where four modules representing the top-level process activities are proposed below:

1. Feature recognition module (interpretation of part design data)
2. Tool selection module (determination of cutting tool, cutting speed and tool life)
3. Parameter selection module (evaluation of the cutting conditions and machining parameters)
4. Machining sequence module (determination of machining layer sequence and tool path strategy)

The proposed process planning methodology is presented in Figure 78 while the internal process flow and logics for solving the tasks for each activity are discussed separately in the following subsections. The process logics for each module are implemented in Excel (Microsoft, 2013) in the development of a simple program to demonstrate the flow of machining data between each activity to populate the process plan datasheet.

6.2.1 Proposed process planning methodology for micromilling

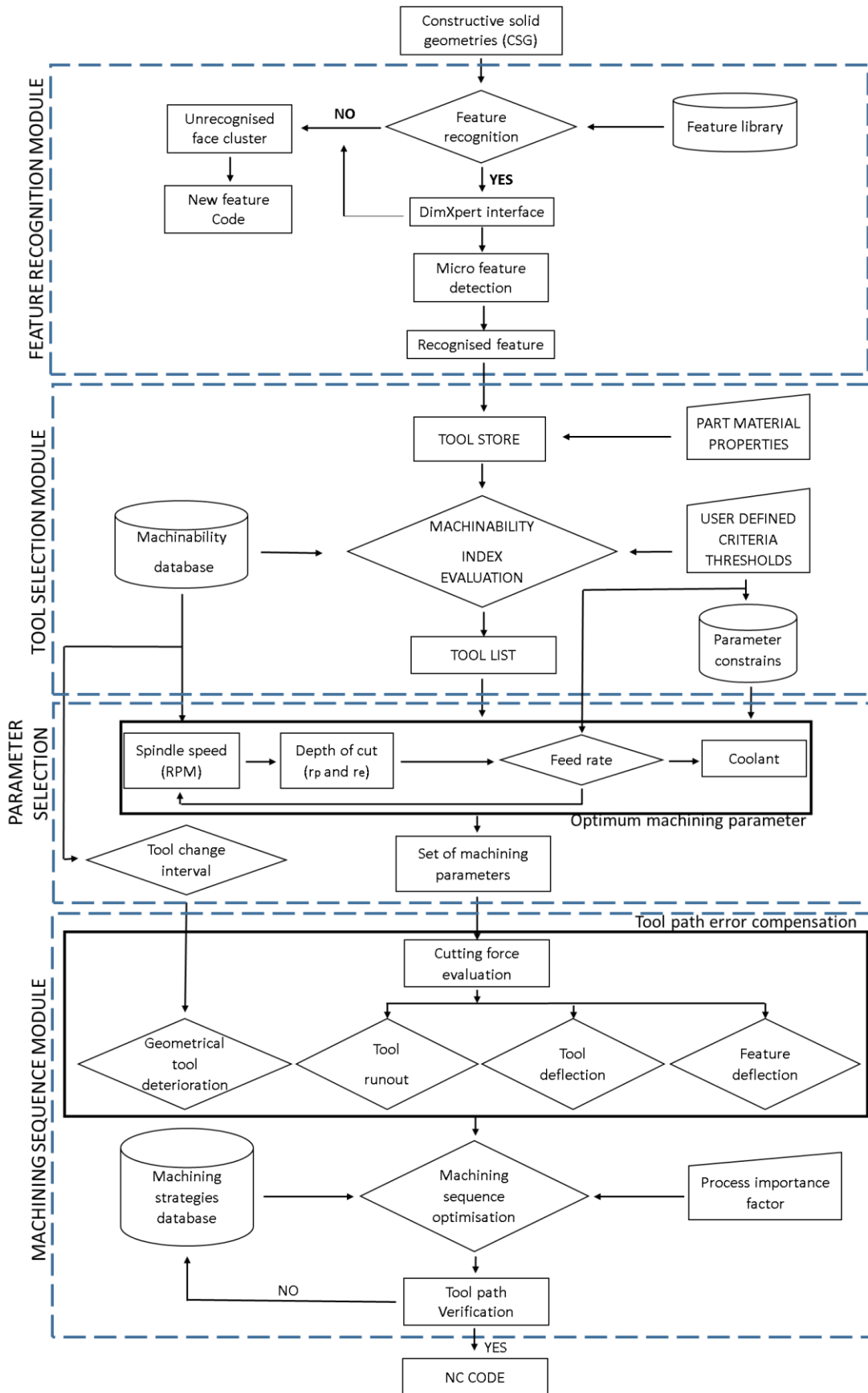


Figure 78: Proposed process planning methodology for micromilling

6.2.2 Feature recognition module

The outline of steps in translating the boundary representation (B-Rep) model described by computer-aided design (CAD) model to computer-aided manufacturing (CAM) through the creation of attributed face adjacency graph (AAG) was demonstrated by Verma et al. [142]. Commonly in the process of listing part features, hybrid of graph partitioning [143] and quasi-clique [144] algorithms are used to break down the part geometry graph into subgraphs to mine subsequent graphs until it matches a predefined feature AAG within CAM system feature library.

However, the limitation in the integration between CAD and CAM, with a deficiency in transferring high-level information, makes feature recognition a key activity to transfer the required feature information (e.g. surface roughness and tolerance) for solving tasks within subsequent process planning activities. Furthermore, feature mining is a process-heavy system, while due to its complexity; defining a new feature tree in feature library or adding new feature attribute required by specific manufacturing process for an existing feature isn't a simple task that operator can carry out before comprehensive feature list is generated. Besides the task of creating part feature list, due to miniaturisation of feature geometries in micromilling; an expert task of features categorisation (e.g. high aspect ratio) and evaluation of key manufacturing attributes to describe the distinct properties of each feature (e.g. aspect ratio, geometry type and key geometrical tolerances) is necessary for subsequent tasks in process planning. Nevertheless, further development of a new and existing feature tree to include additional manufacturing attributes specific to micromilling process cannot be achieved by the operator without expert knowledge of the system used in feature extraction by CAM package.

Therefore, in this section, a feature coding methodology and protocol for the feature extraction process by Sadaiah [145] is proposed for the task of feature extraction in micromilling. The model utilises basic functions to break down the part code in the extraction of sub-features while a simple protocol to define a new feature code with the ability to identify key feature faces was introduced. The model also benefits from the ability to assign manufacturing attribute (customisable to any manufacturing process e.g. micromilling in this application) to individual feature faces while facilitating the linkage between feature and their corresponding manufacturing attributes essential for the processes used in micromilling. The proposed model was implemented in Excel (Microsoft, 2013) as part of a program developed with an additional rule-based scheme in relation to face manufacturing attributes for feature categorisation for micromilling. The internal process flow is displayed in Figure 79.

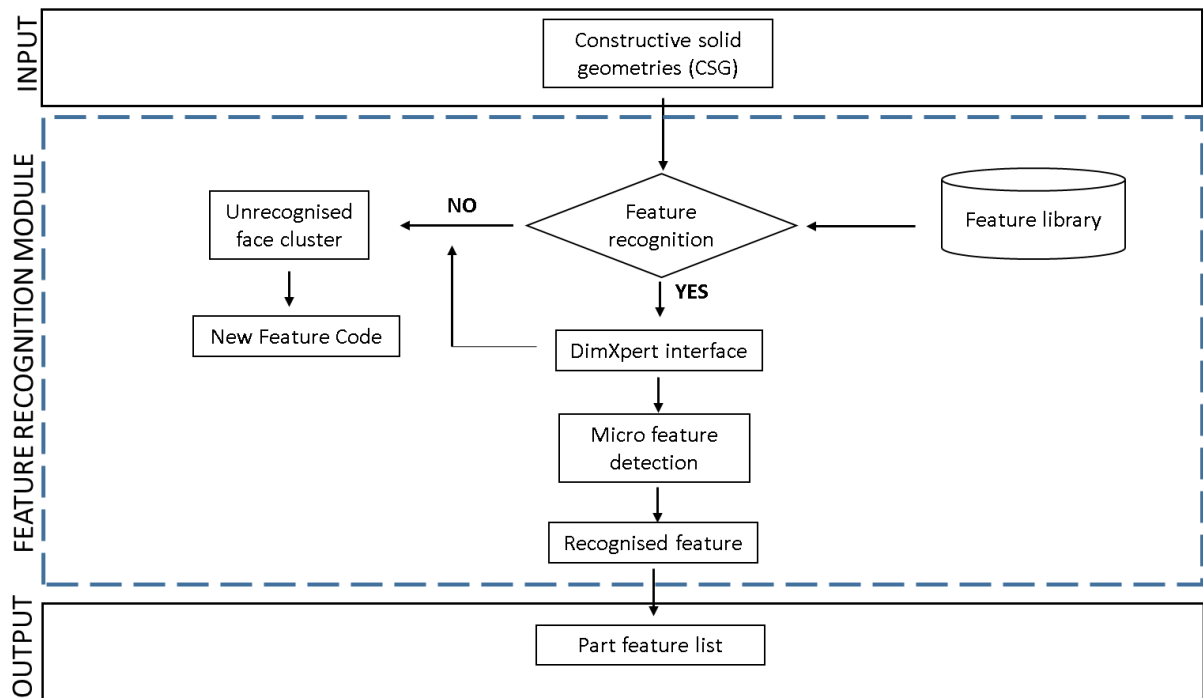


Figure 79: Overview of feature recognition module for micromilling

Following the steps outlined by Verma [142] to extract the B-Rep information of part imported from the CAD model and feature coding methodology by Sadaiah [145], the part code for the imported model was generated. The part code was used as an input to the “feature recognition step”, where the numerical code was compared with a list of feature codes stored within “feature library” using a look-up function in process of feature recognition. The corresponding name of the features that their codes were found within the part code was used to populate the feature list with their assigned manufacturing attributes. However, in conditions where some part of the part code was not matched to a pre-defined code within feature library, new feature code for the cluster of corresponding faces must be generated and stored manually by the operator under a new name. The new feature name must be determined following the ISO classification of prismatic parts (ISO 10303 AP 224) while the list of manufacturing attributes and key faces were manually defined before it was stored in the library. In the process of developing the feature library for all prismatic features, a similar process to add new feature can be repeated where the steps in adding a new feature were described as below.

The steps in the process of sub-feature code generation commence by generating a corresponding Object Multi Attributed Adjacency Matrix (OMAAM) for the part using four integer’s vector to describe the attribute adjacency between faces. The attributes for each integer type are displayed in Table 17 where the first integer represents the adjacency of the attribute to the edge, the second integer represents the type of the edge, the third integer represents the

face type and forth integer quantify the of inner loops. The OMAAM was further subdivided to Feature Multi Attributed Adjacency Matrixes (FMAAM) demonstrating the feature instance where concavity found along row and column in OMAAM highlighted the root faces. Convexity in four-digit vectors along the cell including the root faces indicates to the corresponding boundary faces that were used to generate the submatrix used for new feature code generation.

Table 17: Schematics of the vector and corresponding attributes

Adjacency attributes of edge [x,-,-,-]

Convex	Concave	Non- adjacent
+1	-1	0

Edge type attributes [-,x,-,-]

Straight Edge	Elliptical Edge	Circular Edge	Spline Edge	Non-adjacent
1	2	3	4	8

Face type attributes [-,- ,x,-]

Plane Face	Conical Face	Cylindrical Face	Non adjacent
1	2	3	0

The feature code is consist of (n+1) groups of 3 digits code where n was the number of root faces, the first digit represents the number of passage through the feature, the second digit consists of the number of boundary faces and third digit gives the number of convex adjacencies between pair of the root. The feature code generated with the corresponding manufacturing attributes specified for each feature was stored in the feature library. The steps in process of adding new feature were demonstrated as below by adding the rectangular corner slots with rounded edge shown in Figure 80 (used in the design of an artefact discussed later on in this chapter) to the list of features in feature library established for process planning program.

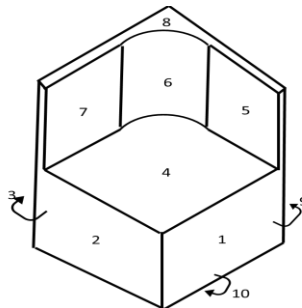


Figure 80: Rectangular corner slots with rounded edge

The corresponding (OMAAM) was generated for the part shown in Figure 81 where the root and boundary faces were identified and used in the generation of the FMAAM in steps to generate the feature code shown in Figure 82.

				B	B						
				R	R	R					
	1	2	3	4	5	6	7	8	9	10	
1	0810	1111	0810	1111	1111	0830	0810	1111	1111	1111	1111
2	1111	0810	1111	1111	0810	0830	1111	1111	0810	1111	1111
3	0810	1111	0811	0831	0810	0830	0810	1110	0810	1111	1111
R 4	1111	1111	0831	0830	-1111	-1331	-1110	0830	0810	0810	0810
R 5	1111	0810	0810	-1110	0810	-1130	0810	1110	0810	0810	0810
R 6	0830	0830	0830	-1331	-1130	0830	-1130	1310	0810	0810	0810
R 7	0810	1111	0810	-1110	0810	-1130	0830	1110	0810	0810	0810
8	1111	1111	1110	0830	1110	-1310	1110	0810	1110	0810	0810
9	1111	0810	0810	0810	0810	0810	0810	0810	0810	1111	1111
10	1111	1111	1111	0810	0810	0810	0810	0810	0810	1111	0810

B-Boundary Face, R- Root face

Figure 81: Object Multi Attributed Adjacency Matrix (OMAAM) for rectangular corner slots with round edge

		4	5	6	7
4	0830	-1110	-1331	-1110	-1110
5	-1110	0810	-1130	0810	0810
6	-1331	-1130	0830	-1130	-1130
7	-1110	0810	-1130	0830	0830

Figure 82: Feature Multi Attributed Adjacency Matrixes (FMAAM) for rectangular corner slots with round edge

The fourth row in FMAAM indicated that a five group (n+1) feature code for a rectangular corner slot was required. The feature properties including feature name, geometry code and corresponding manufacturing attributes specified for key faces summarised in Table 18 were stored in the feature library database. It is worth mentioning the simplicity in adding, removing and modifying the feature properties described by manufacturing attribute within the database that allows the operator to customise manufacturing attributed for a specific process and their manufacturing requirements.

Table 18: Feature properties for rectangular corner slots with round edge

Feature name	Feature code	Manufacturing attributes
Rectangular corner slots with round edge	032 132 331 122 122	<ol style="list-style-type: none"> 1. Datum 2. Reference face 3. Depth 4. Boundry face Width <ol style="list-style-type: none"> a. Face 4 b. Face 5 c. Face 7 5. Boundry face Length <ol style="list-style-type: none"> a. Face 4 b. Face 5 c. Face 7 6. Corner Radius 7. The surface roughness of Root face <ol style="list-style-type: none"> a. Face 4 b. Face 5 c. Face 6 d. Face 7

From the feature recognition stage, the list of features and corresponding manufacturing attribute required were transferred to user interface for the operator to manually assign the value as input to the system (geometrical and surface information are obtained directly from part drawing). In the process of feature categorisation, data validation functions were applied to values given for manufacturing attributes of feature faces to recognise distinct properties of microfeature required to be processed differently in micromilling. Furthermore, the criteria used for data validation can be customised to a specific process or machinery requirement where in this work, logic tests in relation to feature aspect ratio and surface roughness were used in differentiating between standard and microfeature where the conditions were described as below:

- If (Surface roughness of Root face < 1µm, micro, macro)
- If ((Boundary length or width/Depth) >10 , High aspect ratio, Regular)

The outcome of this module is the feature list created at user interface with link to their corresponding manufacturing attributes. The feature faces that satisfied the data validation

criteria's (high aspect ratio and micro surface requirement) were classified for the operator where the output page from this activity is shown in Figure 83.

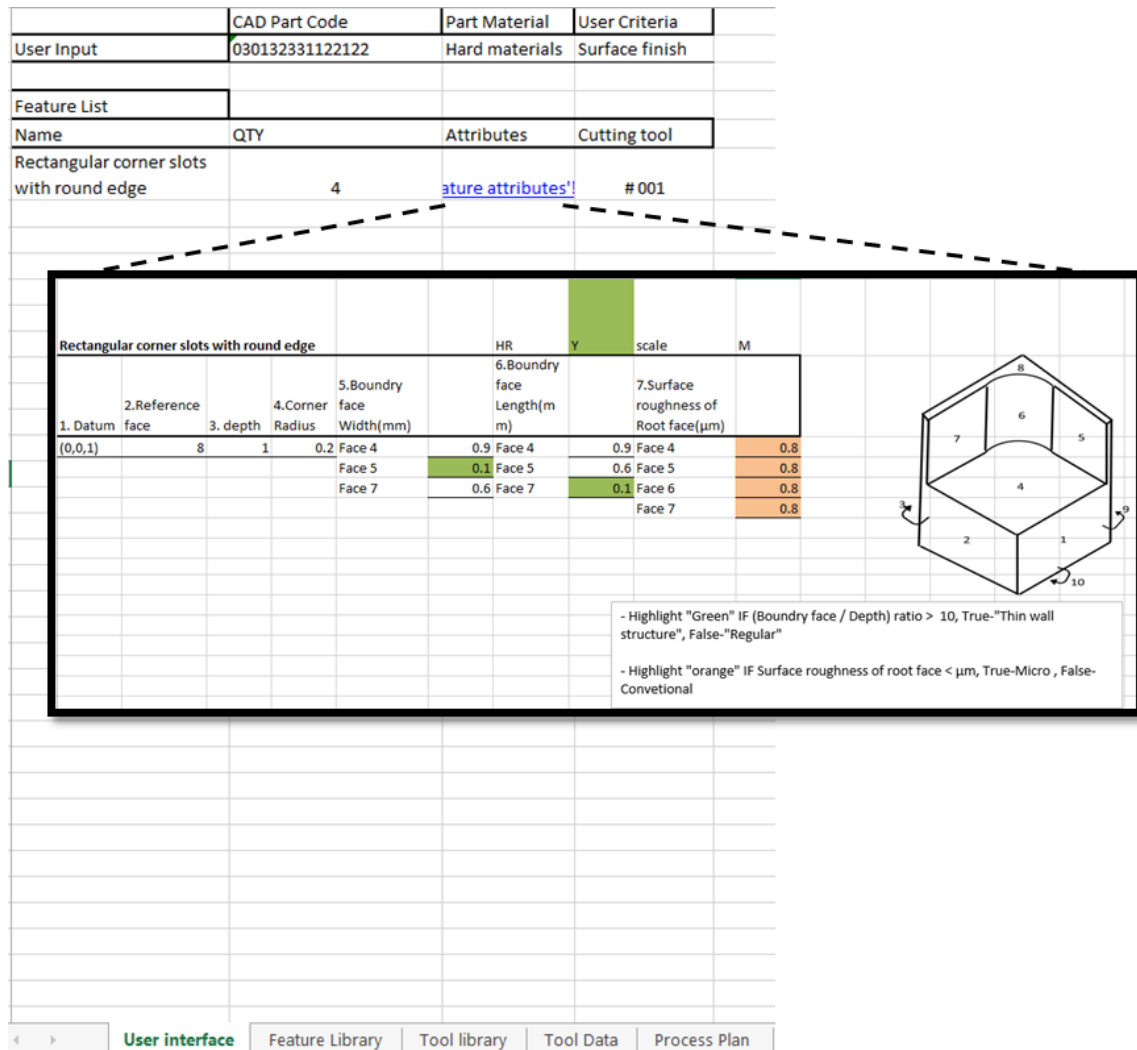


Figure 83: Output- part feature list and corresponding manufacturing attributes

It is worth mentioning that the proposed system is limited to extraction of simple geometries currently used in micro parts wherein the applications using complex geometry such as freeform surfaces in the future; generating a feature list relies on conventional feature extraction system.

6.2.3 Tool selection module

In conventional process planning, endmills are selected as a function of machine tool and operation characteristics, while available tools were further filtered by material suitability and geometrical collision test before a shortlist of tools is produced [146]. During the allocation of each tool to each machining operation, cutting tools are selected from the shortlist in relation to tool machinability rating [147] (widely available for conventional tools evaluated by institutes such as American iron and steel institute (AISI) and tool manufacturer) and their replacement strategy enabling the optimum tool to be selected. The conventional tool

replacement strategy uses static tool life data, evaluated following ISO (ISO 8688-2 procedure for evaluation of the life of endmills) procedure for estimation of tool life, combined with the feedback from the machine to estimate the tool change intervals.

However, due to the lack of readily available tool performance data and replacement strategy data, the comparison of endmills with sub-millimetre dimensions classified as micro endmills used in micromilling is impractical following the conventional approach. Furthermore, due to micromilling being in its infant data is lacking and when data does exist the data is acquired under high laboratory precision making the implementation of this data challenging. The necessity for using multi-process indicators with the close relationship between tool performance and interrelated machining parameters for the evaluation of micro tool life was demonstrated in chapter 4.

The newly created systematic approach for evaluating the machinability index and tool life was developed using Excel (Microsoft, 2013). The machinability approach described by Venkata [148] was used for the evaluation of machinability index in relation to multi- machinability criteria. Furthermore, a weighting system differentiating between the desired machining process requirement; surface roughness, accuracy and machining time, was applied to reflect the operator's requirement. Following on from this, a tool replacement strategy for micro tools was introduced based on the machining data and tool life criteria derived experimentally following the procedure for evaluation of tool life introduced in chapter 4. The micro tool selection system is summarised in Figure 84.

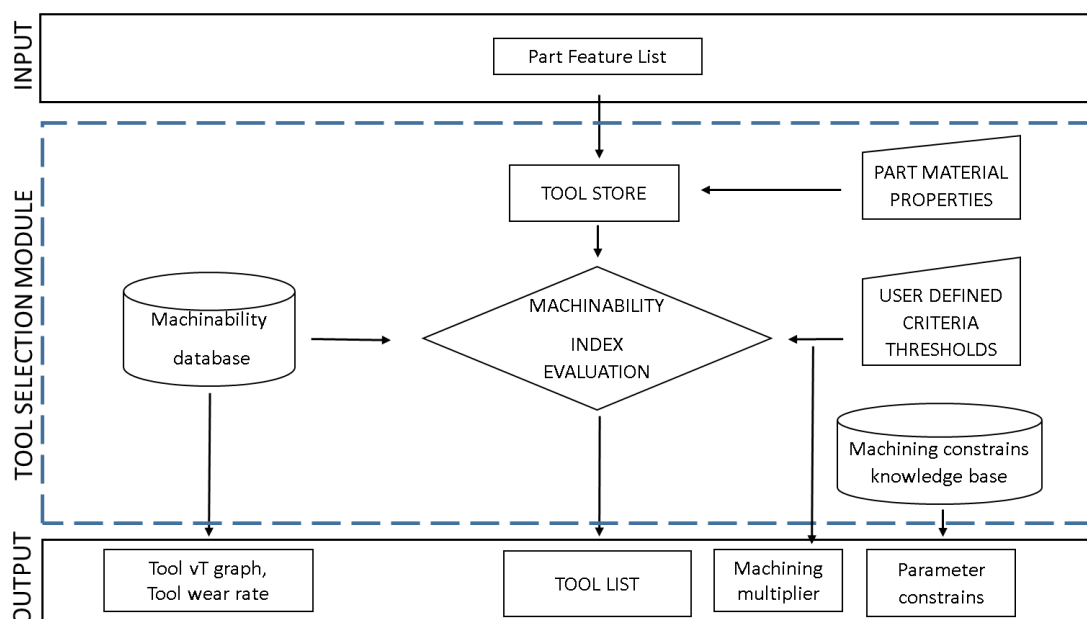


Figure 84: Overview of material module proposed for micromilling

Each time a new tool was added to the tool store the geometrical properties together with the material group capability of the cutting tool were obtained from the manufacturer's catalogue. Whilst the tool replacement strategy was defined by the corresponding vT graph obtained for individual materials (stored in the tool datasheet) following the standard procedure introduced in chapter 4. Following Venkata's mathematical model [148], the machining data obtained from the vT graph was used to form the tool vT table with the rows expressing the number of cutting speeds tested and the columns representing the machining criteria proposed in the evaluation of tool life. The corresponding values for tool life were used to generate the machining data matrix and subsequently normalized matrix to be specified with the tool geometrical properties and displayed in the tool datasheet stored in the machinability database.

The category for part material, specified at the design stage, was manually selected by the operator from the drop-down menu (choosing from six groups of materials defined by ISO 513 for the tool material summarised in Table 19) created in the user interface page. In the process of shortlisting endmills from the tool store, the conventional procedure (initially running a material suitability test followed by a geometrical collision test, in relation to feature depths obtained from the feature list) using the material category indicated by the operator was completed. The depth of each feature was used as criteria to further filter the tool list in relation to the tools maximum axial depth capability before the shortlist of tools was generated.

Table 19: Material categories and colour codes define by ISO513

Material	Steel	Stainless steel	Cast iron	Non-ferrous metals & non-metals	Heat-resistant alloys, titanium	Hard materials
Category	P	M	K	N	S	H
Colour code	Blue	Yellow	Red	Green	Orange	White

The four process relative importance factors used throughout this work; high surface finish, geometrical accuracy, efficiency and optimisation in relation to process objectives were used to assign a weighting to the normalised matrix of tools to calculate the machinability index value. The relative importance factor for the process was selected by the operator from a drop-down list in the user interface page where the corresponding weights to process indicator for the individual process was manually customisable by the operator. The evaluated machinability index was used to compare the performance of tools in the shortlist before a tool was assigned to each feature, represented by a row in the feature list. From the corresponding tool datasheet for the tools selected within the machinability database, the recommended cutting speed and tool change interval was indicated by the row with the maximum machinability index. In comparison, the tool change interval was specified as the lowest machining time in the

corresponding row on the tool vT table. The preview of the datasheet retrieved for the Tungsten carbide tool from machinability database is displayed in Figure 85.

Store Location	#001		
Material Type	H		
vT Raw data			
Cutting speed m/min	Surface roughness	Edge radius	Flank wear
97	6	2.6	12.24
126	11.8	2.5	7.36
157	9.7	0.6	4
188	10.2	0.4	3.53
220	6.2	0.6	5.4

Tool vT Table			Normalised matrix	Equivalent Index	Tool index
0.43	0.19	0.88	0.42227438	0.43144111	
0.84	0.18	0.53	0.3244218		
0.92	0.04	0.29	0.31409542		
0.94	0.03	0.25	0.3069202		
0.75	0.04	0.39			

Figure 85: Example of tool datasheet for individual tool within the tool store

Furthermore, a new machining constraints database was designed to increase the operator's awareness of the key information on tool performance in relation to the selected material and use of recommended cutting speed. As well as enabling the operator to archive additional tool constraints recommended by the tool manufacturer or machining behaviours based on specific materials learned through the experimental investigation specifically customised for industrial application. The summary of machining constraint data for the Tungsten carbide tool as stated below:

- Tool condition: Use of new tools is recommended
- Mounting of the tool: Use culet in clamping the shank is recommended (to minimise tool run-out effect)
- Coolant: Use of pneumatic mist jet impinging cooling (PMJIC) cooling technology is recommended

Following the experimental evaluation of Tungsten carbide tool in the machining of Titanium in chapter 4 further tool-specific limitation was also archived:

- Maximum axial depth of cut (a_p): 30% +/- 5% of flute length
- Maximum radial depth of cut (a_e): Tool diameter
- Maximum feed per tooth (f_z): 0.25 Tool diameter
- Maximum edge radius (r_e): 23 μ m

In process planning for micromilling, this database can act as a central repository of machining knowledge for better communication of gathered machining response and limitation identified

through experimental evaluation of tools and material. The output from this module was the feature list with the assigned cutting tool and their corresponding reference number, recommended cutting speed and tool replacement strategy for individual tool assigned to features in the feature list. Furthermore, a link to the corresponding tool datasheet within the machining constraint knowledge database was included on the feature list to notify the operator with the tool performance limitations.

6.2.4 Machining parameters selection module

The aim of parameter selection in conventional process planning is to provide an efficient range to machining parameters maximising the machining efficiency, typically achieved by increasing the material removal rate. The maximum limit of the machining parameters are widely available within the tool manufacturer catalogue and easily accessed by the operator during the process planning stage and included in the process sheet, whilst the machining parameters are further optimised by the operator during the manufacturing step using the machine feedback received from the material removal process.

However, the drawbacks of tool miniaturisation and selection of aggressive parameters resulting in immature tool failure combined with poor surface roughness, and difficulties in achieving secondary finishing process make the conventional approach unsuitable for micromilling. Additionally, limitations in the operator interaction during the material removal process (restriction with audible and visual inspection) requires the optimal parameter selection to be completed at the process planning stage and an advanced machining knowledge of the tool and material used. Furthermore an excessive tool wear rate and minimum chip thickness effect, with a strong dependency on material properties and tool geometry in combination with a strict requirement for the quality of surface finish and improved machining efficiency, emphasise the need for appropriate selection of the optimal machining parameters at the process planning stage.

Although optimisation of the individual machining parameter was excluded from the scope of this work, a systematic approach to the evaluation of the optimal machining parameter range is proposed. The methodology used in the development of the approach was obtained from the method introduced in chapter 4 and used by others throughout the literature for the task of parameter selection for micromilling. The outline of the parameter selection module is displayed in Figure 86.

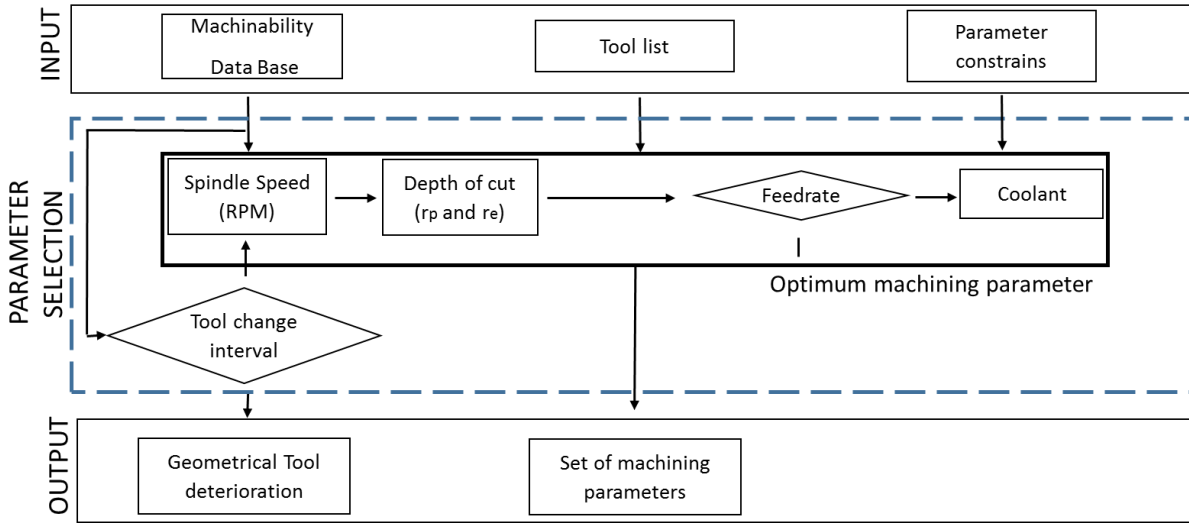


Figure 86: The outline of the machining parameters selection process

Taguchi model and regression analysis have been successfully used by multiple researchers throughout the optimisation of machining parameters [50, 52, 53, 149]. As such, a combination of both were applied when establishing a surface roughness model initially proposed by Lu et al. [50] that was utilised to implement a constrained base optimisation for the evaluation of the optimal feedrate. The statistical model is described in Equation 15 [50].

$$y = \beta_0 + \sum_{i=1}^k \beta_i x_i + \sum_{i=j}^k \sum_{j=i}^k \beta_{i,j} x_i x_j + \varepsilon \quad (15)$$

Where β is a model parameter to be fitted based on the measured value of response factors, k is a number of independent factors and ε is the error. The model uses regression analysis for the evaluation of independent variable coefficients; spindle speed (n), feed per tooth (f_z) and axial depth of cut (a_p), specific to a combination of tool and material using experimentally obtained surface data following that of Lu et al. [50]. As the surface roughness of the root faces was specified during the design stage, the optimal feedrate was evaluated using the linear surface equation (obtained at feature recognition activity and included in feature list), with both the spindle speed and depth of cut known for the selected tool (specified in tool selection activity). In micromilling, the need to accurately evaluate the constraints to the range of individual parameters specific to a tool and material combination was highlighted by the minimum chip thickness effect and the main dynamic problem of self-excited vibration, commonly known as chatter (the consequence of low depth of cut). Therefore, the specific limits to the parameters evaluated were stored in the machining constraints knowledge base (introduced in the tool selection module), whilst the regression equation for the surface roughness was added to the

tool datasheet stored in the machinability database and other parameter range constraints (feedrate and depth of cut) following the standard format expressed in equation 16.

$$V_l \leq V \leq V_u \quad (16)$$

Where V_l and V_u are the values of the lower and upper bound to the parameter value V respectively. When the upper range limit is not specified by the machining constraints knowledge base, the value for the upper bound of feedrate and the depth of cut must be evaluated by load testing [51]. Whilst the lower bound value for depth of cut should be determined from a 3D stability lobe diagram [150] utilising the subsequent plot of the depth of cut versus spindle speed to select the depth of cut corresponding to stable regions on the graph.

The lower bound value of feed per tooth was set by the minimum chip thickness indicated by the transition of material removal to the ploughing effect. In micromilling, when the chip thickness is comparable to the material grain size, the minimum chip thickness is interrelated to the workpiece material properties (microstructure and grain size) which can either be evaluated numerically [151-153] or experimentally [154-158] and published as the ratio of feed per tooth to cutting edge radius. For circumstances where the experimental validation of minimum chip thickness for a workpiece-tool combination is not feasible or available in the literature, minimum chip thickness can be estimated numerically using the mechanistic model taking into consideration the effect of tool run out proposed by Sahoo et al. [151], expressed in equation 17 [151].

$$h(t, i) = r + L \sin \left(wt - \frac{2\pi i}{K} + \eta \right) - \left[r^2 - L^2 - \cos^2 \left(wt - \frac{2\pi i}{K} + \eta \right) \right]^{0.5} \quad (17)$$

Where L is the distance between tool centres, r the tool run out, w the angular speed, K the tool flute and η the angle between connecting the cutter location. However, the exclusion of the impact of material properties in any of the numerical models found in this work limits the estimated value of minimum chip thickness and therefore will not be used in this module [159]. A ratio of 0.15, obtained experimentally by Ikawa et al. [156], for micromilling of titanium was used throughout this study. Therefore, the cumulative lower bound for feed per tooth was described as a function of machining time using an exponential equation describing the trend line of tool edge deterioration measured experimentally in chapter 4 (the experimental data is shown in Figure 42). In the selection of depth of cut and feed rate for optimum material removal rate, the value for the upper bound of depth of cut was suggested by parameter constraints sheet. While, using the corresponding surface regression equation for the selected tool, feed per tooth (f_z) and subsequently optimal feedrate was evaluated expressed in the equation 18.

$$F = f_z \cdot S \cdot N \quad (18)$$

Where f_z is the feed per tooth, S the spindle speed, and N the number of flutes. It is recommended to use the lower bounds of the machining parameters when machining high aspect ratio feature, with the lower bound for feed per tooth (f_z) being evaluated using the exponential equation describing tool edge deterioration. Tool edge deterioration was described by trend line of the experimentally evaluated tool wear graph, similar to one evaluated in chapter 4 (Figure 42) and subsequently, the cumulative feedrate is recommended to be used as a function of machining time. The outcome of this module is the corresponding cutting parameters (spindle speed, depth of cut and feedrate) for allocated tools for machining of the individual feature on the feature list.

6.2.5 Machining sequence module

In conventional machine sequence planning, tool path and machining layer strategy are optimised in relation to tool path length and designed to maximise the tool life. Therefore, in the selection of machining layer strategy, the path with the shortest length was selected with tool entry and exit position optimised for the shortest distance.

However, in micromilling, further considerations to compensate for low stiffness of tool and feature geometry [63], surface accuracy constraints and enhance tool path errors [160] are required thus, changing the machine sequence planning for micromilling. Furthermore, the increased effect of machining vibration, due to excessive tool wear, results in a consequential burr appearance leading to difficulties in achieving the secondary finishing process. As such, this needs to be compensated in the design of tool path strategies to improve tool life and machining stability. Chapter 5 studied the effects of machine layer strategies in micromilling of thin walls, which highlighted the significance of cutter position. This chapter also investigated tool path strategies highlighting the impact of geometry type and strategies on machining stability. These findings combined with the difficulty in accomplishing a secondary finishing process, and the consequence of tool run out and machining vibration in burr appearance reported in literature [24] (due to tool assembly and cutting tool fabrication error); necessitate the selection of tool path strategy that achieve better machining stability yet maximising the machining efficiency.

This module proposes a systematic approach for the evaluation and compensation of tool path error and introducing a methodology for the selection of tool path strategy and machining layer sequencing with application on thin wall structure introduced in chapter 5. The internal process flow is displayed in Figure 87.

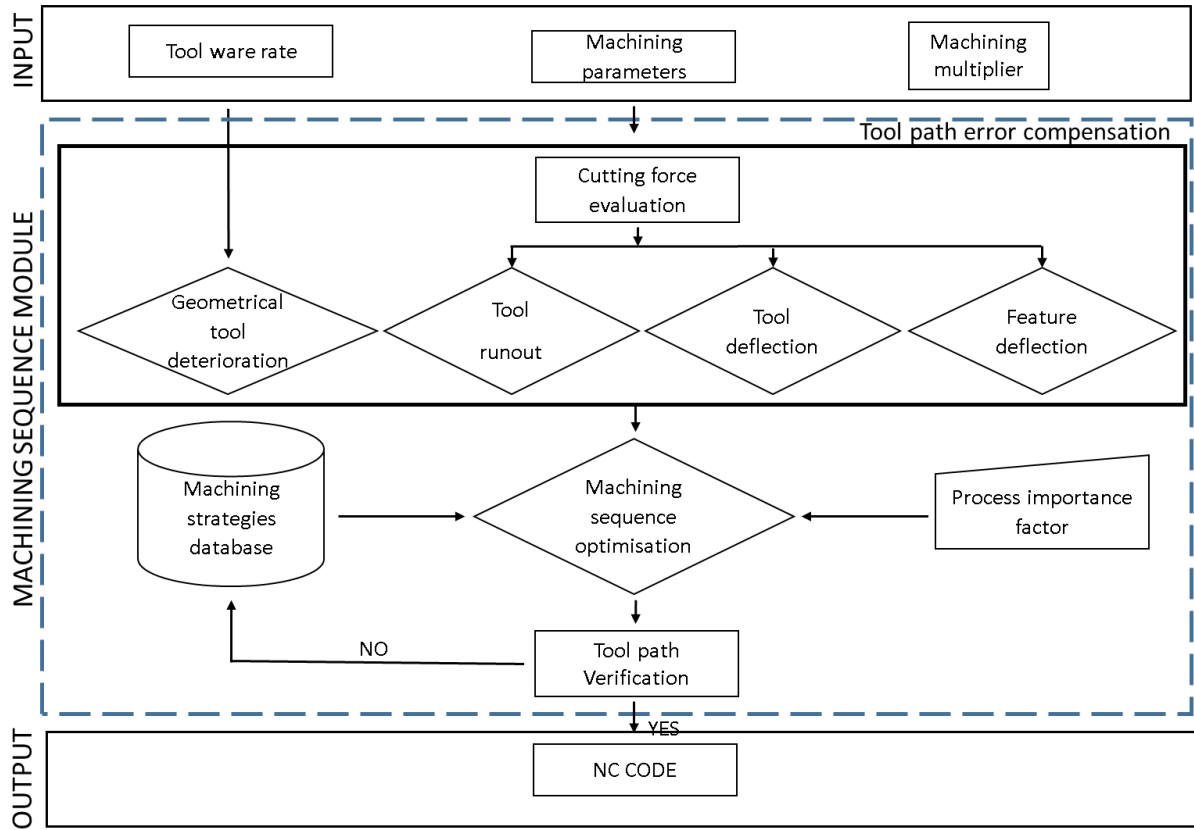


Figure 87: Flow chart of machining toolpath and strategic sequence selection for micromilling

In the evaluation of tool deflection, utilising the list of tools and corresponding machining parameters evaluated in previous activities, the resultant thrust force along the cutting direction of the tools can be estimated using equation 20 [161].

$$F_t = \frac{uHA_c}{3} \left(\frac{\cot \gamma}{\sqrt{3}} + 1 \right) + A_f (0.62H) \sqrt{\frac{43H}{E}} \quad (20)$$

Where F_t is the total thrust force, u the friction coefficient between tool rake face and workpiece, H the hardness of workpiece material, A_c the face area of the chip, γ the shear angle, A_f the flank area of the tool and E the elastic module of the workpiece. The variation in the face area of the chip (A_c) during the tool translation through the material as a function of rotation angle (θ) is described by equation 21 [161].

$$A_c = df_z \sin \theta (1 \pm \zeta) \quad (21)$$

Where d is the tool diameter, f_z the feed per tooth, θ the tool rotational position and ζ the measured run out of the tool (a combination of tool assembly, centring and fabrication error). The flank area of the tool (A_f) was described as the interface area between the flank face of the

tool and workpiece material. The approximation of flank contact area is described by equation 22 [161].

$$A_f = \left(\frac{R_t W_L \phi}{2 - \sin \theta} \right) \quad (22)$$

Where R_t is the radius of the tool, W_L the width of the wear land, ϕ the contact angle between tool and the workpiece and θ the rotational position of the tool. W_L was obtained from the vT table found in the tool datasheet (shown in Figure 85) described for cutting speeds using linear equation as a function of time. Therefore, the linear equation describing the wear land expansion can replace the value of W_L to describe the cutting force as a function of machining time. The calculated cutting force (F) is then used as an input parameter to estimate the bending deflection of the tool described by the relationship between bending moment and bending deflection in equation 23 [162].

$$EI(z)\delta(z) = -M \quad (23)$$

Where M is the bending moment calculated from the equilibrium condition obtained using equation 24 [162].

$$M = -F(L - z) \quad (24)$$

E is a module of elasticity for tool material, $I(z)$ is the second moment of area for a circular cross-section of the tool described by equation 25 [162].

$$I(z) = \frac{\pi d^4(z)}{64} \quad (25)$$

d is the tool diameter of the cutter and the $\delta(z)$ is the tool deflection described by equation 26 [162].

$$\delta(z) = -\frac{F}{6EI_3} z^3 + \frac{FL}{2EI_3} z^2 + B_5 z + B_6 \quad (26)$$

B_{5-6} are constraints for tool describing the contribution of tool section to total tool displacement and I_3 is the depth of cut.

In the application of machining high aspect ratio, the maximum deflection of faces marked as high aspect ratio deformation can be evaluated using the maximum deformation model by Qu et al. [163], assuming the maximum formation occurs at a cutter position of half the tool length as shown in equation 27 [163].

$$W_{max} = \frac{F_z L^3 (13L - 2)}{96(L + 2)EI} \quad (27)$$

Where L is the face length found from the feature list, F_z the thrust force calculated in equation 30, E the elastic modulus of workpiece material, and I the moment of inertia for beam structure described in equation 28:

$$I = \frac{bh^3}{12} \quad (28)$$

Where b is the depth of the feature face and h the height of feature specified by manufacturing attributes for the features in the feature list. In compensation for the geometrical deterioration of the tool due to wear, it is recommended that the actual diameter value obtained experimentally in chapter 4 should be used, however, in this work the tool diameter reduction was described by the trend line equation for selected cutting speeds. In the evaluation of the tool path error compensation, given that the tool deflection, feature deformation, tool run out and tool diameter reduction as a function of machining time were evaluated for each feature on the feature list, the offsetting value of the tool path was obtained as the total sum of the maximum errors.

In the selection of machining sequence, a database was formed using the name and corresponding independent variable score for a range of tool paths and machining layer strategies experimentally evaluated in chapter 5. The selection methodology by Cardoso [139] was used to select the best machining sequence available in cooperating the importance factor weight introduced in tool selection module in section 6.2.3. The mathematical scoring system as a function of independent variable scores is described by equation 29 [139]:

$$f(\alpha, \beta, \gamma) = \frac{1}{(x * (\frac{\alpha}{\alpha_{max}}) + y * (\frac{\beta}{\beta_{max}}) + z * (\frac{\gamma}{\gamma_{max}}))} \quad (29)$$

Where f is the total score, x, y and z are the importance factor, α, β and γ are the independent variable score for accuracies, the surface roughness, and machining time respectively. The name of the tool path and layer strategy with the highest score were then recorded for each tool in conjunction with the layer sequence index sheet. The outcome of this process model is the correspondent tool path, machining layer strategy and tool path offset value that are recorded on the feature list for each tool to complete the process plan datasheet.

The process plan datasheet populated through the process methodology reviewed in this section including the list of part features; tools with their corresponding machining parameters,

replacement strategy, machining sequences and their corresponding parameters. The outcome of this system (process datasheet) is to be submitted in addition to the product design to the next stage (manufacturing) for the machine operator to convert the process steps and parameters using CAM system to set of machine code for the fabrication of the part.

6.3 Experimental validation

The conceptual process planning methodology was benchmarked against the conventional method by fabricating an artefact (a commercially used component with thin wall feature - Micro impeller). The component was designed in CAD (Image of the model from Inventor (Autodesk, Professional 2015) is shown in Figure 88) and assigned with the material, geometrical and surface tolerance (made of Titanium with geometrical tolerance of ± 0.005 mm and surface roughness under 500nm). The part drawing was used as an input during the manufacturing stage submitted to the machine workshop for the fabrication of the parts. Additionally, a process datasheet (shown in Figure 89) was generated using a model developed through the implementation of the proposed methodology in Excel (Microsoft, 2013). In order to generate the machine numerical code (NC) from the selected process datasheet, a commercial computer aided manufacturing (CAM), EdgeCAM (Vero, 2016R2) was used to manually extract feature and assign the corresponding machining parameter and sequences given for each feature geometry from the process datasheet. The overview of these steps are displayed in Table 20 and the copy of the NC code post-processed for selected machine centre included in Appendix 4. For the fabrication of components processed conventionally, the operator was assigned with the task of process planning where the selected tools and machining parameters were obtained from the tool catalogue (Appendix 2).

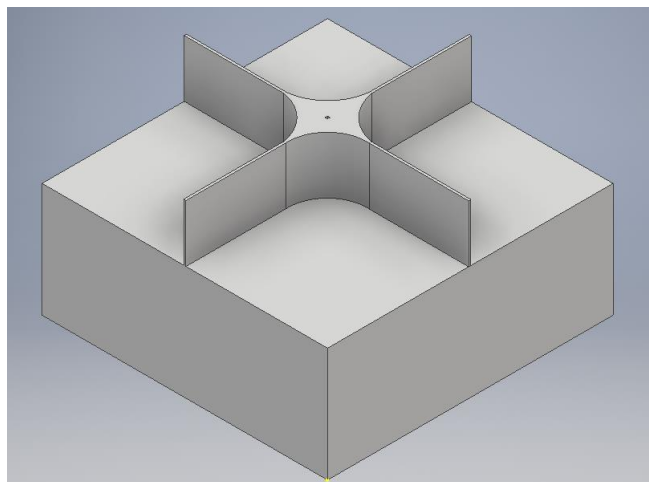


Figure 88: Artefact model - micro impeller

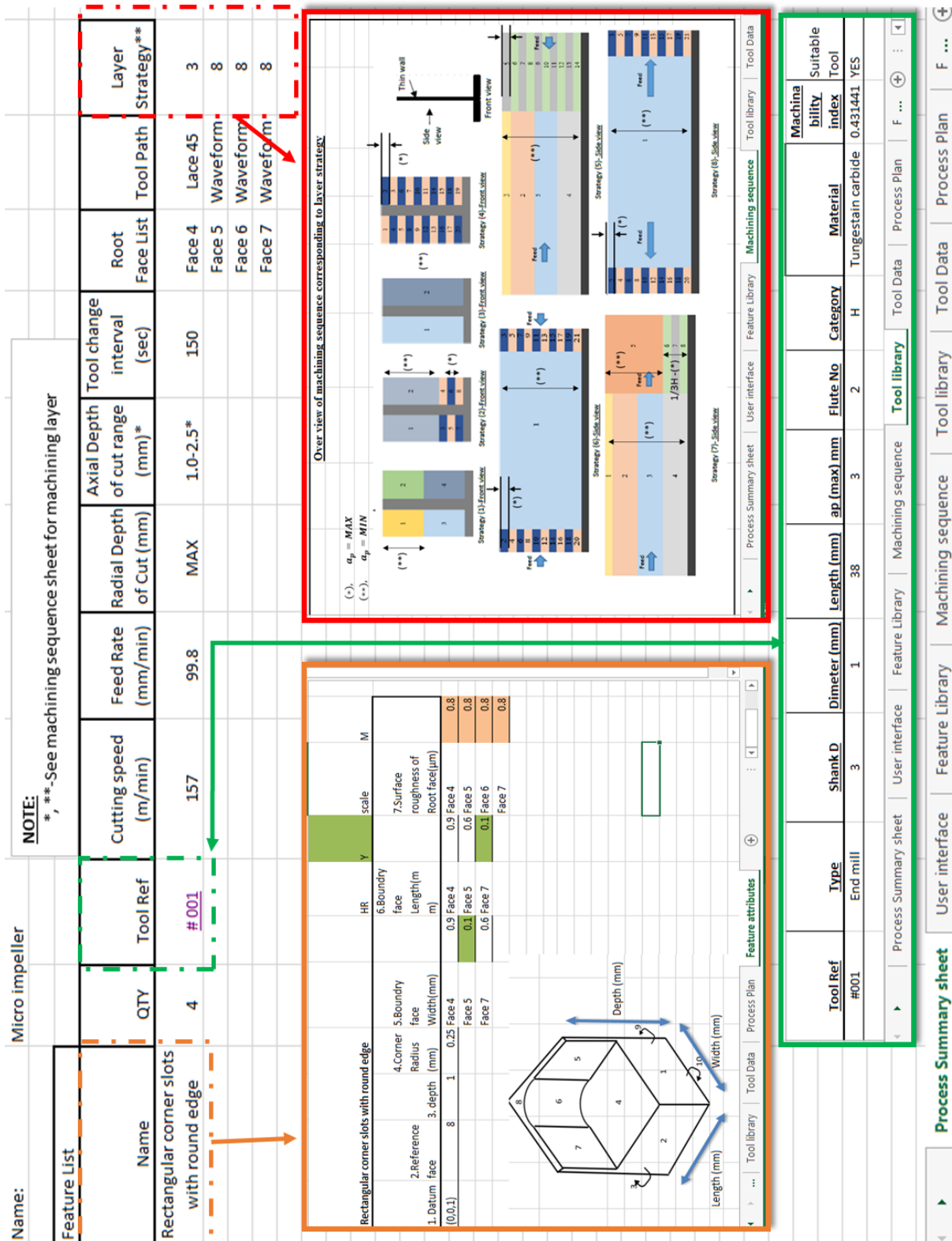
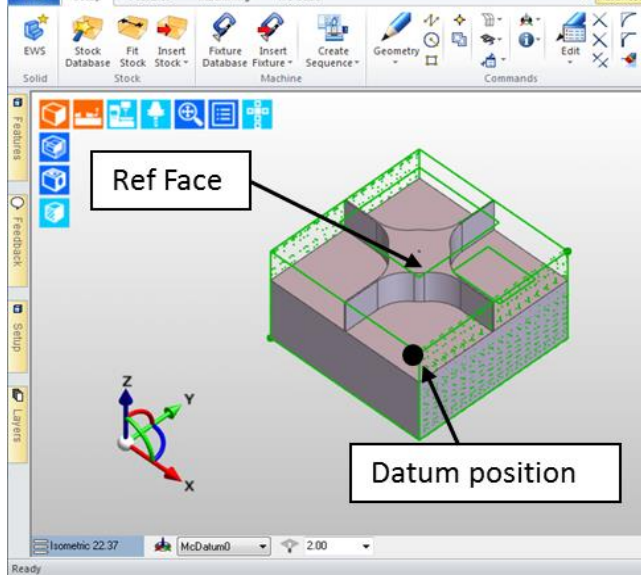
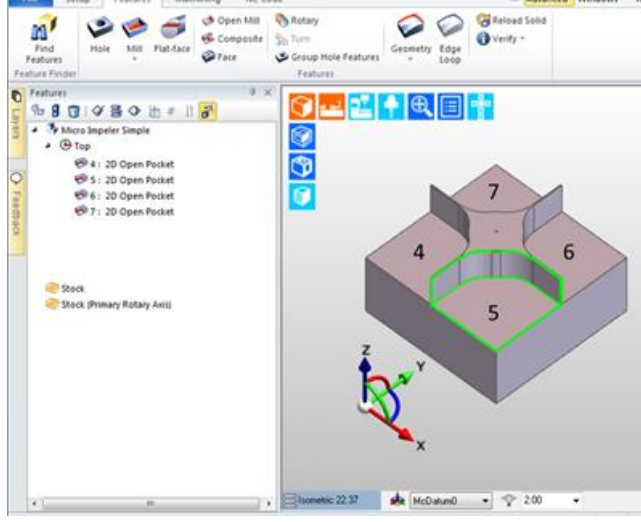
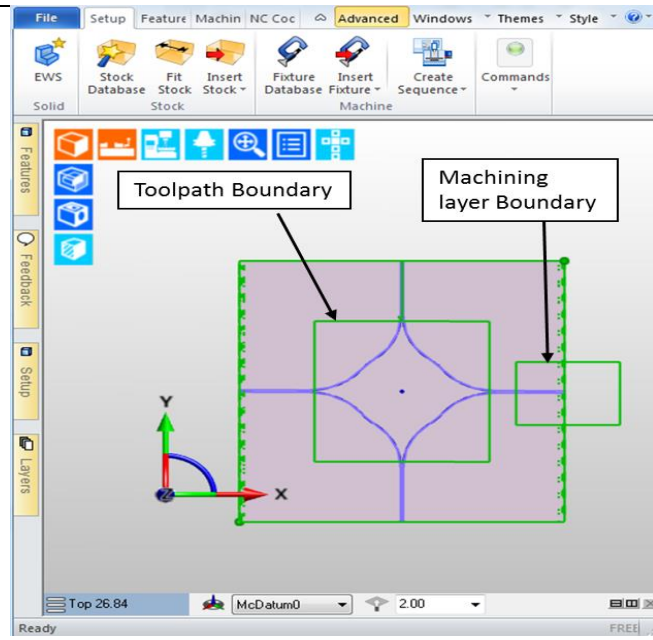


Figure 89: Process datasheet for the fabrication of micro impeller

Table 20: The Step procedure in generating the NC code

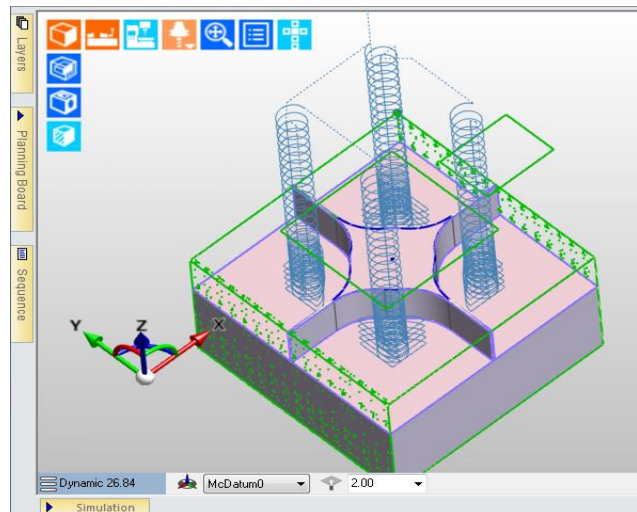
Steps/Description	Demo
<p>1. Stock fit:</p> <p>Following the import of solid model into Edge CAM environment, initially the material stock was defined with dimensions of the block of raw material feed into the machine. While the “Datum position” and “Reference face” was defined in relation to feature attributes defined by Feature attributes.</p>	 <p>The screenshot shows the Edge CAM software interface. The top menu bar includes File, Setup, Features, Machining, and NC Code. The main workspace displays a 3D model of a part with a green wireframe bounding box representing the stock. A callout box labeled 'Ref Face' points to the top surface of the stock, and another callout box labeled 'Datum position' points to a specific point on the top surface. A 3D coordinate system (X, Y, Z) is visible in the bottom left corner.</p>
<p>2. Feature extraction:</p> <p>Following the list of features in Feature List, the quantity of 4 corner slots with circular corner was manually defined (Part symmetrical across X and Y)</p>	 <p>The screenshot shows the Edge CAM software interface with the 'Feature List' window open on the left. The list contains the following items: Top, 4: 2D Open Pocket, 5: 2D Open Pocket, 6: 2D Open Pocket, 7: 2D Open Pocket, Stock, and Stock (Primary Rotary Axis). The main workspace displays a 3D model of the part with the four corner slots highlighted in green and numbered 4, 5, 6, and 7. A 3D coordinate system (X, Y, Z) is visible in the bottom left corner.</p>

3. Boundary segmentation:
 Providing different tool path strategies were selected, tool boundary was defined to reflect the areas machined using different tool path strategy. A secondary boundary was defined to accommodate for different feed direction requirement by tool layer strategy that was selected.

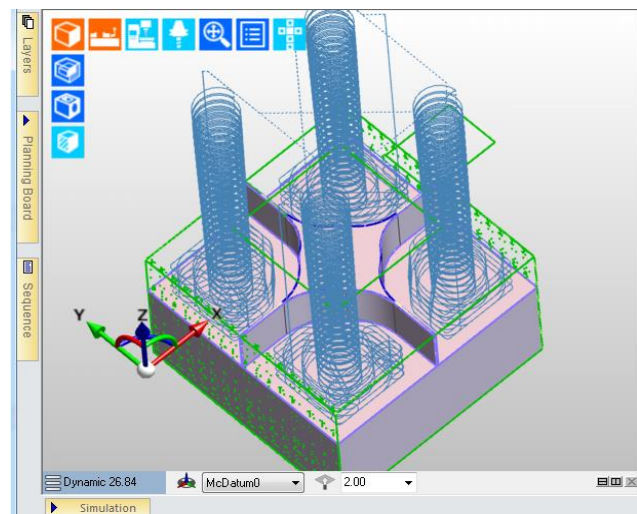


4. Tool selection and machine operation sequencing:
 The tool data obtained from the tool library within the process summary sheet are used to define the cutting tool within the CAM tool store and been assign to machining operation for each root face listed in the feature list. The sequence of machining operation follows the sequence given in layer strategy wherein operation 1 the material around circular geometries were removed first. In the second operation remaining material around the linear geometries were removed leaving the excess supporting material around the thin wall edge that is removed last by operation 3.

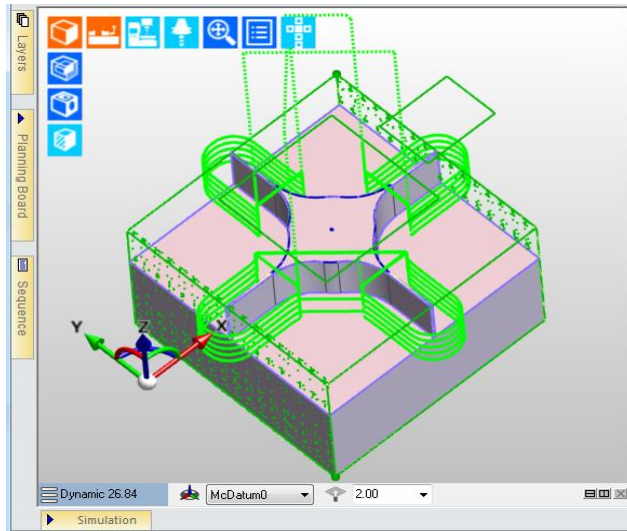
Operation 1:



Operation 2:

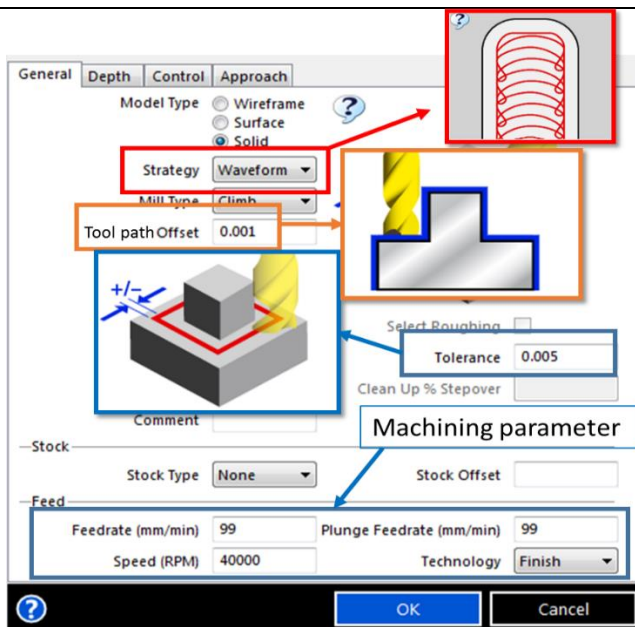


Operation 3:



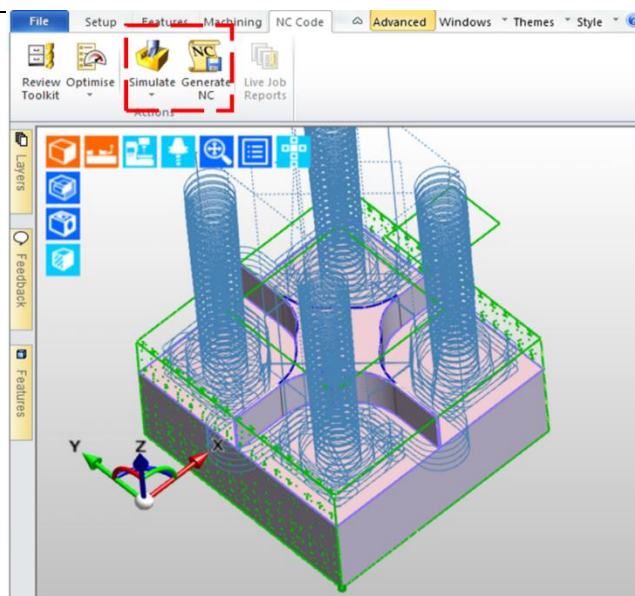
5. Selection of machining parameters:

The given machining parameter and tool path strategy for individual root faces obtained from process datasheet were assigned to the corresponding operation.



6. Tool simulation and NC generation:

The machine operation sequence and tool paths were verified by simulation before the numerical machine code was generated.



6.3.1 Results and discussion

The finish machined parts were examined in relation to geometrical and surface accuracy of thin wall structures in comparison of two process planning methodologies (conventional in comparison to proposed process planning methodology). The geometrical and surface data achieved for parts fabricated are summarised in Figure 90 to Figure 92.

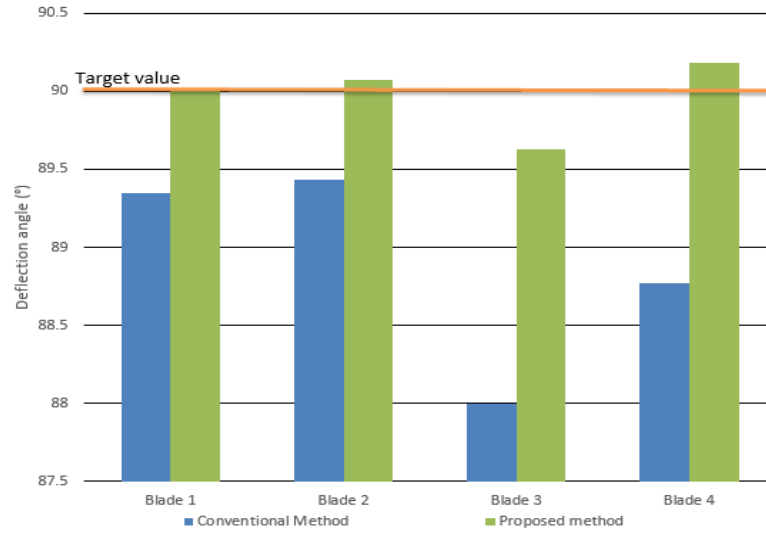


Figure 90: Maximum deflection angle of micro blades

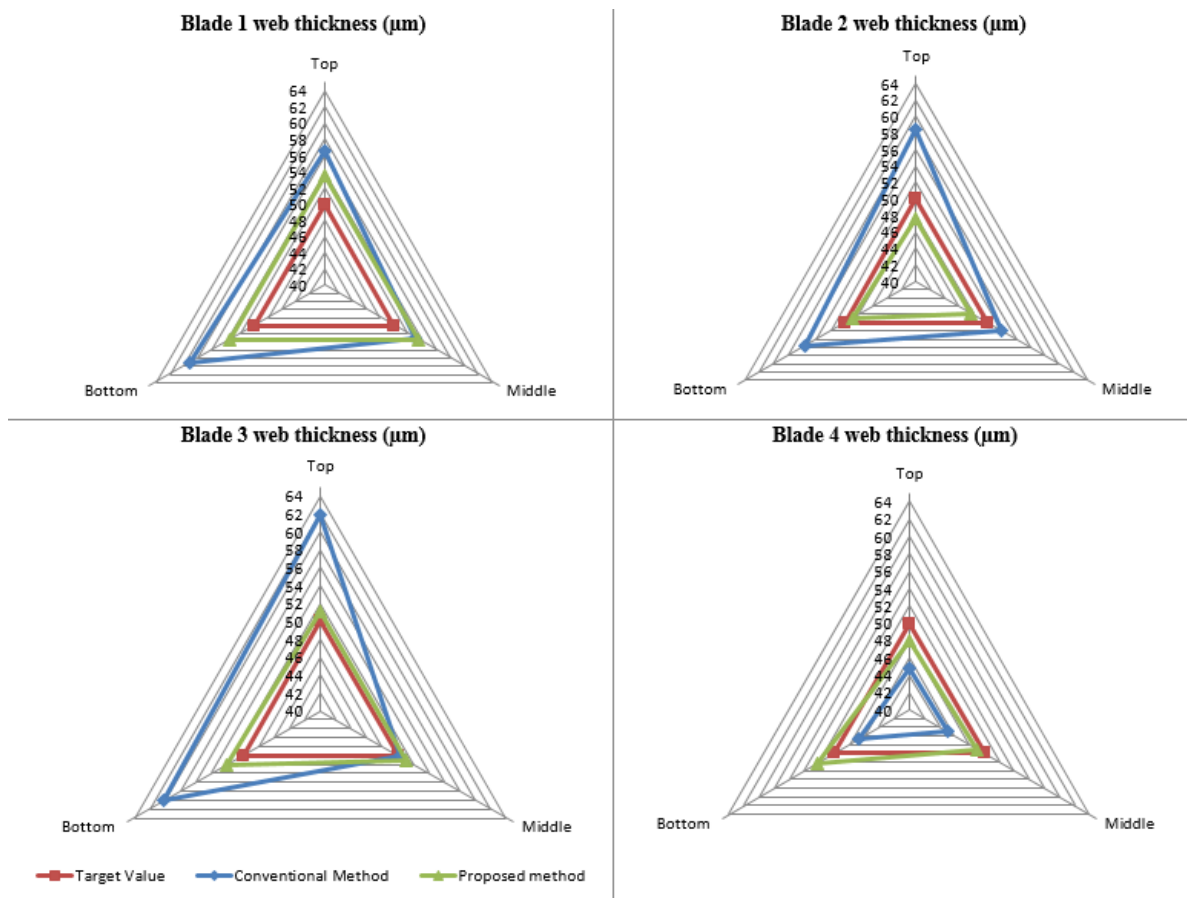


Figure 91: Web thickness of the micro blades

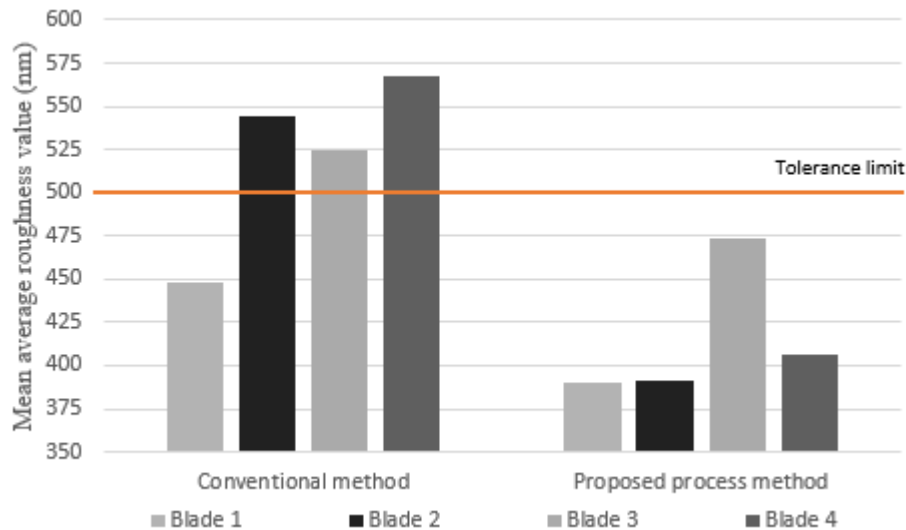


Figure 92: Mean surface roughness of micro blades side face

The comparison of achieved thin wall deflection angle (zero deflection is desired) in Figure 90 shows a drop in deflection error from 3% to 1%. This was achieved by processing the part following the proposed process planning methodology. The reduced deflection error suggests that the superior cutting condition evaluated using the proposed methodology for machining of thin wall structures reduced the impact of cutting forces on the finished thin wall accuracy. Furthermore, the drop in the range of measured deflection angle from 2° to 0.5° indicates improved repeatability of part accuracy when following the proposed process planning methodology. This is a major contribution to the development of process reliability for micromilling.

In the assessment of geometrical accuracy, web thickness of micro blades were measured and shown in Figure 91 (Target web thickness of $0.05\text{mm} \pm 0.005\text{ mm}$). The measured web thickness of the micro blades fabricated using the conventional process plan resulted in a web thickness outside the range of the specified tolerance of $\pm 0.005\text{ mm}$ (blade 1: bottom- $58\ \mu\text{m}$, blade 2: top- $57\ \mu\text{m}$, blade 3: top and bottom- $62\ \mu\text{m}$ and $58\ \mu\text{m}$ respectively and blade 4: top and middle- $44\ \mu\text{m}$ and $44\ \mu\text{m}$ respectively). However, the web thickness measured from the part fabricated using the proposed methodology achieved the web thickness within the specified geometrical tolerances. The large range (up to $12\ \mu\text{m}$) observed for the web thicknesses across the height of supposedly identical thin walls with a constant $50\ \mu\text{m}$ thickness, indicates poor repeatability when using the conventional process. Moreover, the variation of web thickness across the height of thin walls (with the range up to $8\ \mu\text{m}$) fabricated using the conventional process makes the use of a compensation technique difficult. However, the achieved web thickness with lower in range across the height (up to $1\ \mu\text{m}$) by part using the proposed

methodology enabled the use of other compensation techniques such as tool path offsetting to achieve an even lower geometrical tolerance in micromilling. The comparison of the geometrical accuracy also indicates to the improved capability of micromilling by utilising the proposed process planning methodology.

The effectiveness of the proposed methodology was also compared in relation to the average surface roughness of feature faces recorded in Figure 92. The surface roughness achieved by using the conventional method exceeded the surface tolerance required (below 500nm) for blades 2, 3 and 4 (544 nm, 525 nm and 567 nm respectively), therefore, the part produced was categorised as a defect. However, the surface roughness for the feature faces achieved by the proposed methodology was within the tolerance limit for all blades. The jump (from 450 nm to 544 nm) in surface roughness as machining progressed from blade 1 and blade 2, exceeding the surface tolerance limit, highlighted the ineffectiveness of conventional tool change strategy for micromilling. Furthermore, the rapid increase in surface roughness from 410 nm to 570 nm suggests that unsuitable machining parameters led to a higher tool wear rate and lower machining stability.

In micromilling, using the proposed methodology, there was a 17 % reduction in the measured maximum surface finish suggesting the superior conditions selected results in better machining stability and lower tool wear rate, and should therefore be implemented.

6.4 Conclusion and remarks

The task of process planning, a detailed evaluation of process steps and selection of the corresponding variable in micromilling, plays a key role in improving the machine efficiency, achieving geometrical and surface tolerances and prolonging the life of micro tools. The methodology for evaluation of machining parameters and compensation technique with consideration of distinct features of micromilling are outlined in this chapter. The following conclusions are made:

- The quality and accuracy of part interpretation stage directly influence the logic used in the process plan activities. Therefore, the standardisation of feature extraction and feature processing methodology to identify key feature data for use in subsequent planning activities is essential.
- The explicit characteristics of the workpiece material and their impact on tool wear and consequently tool life for micro tools need to be accounted for in the evaluation of machinability index. The machinability index value for a specific tool and workpiece combination is a key indicator for operator tool selection. Likewise, this value can be

beneficial at the design stage, as tool availability can be considered when selecting workpiece material and tolerance requirements.

- Micro endmills replacement strategy should be evaluated in relation to the impact of machining parameters on wear rate, with attention given to tool edge radius, identified as the main tool life criteria.
- Accurate estimation of tool run out, tool deflection and feature deformation are critical for the effectiveness of tool path compensation technique in micromilling. While strategic selection machining layer sequencing applicable to micromilling of high aspect ratio features to control chatter and minimise geometrical inaccuracy is critical in achieving machining tolerances.
- In the task of populating a comprehensive process sheet; standardisation of procedure helps to overcome the traditional knowledge-intensive task in process planning. Whilst improving the communication between the planner and the operator ensuring that the key feature information and corresponding prerequisite variables for machine coding, either manually from the machine interface or using CAM software are provided. An important step towards the automation of process planning.

Chapter 7. Conclusions and future work

7.1 Conclusions

The miniaturisation of the cutting tool and features used in micromilling has majorly impacted the approach towards process planning especially in applications with high aspect ratios. Besides common tasks of feature translation and evaluation of optimum machining process sequences and their corresponding parameters; attention must be given to the compensation of emerging machining errors in process planning. Therefore the proposed modules used in the development of a methodology for process planning for micromilling are valuable guidelines to the operator undertaking the task of process planning for micromilling. The conclusions drawn from this research are as follows:

- In machine sequence planning, the characteristic of tool path motion is shown to be highly sensitive to the geometry type. Also, the constant engagement of the tool along the path and prevention of sharp turns are found to be vital to avoid tool failure and improve stability. In micromilling of thin wall structures, additional structural support by the use of un-machined excess material is required where removal of excess material should proceed from the least supported to the most supported region. Also, tool entry and exit position into excess material should be selected in relation to feature structural stiffness. Optimum selection of tool path and layer strategy are shown to be equally

important as the optimisation of machining parameters, where the balance of machining accuracy and productivity can be achieved. Currently, it has been achieved at the expense of productivity.

- The rate of wear for uncoated tungsten carbide tools in the machining of titanium was separated into three stages that are initial, stable and rapid wear. Wear mode during the initial and stable stage were regarded as non-uniform abrasive wear along the active edge of the tool while in rapid stage a combination of abrasive and adhesive wear was observed. The transition point to rapid stage has been shown to result in degradation of surface roughness indicating an increase in machining vibration; meanwhile, the higher appearance of burrs around the sharp edge of the machined features was observed. The adhesion wear was also associated with increasing tool edge radius that results in rapid extension of wear land width across tool flank face and deterioration of tool diameter. Maximum wear land width of 27 μm and cutting edge radius of 30 μm were proposed as tool life criteria for uncoated tungsten carbide tools.
- In the investigation of machining parameters, small depth of cut used in micromilling was found to be responsible for vibration showing a direct relationship between the depth of cut and machining stability. Higher cutting speeds and lower feed rates are shown to extend the micro endmill's life in relation to the proposed tool life criteria. Increasing the cutting speed also reduced the flank wear rate; consequently, improving the machining stability as suggested by the lower surface roughness. Low feedrate can have an adverse effect if the minimum chip thickness value is disregarded, leading to ploughing effect that increases the vibration and surface roughness; therefore, lower bound for feedrate must be evaluated in relation to micro tool wear. In optimisation of machining parameters in relation to surface roughness, the use of adaptive feedrate is recommended considering the increasing tool edge radius due to wear.
- Process planning plays a key link between design and manufacturing. The results and discussions from the investigation of miniaturisation of cutting tools and feature geometries suggest that the difficulties faced in micromilling arise from the lack of methodological approach to process planning for micromilling. This is particularly valid for applications with high aspect ratio. Also, the accuracy of feature extraction in the process planning stage is essential due to the deficiencies in transferring information between CAD and CAM. Therefore, the proposed standardisation of part interpretation to include key information required for the task of process planning in micromilling is essential to ensure the quality of information feeding into the system. In the assessment

of tool performance, standard reporting procedures must be used if meaningful and comparable data are to be used for evaluation of the machinability index that enables the operator to compare tools in the task of tool selection. Furthermore, a repository of machining knowledge is required to store additional experimental performance data for a specific tool and material combination to deskill the task of decision making in process planning.

7.2 Contributions to knowledge

This thesis incorporates many key findings for process planning activities in the field of micromilling explicitly for the fabrication of thin wall structures. The major contributions of this thesis with a brief description are summarised below:

- This study introduces for the first time a systematic process planning methodology for micromilling with an application to thin wall structures. At the same time, it provides a systematic approach to solve the process planning tasks to assist the operator in the generation of process datasheets without prior knowledge of microscale machining. The newly proposed methodology involves the implementation of internal logics for key activities in Microsoft Excel to generate the process datasheet using a combination of user-system interaction and prior database for input.
- The study of tool wear in Chapter 4 proposed new tool rejection criteria for the evaluation of the life of micro endmills and their replacement strategy. The proposed procedure can be considered as a guideline for academics/manufacturers to evaluate and report comparable tool performance data.
- A new technique to account for multi machinability criteria that affect the micro tool performance was introduced for the evaluations of machinability index. This technique allows a novel and simple way to compare the performance of micro endmills in the task of tool selection by the operator in process planning.
- The findings from the investigation of the impact of machining layer strategy on the accuracy of thin wall structure extended the body of knowledge on the characteristics of layer strategies and their behaviour in relation to geometry type. The results from the comparison of micro tool performance, using different tool path strategies in the machining of linear and circular geometries, enabled a better understanding of the tool path strategy effect on geometry type. The machining knowledge gathered adds to fundamental machining data used in the formulation of the logic test for machine sequence planning module in the process planning system.

7.3 Future work

Although the process planning methodology proposed in this research shows to be effective in achieving tight tolerances and improved the repeatability in micromilling, other improvements can still be made. This section also briefly highlights some interesting research topics that are worth investigating further. The potential areas for future work are outlined below:

- Following the implementation of the proposed process planning methodology in Microsoft Excel, the process datasheet generated was manually inputted to commercial CAM software to generate the NC code. This step can be eliminated if the proposed methodology is implemented as an additional module explicit for micromilling within a CAM package.
- In this research, only the tool life of 2-flutes uncoated Tungsten carbide in combination with Titanium 6061 was evaluated and stored in the tool database. The expansion of this tool database for different tool coating and tool geometry in combination with a wider range of materials benefits the selection of the most suitable tool in process planning. It also contributes to the expansion of machining knowledge on tool wear and tool life, and increases the confidence level of the system.
- The study of tool path strategies in relation to their corresponding tool motion and feature geometry type highlighted the impact of characteristics of tool paths on the performance of the micro tools, indicated by the surface roughness. The change in resultant surface roughness further suggests that tool path strategies could influence the rate of micro tool wear. Therefore, the study of tool path strategies in relation to tool wear may help to increase the life of the micro tool and consequently improve machining stability and tolerances achieved.
- The study evaluating the sequence of machining layers suggested the importance of selecting the tool entry and exit position in particular to the machining of high aspect ratio structures. Therefore, the development of tool motion simulator module used for collision detection in commercial CAM, by enabling the evaluation of structural stiffness of part feature, can assist the operator in improving the machining sequence explicit to part feature.
- Micro components are currently made of simple features where the feature extraction methodology proposed in this research is only capable of extracting. However, further development of the feature extraction module is required, since when more sophisticated features, such as free form surfaces, are used in the design of micro components that still relies on the conventional method.

References

1. Asad, A.B.M.A., et al., *Tool-based micro-machining*. Journal of Materials Processing Technology, 2007. **192–193**: p. 204-211.
2. Lauro, C.H., et al., *Optimization of micro milling of hardened steel with different grain sizes using multi-objective evolutionary algorithm*. Measurement, 2016. **85**: p. 88-99.
3. Weule, H., V. Hüntrup, and H. Tritschler, *Micro-Cutting of Steel to Meet New Requirements in Miniaturization*. CIRP Annals - Manufacturing Technology, 2001. **50**(1): p. 61-64.
4. Geiger, M., et al., *Microforming*. CIRP Annals-Manufacturing Technology, 2001. **50**(2): p. 445-462.
5. Leo Kumar, S.P., J. Jerald, and S. Kumanan, *An intelligent process planning system for micro turn-mill parts*. International Journal of Production Research, 2014. **52**(20): p. 6052-6075.
6. Dornfeld, D., S. Min, and Y. Takeuchi, *Recent advances in mechanical micromachining*. CIRP Annals-Manufacturing Technology, 2006. **55**(2): p. 745-768.
7. Özel, T. and X. Liu. *Modeling based micro-milling process planning for machining mold cavities*. in *Proceedings of the 3rd Int. Conference on High Speed Cutting*. 2008.
8. Rippere, T.B., K.J. Rao, and G.J. Wiens, *Modeling and analysis of fixel designs for micromanufacturing active fixturing*. Journal of Manufacturing Science and Engineering, Transactions of the ASME, 2011. **133**(2).
9. Bissacco, G., H.N. Hansen, and L. De Chiffre, *Micromilling of hardened tool steel for mould making applications*. Journal of Materials Processing Technology, 2005. **167**(2–3): p. 201-207.
10. Budak, E. and I. Tuzla. *Machining stability and Machine Tool Dynamics*. in *Proceedings of 11th International Research/Expert Conference, Trends in the Development of Machinery and Associated Technology*, pp. 111-1129, Hammamet. 2007.
11. Huo, D., *Micro-cutting: fundamentals and applications*. 2013: John Wiley & Sons.
12. Cheng, K. and D. Huo, *Micro-Cutting : Fundamentals and Applications*. 2013.
13. Kang, I.S., et al., *A mechanistic model of cutting force in the micro end milling process*. Journal of Materials Processing Technology, 2007. **187–188**: p. 250-255.
14. Mativenga, P.T., A. Aramcharoen, and D. Huo, *Micro tooling design and manufacturing*. Micro-cutting: fundamentals and applications, 1st edn. Wiley, Chichester, 2013: p. 45-61.
15. Ratchev, S., et al., *An advanced FEA based force induced error compensation strategy in milling*. International Journal of Machine Tools and Manufacture, 2006. **46**(5): p. 542-551.
16. Morgan, C.J., R.R. Vallance, and E.R. Marsh, *Micro machining glass with polycrystalline diamond tools shaped by micro electro discharge machining*. Journal of Micromechanics and Microengineering, 2004. **14**(12): p. 1687.
17. Wang, X., et al., *Research on the prediction model of micro-milling surface roughness*. Int. J. of Nanomanufacturing, 2013. **9**: p. 457-467.
18. Takeuchi, Y., et al., *Creation of Ultra-precision Microstructures with High Aspect Ratios*. CIRP Annals, 2006. **55**(1): p. 107-110.
19. Chae, J., S.S. Park, and T. Freiheit, *Investigation of micro-cutting operations*. International Journal of Machine Tools and Manufacture, 2006. **46**(3): p. 313-332.
20. Dhanorker, A. and T. Ozel, *Meso/micro scale milling for micro-manufacturing*. International Journal of Mechatronics and Manufacturing Systems, 2008. **1**(1): p. 23-42.
21. Wang, J., et al., *Chip formation analysis in micromilling operation*. International Journal of Advanced Manufacturing Technology, 2009. **45**: p. 430-447.
22. Kim, C.J., M. Bono, and J. Ni, *Experimental analysis of chip formation in micro-milling*. Technical Paper - Society of Manufacturing Engineers. MR, 2002(MR02-159): p. 1-8.
23. Okazaki, Y., N. Mishima, and K. Ashida, *Microfactory - Concept, history, and developments*. Journal of Manufacturing Science and Engineering-Transactions of the Asme, 2004. **126**(4): p. 837-844.
24. Swain, N., et al., *An experimental investigation on the machining characteristics of Nimonic 75 using uncoated and TiAlN coated tungsten carbide micro-end mills*. CIRP Journal of Manufacturing Science and Technology, 2017. **16**: p. 34-42.

25. Ayed, Y., et al., *Orthogonal micro-cutting modeling of the Ti17 titanium alloy using the crystal plasticity theory*. Finite Elements in Analysis and Design, 2017. **137**: p. 43-55.
26. Ohbuchi, Y. and T. Obikawa, *Adiabatic shear in chip formation with negative rake angle*. International Journal of Mechanical Sciences, 2005. **47**(9): p. 1377-1392.
27. Shunmugam, M.S., *Machining Challenges: Macro to Micro Cutting*. Journal of The Institution of Engineers (India): Series C, 2016. **97**(2): p. 223-241.
28. Rezaei, H., M.H. Sadeghi, and E. Budak, *Determination of minimum uncut chip thickness under various machining conditions during micro-milling of Ti-6Al-4V*. International Journal of Advanced Manufacturing Technology, 2018. **95**(5-8): p. 1617-1634.
29. Ducobu, F., E. Filippi, and E. Rivière-Lorphèvre. *Chip formation and minimum chip thickness in micro-milling*. in *Proceedings of the 12th CIRP conference on modeling of machining operations*. 2009.
30. Basuray, P.K., B.K. Misra, and G.K. Lal, *Transition from ploughing to cutting during machining with blunt tools*. Wear, 1977. **43**(3): p. 341-349.
31. Shimada, S., et al., *Feasibility study on ultimate accuracy in microcutting using molecular dynamics simulation*. CIRP Annals-Manufacturing Technology, 1993. **42**(1): p. 91-94.
32. Shi, Z.Y. and Z.Q. Liu. *Numerical modeling of minimum uncut chip thickness for micromachining with different rake angle*. in *ASME 2011 International Manufacturing Science and Engineering Conference, MSEC 2011*. 2011.
33. Vogler, M.P., R.E. DeVor, and S.G. Kapoor, *On the modeling and analysis of machining performance in micro-endmilling, part i: Surface generation*. Journal of Manufacturing Science and Engineering, Transactions of the ASME, 2004. **126**(4): p. 685-694.
34. Liu, X., R.E. DeVor, and S.G. Kapoor, *An analytical model for the prediction of minimum chip thickness in micromachining*. Journal of Manufacturing Science and Engineering, Transactions of the ASME, 2006. **128**(2): p. 474-481.
35. Lai, X., et al., *Modelling and analysis of micro scale milling considering size effect, micro cutter edge radius and minimum chip thickness*. International Journal of Machine Tools and Manufacture, 2008. **48**(1): p. 1-14.
36. Rezaei, H., M.H. Sadeghi, and E. Budak, *Determination of minimum uncut chip thickness under various machining conditions during micro-milling of Ti-6Al-4V*. International Journal of Advanced Manufacturing Technology, 2017: p. 1-18.
37. de Oliveira, F.B., et al., *Size effect and minimum chip thickness in micromilling*. International Journal of Machine Tools and Manufacture, 2015. **89**: p. 39-54.
38. Son, S.M., H.S. Lim, and J.H. Ahn, *Effects of the friction coefficient on the minimum cutting thickness in micro cutting*. International Journal of Machine Tools and Manufacture, 2005. **45**(4): p. 529-535.
39. Liu, X., et al., *Cutting Mechanisms and Their Influence on Dynamic Forces, Vibrations and Stability in Micro-Endmilling*. 2004(47136): p. 583-592.
40. Shi, Z., et al., *Determination of minimum uncut chip thickness during micro-end milling Inconel 718 with acoustic emission signals and FEM simulation*. The International Journal of Advanced Manufacturing Technology, 2017: p. 1-9.
41. Wang, J.S., et al., *Surface generation analysis in micro end-milling considering the influences of grain*. Microsystem Technologies, 2008. **14**(7): p. 937-942.
42. Liu, X., R.E. DeVor, and S.G. Kapoor, *Model-Based Analysis of the Surface Generation in Microendmilling—Part I: Model Development*. Journal of Manufacturing Science and Engineering, 2006. **129**(3): p. 453-460.
43. Wang, J.S., et al., *Modeling and experimental study on micro-milling polycrystalline material*. Dongbei Daxue Xuebao/Journal of Northeastern University, 2008. **29**(10): p. 1478-1481.
44. Lee, D.E., et al., *Precision manufacturing process monitoring with acoustic emission*. International Journal of Machine Tools and Manufacture, 2006. **46**(2): p. 176-188.
45. Qin, Y., *Chapter 1 - Overview of Micro-manufacturing*, in *Micromanufacturing Engineering and Technology (Second Edition)*. 2015, William Andrew Publishing: Boston. p. 1-33.

46. Filiz, S., et al., *An experimental investigation of micro-machinability of copper 101 using tungsten carbide micro-endmills*. International Journal of Machine Tools and Manufacture, 2007. **47**(7): p. 1088-1100.
47. Aramcharoen, A. and P.T. Mativenga, *Size effect and tool geometry in micromilling of tool steel*. Precision Engineering, 2009. **33**(4): p. 402-407.
48. Aramcharoen, A. and P.T. Mativenga, *Evaluation of critical parameters in micro machining of hardened tool steel*. International Journal of Nanomanufacturing, 2009. **3**(1-2): p. 100-111.
49. Tlustý, J., *High-Speed Machining*. CIRP Annals, 1993. **42**(2): p. 733-738.
50. Lu, X., et al., *Cutting parameters optimization for MRR under the constraints of surface roughness and cutter breakage in micro-milling process*. Journal of Mechanical Science and Technology, 2018. **32**(7): p. 3379-3388.
51. Sreeram, S., et al., *Optimization of cutting parameters in micro end milling operations in dry cutting condition using genetic algorithms*. The International Journal of Advanced Manufacturing Technology, 2006. **30**(11): p. 1030-1039.
52. Aslantas, K., E. Ekici, and A. Çiçek, *Optimization of process parameters for micro milling of Ti-6Al-4V alloy using Taguchi-based gray relational analysis*. Measurement, 2018. **128**: p. 419-427.
53. Lekkala, R., et al., *Characterization and modeling of burr formation in micro-end milling*. Precision Engineering, 2011. **35**(4): p. 625-637.
54. Oliaei, S.N.B. and Y. Karpaz, *Influence of tool wear on machining forces and tool deflections during micro milling*. International Journal of Advanced Manufacturing Technology, 2015.
55. Moola, M.R., A. Gorin, and K.A. Hossein, *Optimization of various cutting parameters on the surface roughness of the machinable glass ceramic with two flute square end mills of micro grain solid carbide*. International Journal of Precision Engineering and Manufacturing, 2012. **13**(9): p. 1549-1554.
56. Chen, P.C., et al., *An experimental study of micromilling parameters to manufacture microchannels on a PMMA substrate*. International Journal of Advanced Manufacturing Technology, 2014. **71**(9-12): p. 1623-1630.
57. Li, P., et al., *Micromilling of thin ribs with high aspect ratios*. Journal of Micromechanics and Microengineering, 2010. **20**(11).
58. Popov, K., et al., *Micromilling strategies for machining thin features*. Proceedings of the Institution of Mechanical Engineers, Part C: Journal of Mechanical Engineering Science, 2006. **220**(11): p. 1677-1684.
59. Llanos, I., et al., *Micromilling high aspect ratio features using tungsten carbide tools*. Proceedings of the Institution of Mechanical Engineers, Part B: Journal of Engineering Manufacture, 2014: p. 0954405414522214.
60. Jiao, K.R., et al., *Research on the influences of milling way on surface quality of high-volume SiCp/Al composites thin-walled piece in high speed milling*. Rengong Jingti Xuebao/Journal of Synthetic Crystals, 2015. **44**(12): p. 3770-3776.
61. Li, P., et al., *Micromilling of thin ribs with high aspect ratios*. Journal of Micromechanics and Microengineering, 2010. **20**(11): p. 115013.
62. Gao, Y.-y., et al., *Tool path planning and machining deformation compensation in high-speed milling for difficult-to-machine material thin-walled parts with curved surface*. The International Journal of Advanced Manufacturing Technology, 2016. **84**(9): p. 1757-1767.
63. Chen, W., et al., *Deformation prediction and error compensation in multilayer milling processes for thin-walled parts*. International Journal of Machine Tools and Manufacture, 2009. **49**(11): p. 859-864.
64. Popov, K.B., et al., *Micro milling of thin features*. 2005.
65. Yau, H.-T. and M.-J. Kuo, *NURBS machining and feed rate adjustment for high-speed cutting of complex sculptured surfaces*. International Journal of Production Research, 2001. **39**(1): p. 21-41.
66. Lo, C.-C., *Real-time generation and control of cutter path for 5-axis CNC machining*. International Journal of Machine Tools and Manufacture, 1999. **39**(3): p. 471-488.

67. Park, J., S. Nam, and M. Yang, *Development of a real-time trajectory generator for NURBS interpolation based on the two-stage interpolation method*. The International Journal of Advanced Manufacturing Technology, 2005. **26**(4): p. 359-365.
68. Nam, S.-H. and M.-Y. Yang, *A study on a generalized parametric interpolator with real-time jerk-limited acceleration*. Computer-Aided Design, 2004. **36**(1): p. 27-36.
69. Jaleel, A.K. and Z.K. Abdulla, *A study of the effect of cutting parameters on surface roughness and dimensional deviation for B-spline surfaces in CNC milling machine*. International Journal of Mechanical Engineering and Technology, 2018. **9**(9): p. 162-171.
70. Monreal, M. and C.A. Rodriguez, *Influence of tool path strategy on the cycle time of high-speed milling*. Computer-Aided Design, 2003. **35**(4): p. 395-401.
71. Mayor, J.R. and A.A. Sodemann. *Curvature-based tool-path segmentation for feedrate optimization in micromilling*. in *Transactions of the North American Manufacturing Research Institution of SME*. 2008.
72. Narasimhan, J., Z. Yu, and K.P. Rajurkar. *Tool wear compensation and path generation in micro and macro EDM*. in *Transactions of the North American Manufacturing Research Institute of SME*. 2004.
73. Qin, Z., et al., *Optimisation of tool angles and the relation between tool path and cutting force in high-speed milling with micro-end-mill*. International Journal of Computer Applications in Technology, 2007. **28**(1): p. 20-26.
74. Mayor, J.R. and A.A. Sodemann, *Intelligent tool-path segmentation for improved stability and reduced machining time in micromilling*. Journal of Manufacturing Science and Engineering, Transactions of the ASME, 2008. **130**(3): p. 0311211-03112113.
75. Banerjee, A. and E.V. Bordatchev, *Effect of circular tool path on cutting force profile in micro-end-milling*. Proceedings of the Institution of Mechanical Engineers, Part C: Journal of Mechanical Engineering Science, 2012. **226**(6): p. 1589-1600.
76. Banerjee, A. and E.V. Bordatchev, *Effect of circular tool path on cutting force profile in micro-end-milling*. Proceedings of the Institution of Mechanical Engineers, Part C: Journal of Mechanical Engineering Science, 2011: p. 0954406211423575.
77. Banerjee, A. and E.V. Bordatchev. *An experimental analysis of chip formation in circular micro-end-milling*. in *Transactions of the North American Manufacturing Research Institution of SME*. 2010.
78. Vázquez Lepe, E., et al., *Process planning considerations for micromilling of mould cavities used in ultrasonic moulding technology*. © Precision Engineering, 2015, vol. 39, p. 252-260, 2014.
79. Cakir, M.C., O. Irfan, and K. Cavdar, *An expert system approach for die and mold making operations*. Robotics and Computer-Integrated Manufacturing, 2005. **21**(2): p. 175-183.
80. Standard, I., *Tool Life Testing in Milling, Part 2: End Milling*, in *ISO 8688-2*. ISO8688-1989. p. 1-26.
81. Karandikar, J.M., T.L. Schmitz, and A.E. Abbas, *Spindle speed selection for tool life testing using Bayesian inference*. Journal of Manufacturing Systems, 2012. **31**(4).
82. Wang, C.Y., et al., *Wear and breakage of TiAlN- and TiSiN-coated carbide tools during high-speed milling of hardened steel*. Wear, 2015. **336**: p. 29-42.
83. Rahman, M., A. Senthil Kumar, and J.R.S. Prakash, *Micro milling of pure copper*. Journal of Materials Processing Technology, 2001. **116**(1): p. 39-43.
84. Chang, W., et al., *Investigation of microstructured milling tool for deferring tool wear*. Wear, 2011. **271**(9): p. 2433-2437.
85. Attanasio, A., et al., *Influence of material microstructures in micromilling of Ti6Al4V alloy*. Materials, 2013. **6**(9): p. 4268-4283.
86. Romanus, H., et al. *Micromilling of Sintered ZrO2 Ceramic via cBN and diamond coated tools*. in *Procedia CIRP*. 2014.
87. Su, H., et al., *Tool life and surface integrity in high-speed milling of titanium alloy TA15 with PCD/PCBN tools*. Chinese Journal of Aeronautics, 2012. **25**(5): p. 784-790.

88. Jemielniak, K. and P.J. Arrazola, *Application of AE and cutting force signals in tool condition monitoring in micro-milling*. CIRP Journal of Manufacturing Science and Technology, 2008. **1**(2): p. 97-102.
89. Tansel, I., et al., *Micro-end-milling - III. Wear estimation and tool breakage detection using acoustic emission signals*. International Journal of Machine Tools and Manufacture, 1998. **38**(12): p. 1449-1466.
90. Malekian, M., S.S. Park, and M.B.G. Jun, *Tool wear monitoring of micro-milling operations*. Journal of Materials Processing Technology, 2009. **209**(10): p. 4903-4914.
91. Hung, C.W. and M.C. Lu, *Model development for tool wear effect on AE signal generation in micromilling*. International Journal of Advanced Manufacturing Technology, 2013. **66**(9-12): p. 1845-1858.
92. Özel, T., et al., *Experiments and finite element simulations on micro-milling of Ti-6Al-4V alloy with uncoated and cBN coated micro-tools*. CIRP Annals, 2011. **60**(1): p. 85-88.
93. Uçun, I., et al., *Effect of tool coating materials on surface roughness in micromachining of Inconel 718 super alloy*. Proceedings of the Institution of Mechanical Engineers, Part B: Journal of Engineering Manufacture, 2014. **228**(12): p. 1550-1562.
94. Huo, D., C. Lin, and K. Dalgarno, *An experimental investigation on micro machining of fine-grained graphite*. The International Journal of Advanced Manufacturing Technology, 2014. **72**(5): p. 943-953.
95. Bissacco, G., H.N. Hansen, and L. De Chiffre, *Micromilling of hardened tool steel for mould making applications*. Journal of Materials Processing Technology, 2005. **167**(2): p. 201-207.
96. Weule, H., V. Hüntrup, and H. Tritschler, *Micro-Cutting of Steel to Meet New Requirements in Miniaturization*. CIRP Annals, 2001. **50**(1): p. 61-64.
97. Iglesias, A., J. Munoa, and J. Ciurana, *Optimisation of face milling operations with structural chatter using a stability model based process planning methodology*. The International Journal of Advanced Manufacturing Technology, 2014. **70**(1): p. 559-571.
98. Bouzakis, K.D., et al., *Influence of dry micro-blasting grain quality on wear behaviour of TiAlN coated tools*. Wear, 2011. **271**(5): p. 783-791.
99. Zhu, K., Y.S. Wong, and G.S. Hong, *Multi-category micro-milling tool wear monitoring with continuous hidden Markov models*. Mechanical Systems and Signal Processing, 2009. **23**(2): p. 547-560.
100. Oliaei, S.N.B. and Y. Karpaz, *Polycrystalline diamond end mill cutting edge design to improve ductile-mode machining of silicon*. Precision Engineering, 2018. **51**: p. 403-414.
101. Qu, D., et al., *Experimental Study on the Effects of Coolants on Surface Quality and Mechanical Properties of Micromilled Thin-Walled Elgiloy*. Materials (Basel, Switzerland), 2018. **11**(9): p. 1497.
102. Li, M., et al., *Parameter optimization during minimum quantity lubrication milling of TC4 alloy with graphene-dispersed vegetable-oil-based cutting fluid*. Journal of Cleaner Production, 2019. **209**: p. 1508-1522.
103. Choi, S.U.S. *Enhancing thermal conductivity of fluids with nanoparticles*. in American Society of Mechanical Engineers, Fluids Engineering Division (Publication) FED. 1995.
104. Sun, Y., et al., *Enhanced Machinability of Ti-5553 Alloy from Cryogenic Machining: Comparison with MQL and Flood-cooled Machining and Modeling*. Procedia CIRP, 2015. **31**: p. 477-482.
105. Lv, D., et al., *Tool wear in milling Ti40 burn-resistant titanium alloy using pneumatic mist jet impinging cooling*. Journal of Materials Processing Technology, 2016. **229**: p. 641-650.
106. JungHyun, H., M. Pratt, and W.C. Regli, *Manufacturing feature recognition from solid models: a status report*. IEEE transactions on robotics and automation a publication of the IEEE Robotics and Automation Society., 2000. **16**(6): p. 782-796.
107. Sadaiah, M., et al., *A Generative Computer-Aided Process Planning System for Prismatic Components*. The International Journal of Advanced Manufacturing Technology, 2002. **20**(10): p. 709-719.

108. Sakurai, H. and P. Dave, *Volume decomposition and feature recognition, part II: Curved objects*. Vol. 28. 1996. 519-537.
109. Sakurai, H., *Volume decomposition and feature recognition: part 1—polyhedral objects*. Computer-Aided Design, 1995. **27**(11): p. 833-843.
110. Woo, Y. and H. Sakurai, *Recognition of maximal features by volume decomposition*. Computer-Aided Design, 2002. **34**(3): p. 195-207.
111. Woo, Y., *Fast cell-based decomposition and applications to solid modeling*. Computer-Aided Design, 2003. **35**(11): p. 969-977.
112. Yao, H., et al., *Key technologies in intelligent CAPP system for deep-drawn parts*. Shanghai Jiaotong Daxue Xuebao/Journal of Shanghai Jiaotong University, 2000. **34**(3): p. 306-309.
113. Fan, M.C., *Fixture design for turning parts in CAPP based on knowledge*. Huadong Chuanbo Gongye Xueyuan Xuebao/Journal of East China Shipbuilding Institute, 2001. **15**(4): p. 20-24.
114. Franco, P., M. Estrems, and F. Faura. *DNC method for flatness reduction by machine tool error compensation in planing processes*. in *Proceedings of 8th Biennial ASME Conference on Engineering Systems Design and Analysis, ESDA2006*. 2006.
115. Wang, J., B. Du, and H. Ding, *A modified genetic algorithm(GA) for optimization of process planning*. Journal of Computers, 2011. **6**(7): p. 1430-1437.
116. Hazarika, M. and U.S. Dixit, *Process Planning in Machining*, in *Setup Planning for Machining*. 2015, Springer International Publishing: Cham. p. 1-28.
117. Teich, T., et al., *Step standardized product data representation and exchange for optimized product development and automated process planning*, in *Advances in Intelligent and Soft Computing*. 2010. p. 41-56.
118. Hofmann, R., et al. *Optimization of value added chain in manufacturing using step*. in *Annals of DAAAM and Proceedings of the International DAAAM Symposium*. 2011.
119. Prasoon, R., et al., *An algorithm portfolio approach to reconfigurable set-up planning*. International Journal of Computer Integrated Manufacturing, 2011. **24**(8): p. 756-768.
120. Zahid, T. and A.A. Baqai. *Multi-criteria optimization of process plans for reconfigurable manufacturing systems: An evolutionary approach*. in *ASME International Mechanical Engineering Congress and Exposition, Proceedings (IMECE)*. 2013.
121. Goldhahn, L. and R. Eckardt. *Sustainable Process Planning of Manufacturing Variants for High-precision Parts*. in *Procedia CIRP*. 2016.
122. Shi, J. and C. Richard Liu, *The Influence of Material Models on Finite Element Simulation of Machining*. Vol. 126. 2004.
123. Murugesan, M. and D.W. Jung, *Johnson cook material and failure model parameters estimation of AISI-1045 medium carbon steel for metal forming applications*. Materials, 2019. **12**(4): p. 609.
124. Buzyurkin, A.E., I.L. Gladky, and E.I. Kraus, *Determination and verification of Johnson–Cook model parameters at high-speed deformation of titanium alloys*. Aerospace Science and Technology, 2015. **45**: p. 121-127.
125. Murugesan, M., et al., *A Comparative Study of Ductile Damage Models Approaches for Joint Strength Prediction in Hot Shear Joining Process*. Procedia Engineering, 2017. **207**: p. 1689-1694.
126. Saptaji, K. and S. Subbiah. *Finite element study of the effect of substrate properties in micro-cutting thin workpiece materials*. in *IOP Conference Series: Materials Science and Engineering*. 2016. IOP Publishing.
127. Yuan, Y., et al., *Modeling of cutting forces in micro end-milling*. Journal of Manufacturing Processes, 2018. **31**: p. 844-858.
128. Campatelli, G. and A. Scippa, *Prediction of Milling Cutting Force Coefficients for Aluminum 6082-T4*. Procedia CIRP, 2012. **1**: p. 563-568.
129. Schneider, C.A., W.S. Rasband, and K.W. Eliceiri, *NIH Image to ImageJ: 25 years of image analysis*. Nature Methods, 2012. **9**(7): p. 671-675.
130. Chern, G.L., et al., *Study on burr formation in micro-machining using micro-tools fabricated by micro-EDM*. Precision Engineering, 2007. **31**(2): p. 122-129.

131. Ezugwu, E.O. and Z.M. Wang, *Titanium alloys and their machinability—a review*. Journal of materials processing technology, 1997. **68**(3): p. 262-274.
132. Filiz, S., et al., *An experimental investigation of micro-machinability of copper 101 using tungsten carbide micro-endmills*. International Journal of Machine Tools and Manufacture, 2007. **47**(7-8): p. 1088-1100.
133. Ramaswami, R., *The effect of the built-up-edge(BUE) on the wear of cutting tools*. Wear, 1971. **18**(1): p. 1-10.
134. Teng, X., et al., *An experimental study on tool wear behaviour in micro milling of nano Mg/Ti metal matrix composites*. The International Journal of Advanced Manufacturing Technology, 2018. **96**(5): p. 2127-2140.
135. Meng, H. and X. Li. *Grey relational analysis for impact factors of micro-milling surface roughness*. in *2015 IEEE 12th International Conference on Electronic Measurement and Instruments, ICEMI 2015*. 2016.
136. Annoni, M., L. Rebaioli, and Q. Semeraro, *Thin wall geometrical quality improvement in micromilling*. International Journal of Advanced Manufacturing Technology, 2015. **79**(5-8): p. 881-895.
137. Wu, X., L. Li, and N. He, *Investigation on the burr formation mechanism in micro cutting*. Precision Engineering, 2017. **47**: p. 191-196.
138. Liu, X., R.E. DeVor, and S.G. Kapoor, *An Analytical Model for the Prediction of Minimum Chip Thickness in Micromachining*. Journal of Manufacturing Science and Engineering, 2005. **128**(2): p. 474-481.
139. Cardoso, P. and J.P. Davim, *Optimization of surface roughness in micromilling*. Materials and Manufacturing Processes, 2010. **25**(10): p. 1115-1119.
140. Alting, L. and H.-C. Zhang, *Computer Aided Process Planning: the state-of-the-art survey*. International Journal of Production Research - INTJ PROD RES, 1989. **27**: p. 553-585.
141. Leo Kumar, S.P., *Knowledge-based expert system in manufacturing planning: state-of-the-art review*. International Journal of Production Research, 2019. **57**(15-16): p. 4766-4790.
142. Verma, A.K. and S. Rajotia, *Feature vector: a graph-based feature recognition methodology*. International Journal of Production Research, 2004. **42**(16): p. 3219-3234.
143. Jianbo, S. and J. Malik, *Normalized cuts and image segmentation*. IEEE Transactions on Pattern Analysis and Machine Intelligence, 2000. **22**(8): p. 888-905.
144. Jian, P., J. Daxin, and Z. Aidong, *On mining cross-graph quasi-cliques*, in *Proceedings of the eleventh ACM SIGKDD international conference on Knowledge discovery in data mining*. 2005, ACM: Chicago, Illinois, USA.
145. Sadaiah, M., *An integrated computer aided process planning system for prismatic components*. 2002.
146. Nau, D.S. and M. Luce, *Knowledge Representation and Reasoning Techniques for Process Planning: Extending SIPS to do Tool Selection*. 1987.
147. Arriola, I., et al., *Relationship between machinability index and in-process parameters during orthogonal cutting of steels*. CIRP Annals, 2011. **60**(1): p. 93-96.
148. Venkata Rao, R., *Machinability evaluation of work materials using a combined multiple attribute decision-making method*. The International Journal of Advanced Manufacturing Technology, 2006. **28**(3): p. 221-227.
149. Gologlu, C. and N. Sakarya, *The effects of cutter path strategies on surface roughness of pocket milling of 1.2738 steel based on Taguchi method*. Journal of Materials Processing Technology, 2008. **206**(1-3): p. 7-15.
150. Palpandian, P., R.V. Prabhu, and S.S. Babu, *Stability Lobe Diagram for High Speed Machining Processes: Comparison of Experimental and Analytical Methods—A Review*. International Journal of Innovative Research in Science, Engineering and Technology, 2013. **2**(3): p. 747-752.
151. Sahoo, P. and K. Patra, *Mechanistic modeling of cutting forces in micro-end-milling considering tool run out, minimum chip thickness and tooth overlapping effects*. Machining Science and Technology, 2018.

152. Vogler, M.P., R.E. DeVor, and S.G. Kapoor, *On the Modeling and Analysis of Machining Performance in Micro-Endmilling, Part I: Surface Generation*. Journal of Manufacturing Science and Engineering, 2005. **126**(4): p. 685-694.
153. Yuan, Z.J., M. Zhou, and S. Dong, *Effect of diamond tool sharpness on minimum cutting thickness and cutting surface integrity in ultraprecision machining*. Journal of Materials Processing Technology, 1996. **62**(4): p. 327-330.
154. Hassanpour, H., et al., *Experimental Study of Cutting Force, Microhardness, Surface Roughness, and Burr Size on Micromilling of Ti6Al4V in Minimum Quantity Lubrication*. Materials and Manufacturing Processes, 2016. **31**(13): p. 1654-1662.
155. Aslantas, K., et al., *Cutting performance of nano-crystalline diamond (NCD) coating in micro-milling of Ti6Al4V alloy*. Precision Engineering, 2016. **45**: p. 55-66.
156. Ikawa, N., et al., *An Atomistic Analysis of Nanometric Chip Removal as Affected by Tool-Work Interaction in Diamond Turning*. CIRP Annals - Manufacturing Technology, 1991. **40**(1): p. 551-554.
157. Sahoo, P., et al., *Size effects in Micro End-Milling of Hardened P-20 Steel*. Materials Today: Proceedings, 2018. **5**(11, Part 3): p. 23726-23732.
158. Son, S.M., H.S. Lim, and J.H. Ahn, *Effects of the friction coefficient on the minimum cutting thickness in micro cutting*. International Journal of Machine Tools and Manufacture, 2005. **45**(4-5): p. 529-535.
159. Elkaseer, A.M., et al., *Material microstructure effects in micro-endmilling of Cu99.9E*. Proceedings of the Institution of Mechanical Engineers, Part B: Journal of Engineering Manufacture, 2018. **232**(7): p. 1143-1155.
160. Mamedov, A. and I. Lazoglu, *Machining forces and tool deflections in micro milling*. Procedia CIRP, 2013. **8**: p. 147-151.
161. Dow, T.A., E.L. Miller, and K. Garrard, *Tool force and deflection compensation for small milling tools*. Precision Engineering, 2004. **28**(1): p. 31-45.
162. Yi, J., et al., *Micro-flank milling forces considering stiffness of thin-walled parts*. The International Journal of Advanced Manufacturing Technology, 2018. **95**(5): p. 2767-2782.
163. Qu, D., et al., *Applications of integrated auxiliary methods based on deformation analysis for micro-milling thin-walled slot on micro-neck*. The International Journal of Advanced Manufacturing Technology, 2017. **91**(5): p. 1945-1955.
164. Afazov, S.M., S.M. Ratchev, and J. Segal, *Modelling and simulation of micro-milling cutting forces*. Journal of Materials Processing Technology, 2010. **210**(15): p. 2154-2162.

Appendix

Appendix A

A1 Cutting parameter validation

A series of machining experiments have been conducted in order to validate the cutting forces used in the simulation of machining layers evaluated numerically. Also, the effect of tool run out (the combination of tool assembly and fabrication error) not applicable to numerical model was measured and applied as an offset value to tool path used in experimental validation.

A1.1 Run out measurement

This experiment was designed to measure the spindle run out for micro tool clamped using ultra-precision collet in slot milling of Aluminium 6061-T6. The cutting parameters used in the experiment are summarised in Table 21.

Table 21: Machining parameters used in tool run out experiment

<i>Machining parameter</i>	<i>Value</i>
<i>Spindle speed (n)</i>	60000 RPM
<i>Radial cutting depth (a_e)</i>	1 mm
<i>Cutting width (a_p)</i>	0.5 mm
<i>Feed rate (f)</i>	200 mm/min

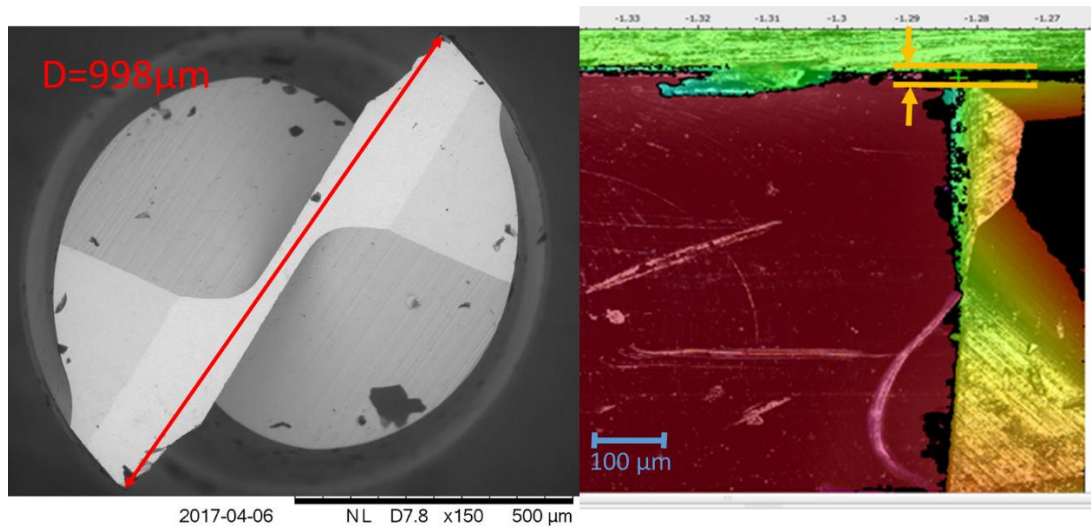


Figure 93: Comparison of tool diameter (SEM image-Left) with the resultant slot width measured using Alicona (Right)

Figure 93 shows the Alicona measurement environment whereas a result of tool run-out, the width of the machined slot is 1.6694 μm larger than the machine tool diameter. The tool run out value was close to the assumed value of 1 μm for the machining parameter used. The slightly

higher experimental value is believed to be the error due to tool assembly and machine vibration from the siting of the CNC machine in a multi-disciplinary machine shop. The measured run out is compensated for in the next stages of the experiment.

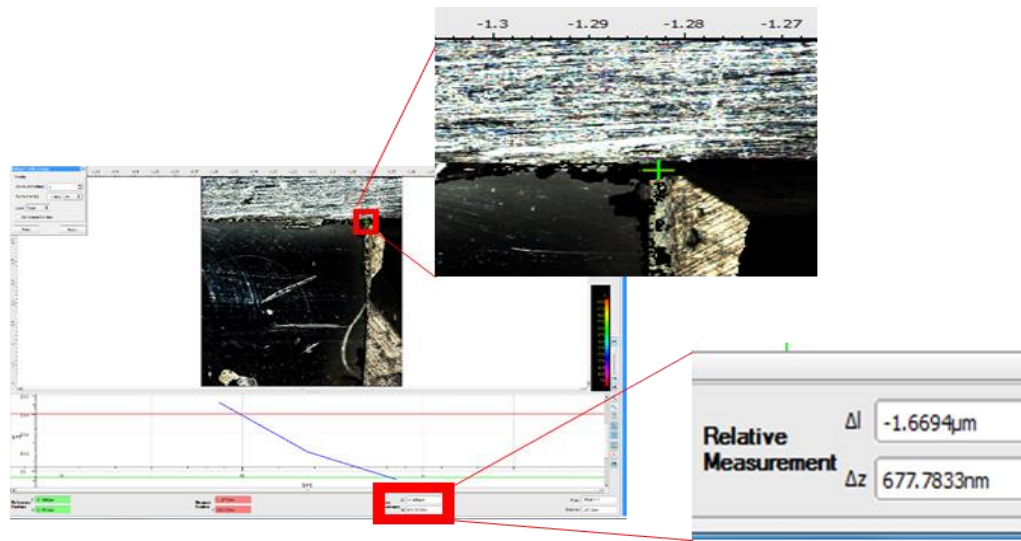


Figure 94: Alicona measurement interface

A1.2 Cutting force validation

The resultant cutting forces along X, Y and Z was measured using a dynamometer fixed to the vice in the machining centre during slot milling. The signals from the force sensors were plotted using the Kistler software DynoWare to measure average force recorded across three axes.

The cutting forces calculated using the numerical model have been experimentally validated by undertaking slot milling using a range of depths of cut; $0.1\mu\text{m}$, $0.2\mu\text{m}$ and $0.3\mu\text{m}$ the average cutting forces after the filtration plotted in

Figure 96. Cutting forces calculated using the mechanistic model and used in the simulation model shows a good agreement with the measured forces experimentally [164].

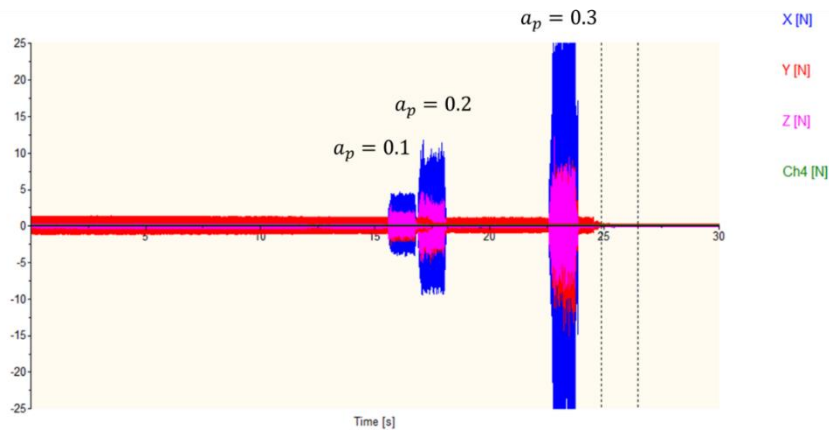


Figure 95: Cutting forces measured in full slot milling of Aluminum 6061-T6 using 1 mm uncoated tungsten carbide endmill

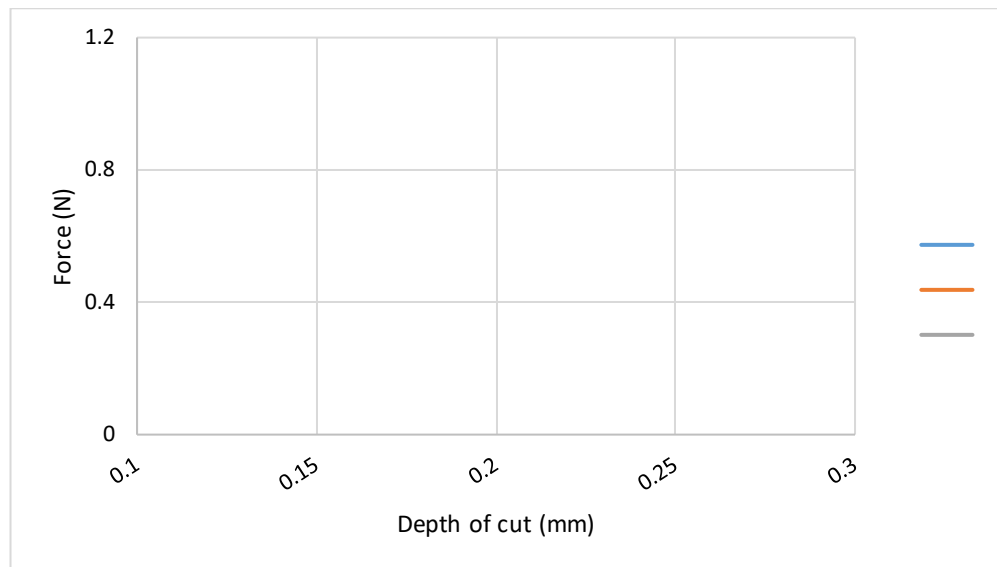


Figure 96: Average cutting forces measured for 1 mm uncoated tungsten carbide endmill

Appendix B

B1 Cutting tool datasheet

https://asia.kyocera.com/products/cuttingtools/wpcontent/uploads/2017/09/Solid_Round_Cutting_Tools_Catalog-2017.pdf

B2 HURCO CNC machine centre

<https://www.hurco.com/media/Brochures/Hurco-VerticalMachines-Technical-Catalog.pdf>

B3 NAKANISHI High speed spindle

<http://www.nsk-nakanishi.co.jp/industrial-eng/hpms/hes/hes.pdf>